AN APPROACH TO ESTIMATING LONG-TERM MULTIAXIAL CREEP BEHAVIOR FROM SHORT-TERM UNIAXIAL CREEP RESULTS

By John W. Chuang, Thomas W. Kennedy,
and Ervin S. Perry

RESEARCH REPORT 2864-3

to

OAK RIDGE NATIONAL LABORATORY

operated by

UNION CARBIDE CORPORATION

for

U.S. ATOMIC ENERGY COMMISSION

DEPARTMENT OF CIVIL ENGINEERING

THE UNIVERSITY OF TEXAS AT AUSTIN

JUNE 1970

AN APPROACH TO ESTIMATING LONG-TERM MULTIAXIAL CREEP BEHAVIOR FROM SHORT-TERM UNIAXIAL CREEP RESULTS

by

John Wu-Shuang Chuang
Thomas W. Kennedy
Ervin S. Perry

Research Report Number 2864-3

An Investigation of the Time-Dependent
Deformation of Concrete Under Triaxial Stress
Conditions in Prestressed Reactor Vessels

conducted for

Oak Ridge National Laboratory

operated by
Union Carbide Corporation
for the
United States Atomic Energy Commission

by the

DEPARTMENT OF CIVIL ENGINEERING

THE UNIVERSITY OF TEXAS AT AUSTIN

June 1970

PREFACE

This is the third in a series of reports dealing with the findings of a research project concerned with the evaluation of the creep behavior of concrete subjected to triaxial compressive stresses and elevated temperature. This report develops and evaluates a method of predicting long term triaxial creep behavior from relatively short term uniaxial creep data.

The investigation was conducted and financed under Union Carbide Subcontract 2864 for the Oak Ridge National Laboratory, which is operated by the Union Carbide Corporation for the United States Atomic Energy Commission. The planning, conducting, and analyzing of data for this experiment required the assistance and cooperation of many individuals and organizations; the authors would like to acknowledge the cooperation and assistance obtained from the Concrete Division of the Waterways Experiment Station, Jackson, Mississippi, and the Department of Civil Engineering of The University of California at Berkeley. In addition, special thanks are extended to Mr. G. D. Whitman, Coordinator, Pressure Vessel Technology Program, whose active participation and support allowed this investigation to be successfully conducted and to Dr. J. P. Callahan, Mr. J. G. Stradley, and Dr. J. M. Corum of the Oak Ridge National Laboratory. Appreciation is also extended to Professor Clyde E. Kesler, Department of Civil Engineering, University of Illinois, who served as a consultant to the project. Special appreciation is due Mr. Victor N..Toth, Dr. Nabil Jundi, and Dr. Guy P. York for their aid in the planning of the experiment, the preparation of the specimens, and the collection of the data. And finally, the aid extended by personnel of the Center for Highway Research, The University of Texas at Austin, is acknowledged.

Future reports will be concerned with a detailed inspection and evaluation of the specimens used in this investigation, a more detailed investigation of certain aspects of the data, and an extension of this investigation to include the effect of time after loading on creep behavior.

John W. Chuang
Thomas W. Kennedy
Ervin S. Perry

June 1970

ABSTRACT

This report describes an experimental investigation of the creep behavior of concrete subjected to (1) multiaxial stresses ranging from 0 to 3600 psi, (2) two different temperatures during loading (75° F and 150° F), and (3) two different curing histories (sealed and air-dried) and suggests predictive equations for estimating creep strains in the principal directions for stresses less than the creep proportional limit.

The predictive equations for multiaxial states of stress were derived by establishing a linear time-dependent relationship between creep strain and stress from uniaxial creep tests and by assuming (1) that concrete is a homogeneous, isotropic body and (2) that the application of the law of superposition to creep strain is valid. On the basis of the experimental results it appeared that these assumptions were reasonably valid. A comparison of measured creep strains with calculated creep strains indicated that when the stress level was less than the creep proportional limit, the predictive equations provided a satisfactory estimate of the actual creep strains. The standard errors of estimate for the sealed and air-dried curing conditions at 75° F were 16 and 27 micro-units and at 150° F were 33 and 40 micro-units.

The concept of introducing creep strain into stress-strain analyses of concrete is considered and discussed together with effective modulus of elasticity, time-dependent flexibility, and time-dependent lateral expansion per unit stress of concrete.

TABLE OF CONTENTS

LIST OF FIGURES

LIST OF TABLES

CHAPTER 1. INTRODUCTION

The effective use of concrete demands detailed knowledge of its many properties and characteristics. One of these characteristics is the creep behavior of concrete subjected to long-term sustained loads. Although a great deal of information is available on the load-deformation characteristics of concrete, information concerned with the creep characteristics is limited, especially for concrete subjected to triaxial stresses.

With the advent of prestressed concrete nuclear reactor vessels, it has become mandatory that information be obtained on the creep behavior of concrete subjected to sustained triaxial compressive stresses, and it is essential that the time-dependent characteristics be investigated and defined as completely as possible.

In order to obtain such information, the United States Atomic Energy Commission at the request of the Oak Ridge National Laboratory formulated and initiated a basic research program for developing and improving the technology of prestressed concrete reactor vessels. As a part of this program, an extensive experimental investigation to study the creep behavior of concrete subjected to multiaxial states of stress and elevated temperatures was begun at The University of Texas at Austin.

In view of the fact that long-term creep tests are time consuming and that creep tests on concrete subjected to multiaxial compressive stresses are much more difficult to conduct than uniaxial creep tests, it was considered desirable to be able to estimate long-term creep behavior of concrete subjected to triaxial stress conditions from short-term uniaxial creep tests. The theoretical development of a method for estimating long-term creep behavior by utilizing information obtained from relatively short-term uniaxial creep tests is discussed in this report, and information obtained from the experimental portion of the overall investigation is used to develop predictive equations and to evaluate their accuracy.

This report contains seven chapters. Chapter 2 summarizes the current status of knowledge concerning stress-strain-time relationships for concrete

and methods for estimating creep behavior. Chapter 3 discusses stress-strain-time relationships and develops concepts and equations for estimating creep behavior. Chapter 4 describes the experimental program from which creep data were obtained for developing the predictive equations and evaluating their accuracy. The results from these tests are summarized and discussed in Chapter 5. The derived prediction equations for various curing conditions and their applications with regard to predicting creep strains are discussed in Chapter 6. Conclusions and recommendations are contained in Chapter 7.

CHAPTER 2. CURRENT STATUS OF KNOWLEDGE

At any given time the total strain for concrete subjected to a sustained load consists of instantaneous elastic strain ϵ_e, shrinkage strain ϵ_s, and creep strain ϵ_c. The relationships between these three are shown in Fig 1.

Creep strain is that portion of the time-dependent strain attributed to load, shrinkage strain is attributed to physical or chemical causes other than applied load, and elastic strain, which occurs instantly at the time of loading, is associated with the elastic characteristics of concrete.

The actual or theoretical elastic strain, as shown in Fig 1, decreases with time although it is often assumed to be constant and to be equal to the instanteneous strain at the time of loading. The decrease is the result of increase in the modulus of elasticity or stiffness of the concrete with time. However, for this study elastic strain at any time will be considered both equal to the instantaneous elastic strain and constant.

Although Fig 1 is based on the assumption that creep strain and shrinkage strain are mutually exclusive, they are in reality interrelated and difficult to distinguish. Nevertheless, they are normally considered as independent quantities, since shrinkage strain can be easily determined by measurements on unloaded specimens which are similar to the loaded specimens and which are subjected to the same environmental conditions. In this study, therefore, creep strain is considered to be that portion of the time-dependent strain in excess of shrinkage.

Creep behavior of concrete has been the subject of extensive investigations during the past 50 years. The findings of these investigations have been summarized by Fluck and Washa (Ref 9) in 1958, Neville and Meyers (Ref 23) in 1964, and most recently by a special committee of the American Concrete Institute (Ref 31). In addition, a comprehensive review has been conducted and reported by this project (Ref 33). Therefore, no attempt has been made in this study to review and summarize the effects produced by most factors involving the constituents of concrete, environment, and loading conditions. Rather, emphasis has been placed on findings concerned with stress-creep

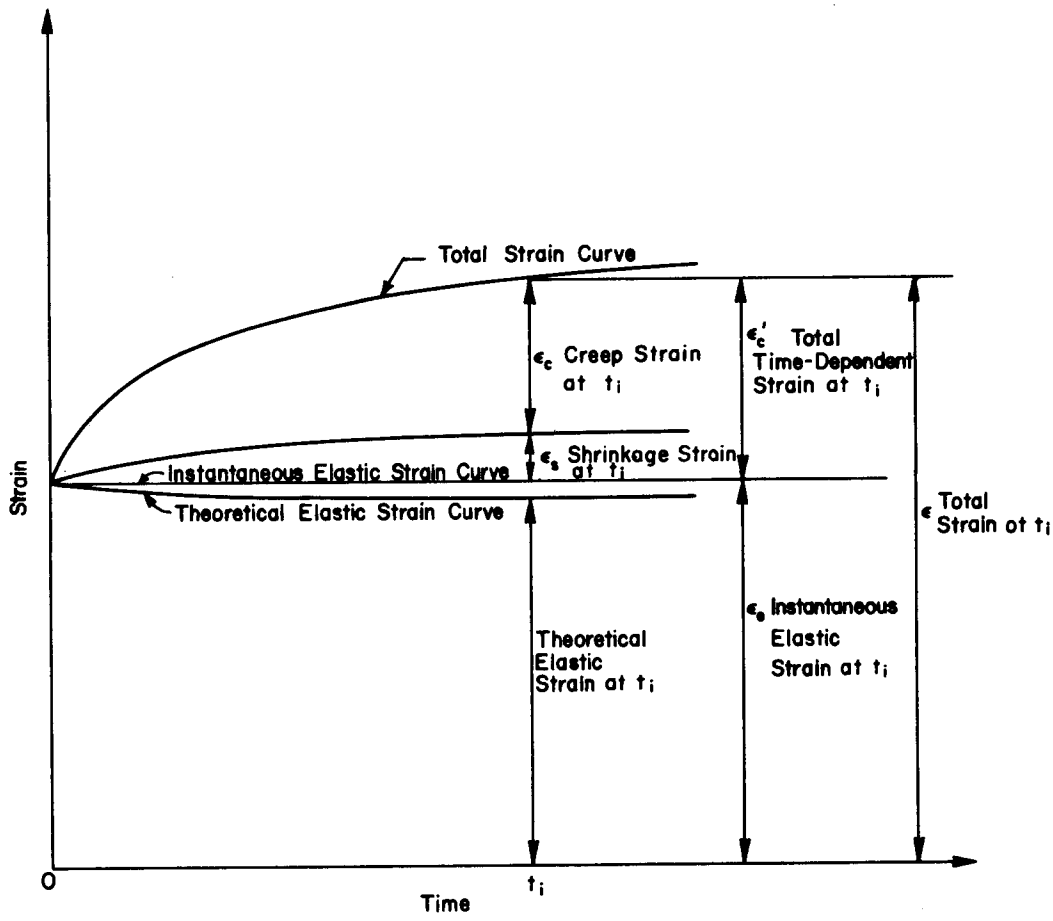

Fig 1. Relationship between creep, shrinkage, and elastic strains.

strain-time relationships, the effects of curing history and temperature, and methods of predicting creep behavior.

STRESS-CREEP STRAIN-TIME RELATIONSHIPS

Uniaxial Stress

In 1960, Rüsch (Ref 29) reported the results from a study to determine the effect of sustained loads on the strength and deformation of concrete and developed two groups of stress-strain curves. One showed that for loads higher than the sustained load strength, i.e., the maximum stress which can be sustained indefinitely, the strain increased rapidly with time and failure occurred. The other group indicated that for a stress lower than the sustained load strength, the creep strain approached an ultimate strain value as time increased, and it was estimated that the sustained load strength was approximately 75 percent of the ultimate compressive strength.

Results from a number of investigations show that creep strain is proportional to the stress applied. This linear relationship between stress and creep strain was reported as early as 1940 by Lorman (Ref 18). Later McHenry (Ref 20) and Shank (Ref 30) introduced the concept of specific creep, which is creep strain per unit stress. Their findings indicated that although specific creep varied with time it was constant for any given time, pointing out a linear relationship between creep and stress. In 1964 Ali and Kesler (Ref 2) reported that creep consists of basic creep, which is without moisture loss, and drying creep, which is with moisture loss. They also noted that for the same concrete, a linear relationship existed between stress and basic creep strain and between stress and drying creep strain but that the slopes of the two relationships were different. In recent tests, Roll (Ref 26) found that the stress-creep strain relationship was linear up to stress levels of approximately 30 to 35 percent of ultimate strength. He also reported that other investigators have found that this linearity existed up to 20 to 40 percent and was linear at any given time after loading but that the slope of the relationship decreased with increased time after load throughout the loading history. Results from tests performed by Gopalakrishnan et al (Ref 11) on concrete cubes under sequential loading showed that the linear stress-creep strain relationship was valid for both uniaxial and multiaxial states of stresses. Tests conducted by Hannant (Ref 12) showed that creep strain was proportional to stress at stress levels less than 2000 psi and at temperatures between 81° F and 163° F.

Multiaxial Stress

The majority of the investigations have been concerned with creep behavior under uniaxial loading conditions; nevertheless, creep under multiaxial stresses has recently received attention, partially because of the development of nuclear reactor vessels and other structures in which a complex state of stress exists.

Experiments conducted by Hannant (Ref 12) concerned with creep behavior resulting from multiaxial states of stress indicated a linear relationship between axial stress and axial creep strain. The slope of this linear relationship varied with time, but was constant at any given time. Later, tests conducted by Gopalakrishnan et al (Ref 11) also showed a linear relationship for multiaxial states of stress and indicated that the relationship was linear at any time during the period in which the concrete was loaded. These investigators, however, suggested that the linear stress-creep strain relationship for multiaxial stresses was different than for uniaxial stresses.

Little information is available concerning a Poisson's effect for creep and the information that is available often conflicts. Values for creep Poisson's ratio have been found to range from 0.0 to 0.2. In 1954 Ross (Ref 28) reported that creep in the direction of the major principal stress appeared to be unaffected by the presence of minor stresses, thus suggesting that creep Poisson's ratio was zero. This is in contrast to the results reported by most other investigators. Earlier investigations conducted by Duke and Davis (Ref 7) on the creep behavior of concrete subjected to combined stresses indicated that under axial load, creep strains occurred laterally as well as axially and a value of 0.17 was suggested for creep Poisson's ratio. Arthanari and Yu (Ref 3) reported an overall creep Poisson's ratio of 0.2. Recent creep tests performed by Hannant (Ref 12) on sealed concrete cylinders under a multiaxial state of stress also showed that creep strain in the axial direction was reduced by stresses at right angles to the axial stress, and a creep Poisson's ratio, similar in magnitude to the elastic Poisson's ratio, was suggested. It should be noted, however, that Hannant measured strains only in the axial direction. Recent work by Gopalakrishnan et al (Ref 11) showed that the uniaxial creep Poisson's ratio was approximately the same as the elastic Poisson's ratio but that its value varied when stresses in the orthogonal direction were applied. They concluded that creep under a multiaxial state of stress could be

estimated by an equation based on the theory of elasticity, assuming an anisotropic material with different values for creep Poisson's ratio in each direction.

EFFECT OF TEMPERATURE AND MOISTURE CONDITION

Various studies concerned with the effects of temperature during loading and moisture condition during curing and loading have indicated that both significantly influence the creep behavior of concrete.

Temperature

Test results reported by Hannant (Ref 12), Arthanari and Yu (Ref 3), and England and Ross (Ref 8) showed that in the temperature range of 68° F to 284° F the rate and magnitude of creep strain increased with increased temperature for sealed and unsealed specimens. Also, Hansen (Ref 13) reported that for concrete beams tested and cured under water for 6 months, creep deformation in flexure increased when the temperature was increased in the range of 68° F to 140° F. Nasser and Neville (Ref 21) reported that a linear relationship between temperature decreased the creep. In addition, results reported by Hannant (Ref 12) and Arthanari and Yu (Ref 3) showed that the creep of concrete increased linearly with temperature up to 176° F and that a further increase in temperature accelerated the creep rate. Arthanari and Yu also found that the creep strain of concrete was greater when the temperature was increased in steps than when the maximum temperature was maintained constant for the same period of time.

Tests performed by Cruz (Ref 6) on concrete specimens loaded to a 0.45f'c stress level for five hours, and maintained at 300° F, 600° F, 900° F, and 1200° F, showed creep strains to be 3.3, 6.4, 14.9, and 32.6 times greater than the strain recorded at 75° F.

Moisture Condition

The moisture condition for concrete during curing and while under load is one of the more important factors influencing the creep behavior of concrete. It is generally concluded that when concrete is not in hygroequilibrium, creep strain is higher when the relative humidity of the environment is low (Ref 23).

Long-term creep tests conducted by Troxell et al (Ref 32) indicated that at the end of 20 years creep strain of unsealed specimens stored at 50 percent relative humidity was three times that in specimens stored at 100 percent relative humidity. Hannant (Ref 12) found that 200 days after loading, creep

strains in concrete which was dried prior to loading were relatively small when compared with those in saturated concrete. Glucklick and Ishai (Ref 10) have also shown that creep strains in well-cured concrete with low moisture content at the time of loading were less than when the concrete had a high moisture content.

PREDICTION OF CREEP

Uniaxial Stress

Various prediction equations for estimating creep strain ε_c or specific creep c, i.e., creep strain per unit stress, at any time t after being subjected to a uniaxial stress σ which is less than the creep proportional limit have been suggested. These equations can be categorized as hyperbolic, exponential, or logarithmic.

In the hyperbolic group, for example, Lorman (Ref 18) proposed

$$\varepsilon_c = \frac{mt}{n + t}\sigma$$

where m and n are constants.

Neville and Meyers (Ref 23) reported that Ross (Ref 27) suggested

$$\varepsilon_c = \frac{t}{a + bt}$$

where a and b are constants for any given concrete, age of loading, and stress level.

Shank (Ref 30) suggested that specific creep could be estimated by the following exponential relationship:

$$c = Kt^{1/d}$$

where d and K are constants.

McHenry (Ref 16) suggested that specific creep could be predicted by

$$c = \alpha(1 - e^{-rt}) + \beta e^{-p\tau}(1 - e^{-qt})$$

where α , β , r , p , and q are constants, and τ is the age at loading.

Ali and Kesler (Ref 1) concluded that specific creep consists of basic creep c_b and drying creep c_d which could be expressed as follows:

$$c = c_b + c_d$$

$$c_b = \beta\left[\alpha_1\left(1 - e^{-\frac{t}{\tau_1}}\right) + \alpha_2\left(1 - e^{-\frac{t}{\tau_2}}\right) + \phi t\right]$$

$$c_d = \gamma\beta\epsilon_s\left(a_1 + \frac{b_1}{t}\right)$$

where

β = is a compliance factor representing the ratio of the deformation of the gel component of the concrete to the deformation of a hypothetical specimen of pure gel subjected to the same stress as the concrete,

ϵ_s = free shrinkage strain,

α_1 and α_2 = compliances of the Kelvin springs,

τ_1 and τ_2 = retardation times of the Kelvin elements,

ϕ = effective fluidity of the free dash pot,

γ = shrinkage correction factor,

a_1 and b_1 = constants.

In the logarithmic group, Hanson (Ref 14) suggested

$$\epsilon_c = F(T)\log_e(t + 1)$$

where $F(T)$ is the rate of creep.

Multiaxial Stress

There is very limited information on prediction of creep of concrete under multiaxial stress. In 1944 Duke and Davis (Ref 7) suggested that the ratio Ra of the axial strain in a cylinder under triaxial stresses σ_1 , σ_2 , and

σ_3 to the axial strain in a cylinder subject to simple axial stress σ_A can be estimated by

$$Ra = \frac{\sigma_1}{\sigma_A} - \nu_c \frac{\sigma_2}{\sigma_A} - \nu_c \frac{\sigma_3}{\sigma_A}$$

where ν_c is creep Poisson's ratio.

Hannant (Ref 12) proposed an equation for predicting creep under multiaxial stress as follows:

$$(\epsilon_c)_{mx} = (\epsilon_c)_x \left[1 - \nu_c \left(\frac{\sigma_y + \sigma_z}{\sigma_x} \right) \right]$$

where

σ_x, σ_y, and σ_z = principal stresses,

$(\epsilon_c)_x$ = creep strain under uniaxial stress in the direction of σ_x,

ν_c = creep Poisson's ratio,

$(\epsilon_c)_{mx}$ = ultimate creep strain in the direction of σ_x for the multiaxial stress condition.

The concept of applying superposition principles to creep deformation was suggested in 1944, by Duke and Davis (Ref 7). Later, Arutyunyan (Ref 4) used superposition for solving problems involving creep of concrete subjected to multiaxial stresses. In a more recent study of creep in sealed specimens, Hannant (Ref 12) found that the reduction in creep strain in one direction is approximately proportional to the stress magnitudes in the orthogonal direction. In contrasting tests performed by Gopalakrishnan et al (Ref 11) with unsealed specimens, creep Poisson's ratio was shown to be influenced by the presence of orthogonal stress, and the investigators concluded that creep under multiaxial compression can be predicted using an equation similar to the elasticity equation for anisotropic materials.

SUMMARY

Previous creep studies have been primarily concerned with the effect of factors such as type of cement, aggregate, age at loading, size and shape of specimens, relative humidity, and mixture proportions. This effort has contributed significant knowledge to an understanding of creep behavior, but since much of the work has been based on uniaxial tests very little information was obtained relative to creep characteristics and the behavior of concrete under multiaxial states of stress. In addition, most of the creep prediction equations discussed previously apply only to uniaxial loadings under the particular conditions examined. The knowledge of creep behavior of concrete subjected to multiaxial stresses and elevated temperatures is still very limited.

In general it appears that creep strain and stress are linearly related at low stress levels and that creep strain and temperature vary linearly up to a temperature of about 200° F. It also appears that creep strains are larger when the concrete is allowed to lose moisture while under load but that creep strains are lower for well-cured concrete that is dried prior to loading than for concrete with a higher moisture content. Creep Poisson's ratio as well as the creep prediction equation for a multiaxial state of stress is not well established, and there is disagreement as to the validity of applying the principle of superposition to creep behavior of concrete.

Since there is a need for information on the creep behavior of concrete subjected to multiaxial states of stress and since experimental creep studies involving multiaxial stresses are very difficult to conduct, it would be desirable to develop a method of estimating multiaxial creep behavior from uniaxial tests.

CHAPTER 3. UNIT CREEP FUNCTION

The purpose of this chapter is to develop a method of estimating long-term creep strains in plain concrete subjected to sustained uniaxial or multiaxial states of stress. This method utilizes creep strain information from uniaxially loaded specimens and is based on the principle of superposition.

CREEP UNDER UNIAXIAL STRESS

Rüsch (Ref 29) presented stress-strain-time relationships for concrete similar to those shown in Fig 2, where the instantaneous stress-strain relationship is represented by curve OA and the stress-ultimate strain relationship for infinite time under a sustained load is represented by curve OB. If only creep strain is considered, a similar relationship between stress and creep strain can be developed by subtracting the instantaneous strain from the total strain in Fig 2. From Figs 2 and 3 it can be seen that if the applied stress is equal to σ, where $\sigma < f'_c$, and if this stress is maintained for a period of time t_i where $t_i > 0$ the total strain is equal to ϵ_i, which is composed of both instantaneous strain ϵ_e and creep strain ϵ_c.

Examination of Fig 3 indicates that the relationship between stress and creep strain is linear up to the creep proportional limit and that the slope of the relationship decreases with increased time under load. The inverse of the slopes of these relationships represents the creep strain per unit stress $\frac{\epsilon_\sigma}{\sigma}$; thus, for concrete loaded under controlled conditions, the creep strain per unit stress at any time after loading is a function of time after loading t, age of loading τ, and stress level σ, and can be expressed as

$$\frac{\epsilon_c}{\sigma} = F(t,\tau,\sigma) \tag{3.1}$$

in which $F(t,\tau,\sigma)$ is defined as the unit creep function.

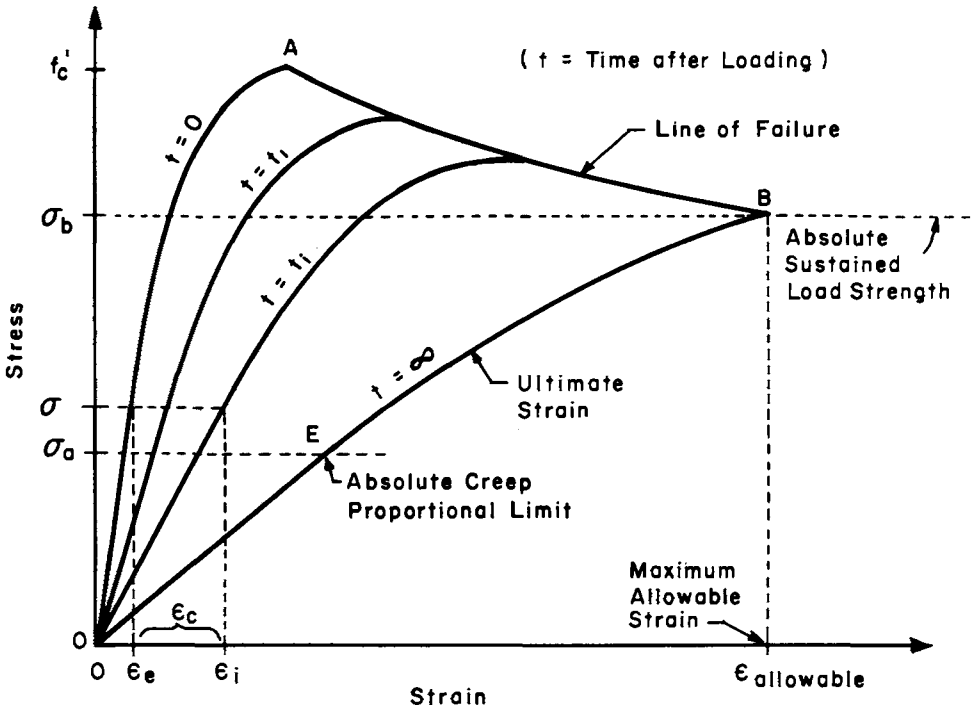

Fig 2. Stress-strain-time relationship for concrete subjected to a sustained uniaxial load (after Rüsch, Ref 29).

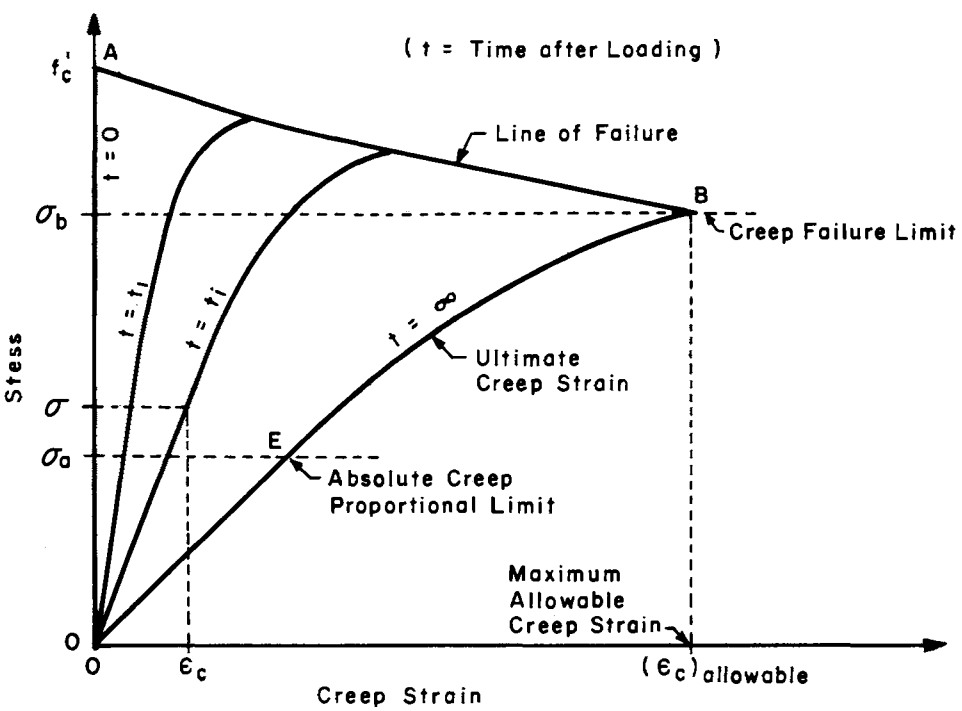

Fig 3. Stress-creep strain-time relationship for concrete subjected to a sustained uniaxial load.

The relationship between the unit creep function and stress is shown in Fig 4, which indicates that the unit creep function is constant at stress levels less than the creep proportional limit and then increases as the stress level increases. Figure 5 illustrates the unit creep function-time relationship. As shown in this figure the unit creep function terminates when the stress level is greater than the sustained load strength σ_b since the concrete will ultimately fail. For stress levels less than the creep proportional limit σ_a the unit creep functions are stress independent, as shown by the $F(t,\tau)$ relationship. This relationship also represents the lower limit for the unit creep function. For stress levels greater than the creep proportional limit but less than the sustained load strength, the unit creep function is between $F(t,\tau)$ and $F(t,\tau,\sigma_b)$, which is the nonfailure region.

In Figs 2 and 3, curve OB represents ultimate creep strain at time equal to infinity and point σ_a represents the absolute creep proportional limit. At a stress level less than σ_a, the relationship between stress and creep strain at time t_i is defined by the appropriate $F(t_i,\tau,\sigma)$ curve. As an example, at $t = 0$ the creep-stress relationship is shown by line OA, which means that at $t = 0$ at any stress level, the creep strain is zero. The creep strain at infinite time is expressed by the OB curve, which is interpreted to mean that as time approaches infinity, the ultimate creep increases with stress. Above the stress level represented by σ_a, the creep-stress relationship becomes nonlinear, and creep strain increases faster than stress.

Curve AB represents the stress and creep failure relationship and point B is the strain failure limit, at which level the creep strain plus elastic strain will reach the maximum concrete strain and failure will occur. If the stress applied is higher than the creep failure limit, the creep rate increases as stress increases, but more rapidly, and the creep body will fail in a shorter time, due to a combination of creep and stress.

These relationships graphically illustrate the unit creep function, and their important characteristics are summarized below:

(1) At the instant of loading, the value of $F(t,\tau,\sigma)$ is zero.

(2) From previous discussion, in Chapter 2, for each $F(t,\tau,\sigma)$ curve there is a creep proportional limit below which the stress-creep strain relationship is linear. This proportional limit varies with time and with age at loading. Thus, there are an infinite number of proportional limits. If, however, only one age of loading is considered there exists a minimum proportional limit, which is defined as the absolute creep proportional limit of the concrete.

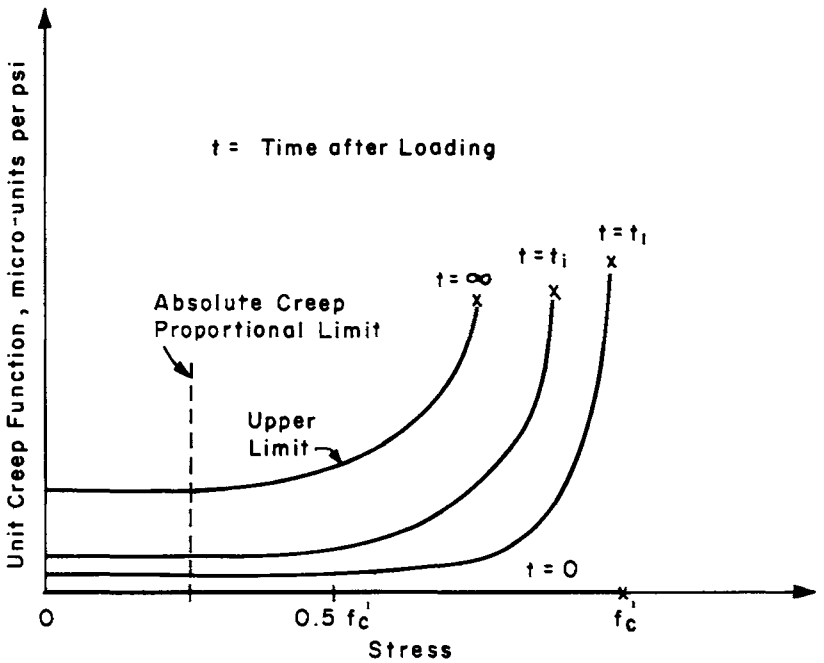

Fig 4. Relationship between the unit creep function and stress for concrete subjected to a sustained uniaxial load.

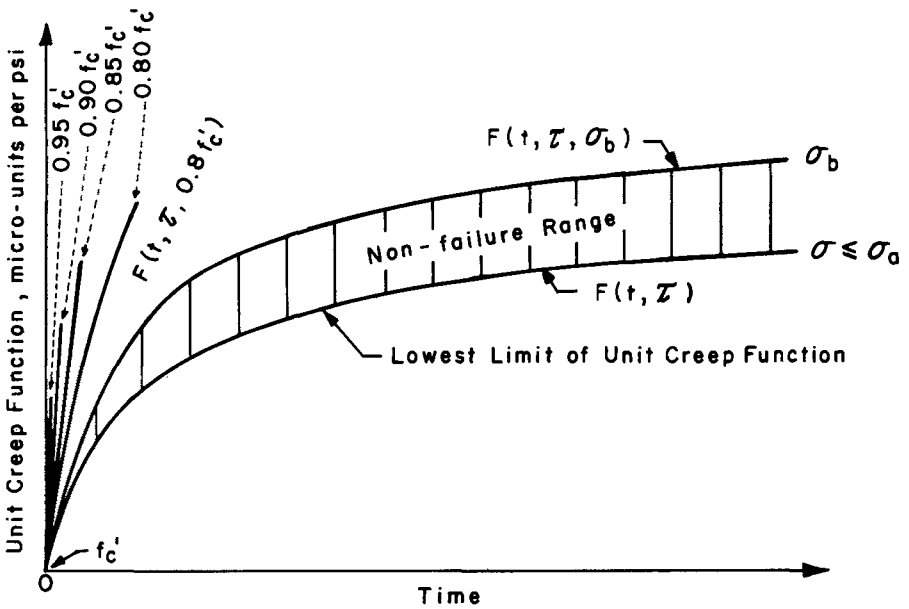

Fig 5. Relationship between the unit creep function and time for concrete subjected to a sustained uniaxial load.

(3) There is also a stress level at which the sum of the elastic strain and the creep strain will equal the maximum allowable strain of concrete, or the maximum strain which will not result in failure. This stress level is a function of time and age of loading. For any given concrete at any given time of loading, there is a maximum stress level, which is defined as the creep failure limit. If the stress level is lower than the creep failure limit, the strain will finally approach a constant value, ultimate creep strain, as time approaches infinity. Conversely, if the stress applied is higher than the creep failure limit, the concrete will ultimately fail.

(4) When the stress level is lower than the sustained load strength, the creep rate becomes zero, and creep strain approaches some ultimate value as time approaches infinity.

At a stress level less than the creep proportional limit, the relationship between creep strain and stress is linear, but the slope varies with time. Since the stress-creep strain relationship is linear at any given time, then, when the stress level is less than the creep proportional limit, the creep per unit stress becomes stress independent and the unit creep function $F(t,\tau,\sigma)$ can be expressed as

$$F(t,\tau) = \frac{\varepsilon_c}{\sigma}$$

where σ is less than the creep proportional limit.

The functional relationship between the unit creep function and both time t and age at loading τ must satisfy the following boundary conditions.

(1) At the time of loading, $t = 0$, unit creep function is zero:

$$\lim_{t \to 0} F(t,\tau) = 0$$

(2) At infinite time, unit creep function approaches a limit:

$$\lim_{t \to \infty} F(t,\tau) = K$$

(3) At infinite time, rate of unit creep function approaches zero:

$$\lim_{t \to \infty} \frac{\partial F(t,\tau)}{\partial t} = 0$$

Several mathematical functions fit these conditions; however, after various trials, the following expression appeared to be the best:

$$F(t,\tau) = K(1 - e^{-\alpha t^{\beta}}) \tag{3.2}$$

where

α and β = constants,

K = a function which is independent of stress level,

t = time after loading.

Since $F(t,\tau)$ is a function of concrete age at loading τ and time after loading t, K must be either a function of τ or constant. The function for K is expressed as $K(\tau)$.

Previous studies (Refs 17, 24, and 32) have shown that ultimate creep strains are much larger when the concrete is loaded at an early age, and Arutyunyan (Ref 4) suggested that ultimate unit creep strain could be expressed as a function of the age at loading. Thus, the unit creep function $F(t,\tau)$ is expressed as

$$F(t,\tau) = K(\tau)(1 - e^{-\alpha t^{\beta}})$$

where $t \geq 0$.

The characteristics of $F(t,\tau)$ are

$$\lim_{t \to 0} F(t,\tau) = K(\tau)(1 - \lim_{t \to 0} e^{-\alpha t^{\beta}}) = 0$$

$$\lim_{t \to \infty} F(t,\tau) = K(\tau)(1 - \lim_{t \to \infty} e^{-\alpha t^{\beta}}) = K(\tau)$$

$$\lim_{t \to \infty} \frac{\partial F(t,\tau)}{\partial t} = \alpha\beta K(\tau) \lim_{t \to \infty} (t^{\beta-1} e^{-\alpha t^{\beta}}) = 0$$

The assumption that the ultimate unit creep strain K is only a function of age at loading is questionable since creep behavior is known to be influenced by many factors, such as temperature, relative humidity, and stress level. Nevertheless, based on the limited investigations in the past (Refs 28 and 29), the assumption seems somewhat reasonable.

Once the $F(t,\tau)$ function is determined, the creep strain of concrete subjected to a sustained uniaxial stress can be predicted as follows:

$$\varepsilon_c = \sigma F(t,\tau) \tag{3.3}$$

If the time after loading is set equal to infinity the ultimate creep strain can be calculated and will be equal to $\sigma K(\tau)$.

In the mathematical theory of elasticity, when an elastic material is subjected to a stress in one direction, there are elastic deformations in the transverse directions. If this concept of a Poisson's effect is extended and applied to creep behavior the creep strain in the y or z-direction is

$$(\varepsilon_c)_y = (\varepsilon_c)_z = -\nu_c(\varepsilon_c)_x \tag{3.4}$$

If ν_c is creep Poisson's ratio and $(\varepsilon_c)_x$ is the creep strain in the loaded direction, which can be calculated from the unit creep function as

$$(\varepsilon_c)_x = \sigma_x F(t,\tau_x) \tag{3.5}$$

then the creep in the transverse direction becomes

$$(\varepsilon_c)_y = (\varepsilon_c)_z = -\nu_c\sigma_x F(t,\tau_x) \tag{3.6}$$

CREEP UNDER MULTIAXIAL STATES OF STRESS

Previous studies have differed with regard to the validity of applying the principle of superposition to creep behavior (Chapter 2); nevertheless, preliminary evaluation of information from the test program associated with this study indicated superposition to be reasonably valid and sufficiently accurate for the material and test conditions examined.

Thus, for a multiaxial state of stress, if the loads are applied at ages τ_x , τ_y , and τ_z in the x , y , and z-directions, respectively, then creep in the x , y , and z-directions can be expressed as

$$(\varepsilon_c)_x = \sigma_x F(t,\tau_x) - \nu_c \sigma_y F(t,\tau_y) - \nu_c \sigma_z F(t,\tau_z) \tag{3.7}$$

$$(\varepsilon_c)_y = \sigma_y F(t,\tau_y) - \nu_c \sigma_z F(t,\tau_z) - \nu_c \sigma_x F(t,\tau_x) \tag{3.8}$$

$$(\varepsilon_c)_z = \sigma_z F(t,\tau_z) - \nu_c \sigma_x F(t,\tau_x) - \nu_c \sigma_y F(t,\tau_y) \tag{3.9}$$

If the loads are applied simultaneously at age τ , creep strains are expressed as

$$(\varepsilon_c)_x = [F(t,\tau)]\,[\sigma_x - \nu_c(\sigma_y + \sigma_z)] \tag{3.10}$$

$$(\varepsilon_c)_y = [F(t,\tau)]\,[\sigma_y - \nu_c(\sigma_x + \sigma_z)] \tag{3.11}$$

$$(\varepsilon_c)_z = [F(t,\tau)]\,[\sigma_z - \nu_c(\sigma_x + \sigma_y)] \tag{3.12}$$

For hydrostatic loading of stress equal to σ , the creep strains are expressed as

$$(\varepsilon_c)_x = (\varepsilon_c)_y = (\varepsilon_c)_z = F(t,\tau)\sigma(1 - 2\nu_c) \tag{3.13}$$

If concrete is subjected to multiaxial stresses but none of the stresses exceed the creep proportional limit, the total strain due to load at any instant t is the sum of elastic strain and creep strain and is expressed as

$$\varepsilon_i = (\varepsilon_e)_i + (\varepsilon_c)_i$$

where

$$i = x\ ,\ y\ ,\ \text{or}\ z\ .$$

If loads in the x , y , and z-directions are applied at τ_x , τ_y , and τ_z , respectively, then the total strain in each direction is expressed as

$$\epsilon_x = \frac{1}{E}[\sigma_x - \nu(\sigma_y + \sigma_z)] + \sigma_x F(t,\tau_x) - \nu_c[\sigma_y F(t,\tau_y) + \sigma_z F(t,\tau_z)] \tag{3.14}$$

$$\epsilon_y = \frac{1}{E}[\sigma_y - \nu(\sigma_z + \sigma_x)] + \sigma_y F(t,\tau_y) - \nu_c[\sigma_z F(t,\tau_z) + \sigma_x F(t,\tau_x)] \tag{3.15}$$

$$\epsilon_z = \frac{1}{E}[\sigma_z - \nu(\sigma_x + \sigma_y)] + \sigma_z F(t,\tau_z) - \nu_c[\sigma_x F(t,\tau_x) + \sigma_y F(t,\tau_y)] \tag{3.16}$$

For the case of $\tau_x = \tau_y = \tau_z = \tau$ the above relationships become

$$\epsilon_x = \frac{1}{E}[\sigma_x - \nu(\sigma_y + \sigma_z)] + F(t,\tau)[\sigma_x - \nu_c(\sigma_y + \sigma_z)] \tag{3.17}$$

$$\epsilon_y = \frac{1}{E}[\sigma_y - \nu(\sigma_z + \sigma_x)] + F(t,\tau)[\sigma_y - \nu_c(\sigma_z + \sigma_x)] \tag{3.18}$$

$$\epsilon_z = \frac{1}{E}[\sigma_z - \nu(\sigma_x + \sigma_y)] + F(t,\tau)[\sigma_z - \nu_c(\sigma_x + \sigma_y)] \tag{3.19}$$

These equations can be reorganized as

$$\epsilon_x = \sigma_x\left[\frac{1}{E} + F(t,\tau)\right] - (\sigma_y + \sigma_z)\left[\frac{\nu}{E} + \nu_c F(t,\tau)\right] \tag{3.20}$$

$$\epsilon_y = \sigma_y\left[\frac{1}{E} + F(t,\tau)\right] - (\sigma_z + \sigma_x)\left[\frac{\nu}{E} + \nu_c F(t,\tau)\right] \tag{3.21}$$

$$\varepsilon_z = \sigma_z \left[\frac{1}{E} + F(t,\tau) \right] - (\sigma_x + \sigma_y) \left[\frac{\nu}{E} + \nu_c F(t,\tau) \right] \quad (3.22)$$

Then the time-dependent flexibility and time-dependent coefficient of lateral strain can be defined as

time-dependent flexibility

$$H(t,\tau) = \frac{1}{E} + F(t,\tau) \quad (3.23)$$

time-dependent coefficient of lateral strain

$$\omega(t,\tau) = \frac{\nu}{E} + \nu_c F(t,\tau) \quad (3.24)$$

The total strains are then expressed as

$$\varepsilon_x = H(t,\tau)\sigma_x - \omega(t,\tau)(\sigma_y + \sigma_z) \quad (3.25)$$

$$\varepsilon_y = H(t,\tau)\sigma_y - \omega(t,\tau)(\sigma_z + \sigma_x) \quad (3.26)$$

$$\varepsilon_z = H(t,\tau)\sigma_z - \omega(t,\tau)(\sigma_x + \sigma_y) \quad (3.27)$$

SUMMARY

The above discussion indicates that total strain as well as creep strain at stress levels less than the creep proportional limit can be estimated by unit creep prediction equations, providing that the modulus of elasticity, the unit creep function, Poisson's ratio, and creep Poisson's ratio can be determined.

Although total strain as well as creep strain data were available from this study, it has been limited to the development and evaluation of prediction methods for creep strain resulting from stresses less than the creep proportional limit. Thus, it is necessary to develop expressions in the form given by Eq 3.2 and to obtain estimates of creep Poisson's ratio. Using this information, predictions of creep strain can be made and compared to actual creep strains measured experimentally.

CHAPTER 4. EXPERIMENTAL PROGRAM

This chapter presents a discussion and description of the factors investigated, the design of the experiment, the techniques used to prepare specimens, the various equipment components, and the test procedures. A more detailed discussion and description are contained in Refs 16 and 33.

The tests consisted of applying compressive loads along the three principal axes of cylindrical concrete specimens (Fig 6) and measuring the axial and radial strains throughout the loading period. The axial and radial loads were varied independently, permitting triaxial, biaxial, and uniaxial states of stress to be achieved. The loads were applied by means of a hydraulic loading system and the resulting strains were measured by two vibrating wire strain gages cast in the concrete along the axes of the axial and radial loads.

For approximately nine months prior to casting the actual test specimens used in this investigation, preliminary experiments were conducted with the actual test equipment and materials, since much of the equipment and materials used in this study were new and had been designed specifically for this project. The purpose of these preliminary tests was to evaluate the equipment and to establish techniques and procedures prior to the beginning of the actual test program. Many of the final techniques resulted from these preliminary experiments as well as from planning conferences conducted during a two-year period prior to beginning the actual testing program.

TEST CONDITIONS

Although numerous factors affect the creep behavior of concrete, this study included only temperature during loading, curing history, and state of stress.

Temperature During Loading

Two temperature levels during loading were selected, representative of the limits of the range of concrete temperature in a nuclear reactor. The low level was set at 75° F, which could be expected at the outer surface of a reactor, and the high level at 150° F, which is representative of the temperature occurring at the inner surface.

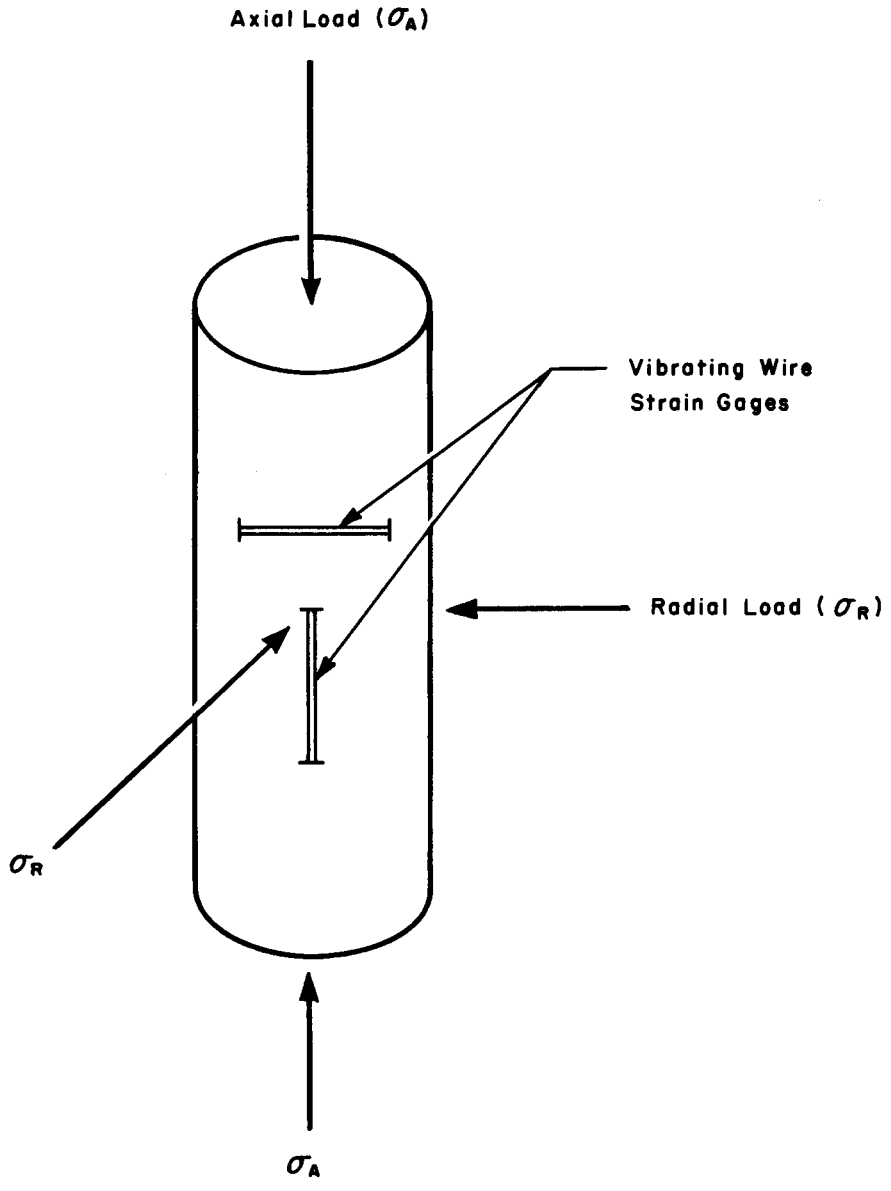

Fig 6. Loading condition and gage placement for creep specimens (Ref 33).

Environmental control provided temperatures which were within $\pm 2^{\circ}$ F of the desired temperature, and they were recorded continuously. Relative humidity of the 75° F environment was maintained at 60 percent $\pm$ 5 percent. The relative humidity of the 150° F environment was not controlled and no measurements were made since all specimens were sealed during the period of time they were subjected to this temperature.

Curing History

In this investigation the most difficult variable to define was curing history, which was investigated at two levels, as-cast and air-dried, representing the expected limits of the range of moisture conditions in a prestressed concrete reactor vessel. The air-dried condition is representative of the curing history at the outer surface of a reactor and the as-cast condition is representative of the moisture content at the inner face of the reactor or that which might be expected in mass concrete.

In this study as-cast and air-dried are terms which refer primarily to the curing history of the specimens prior to loading. As-cast specimens were removed from the molds 24 hours after casting and placed in a curing room for an additional 24 hours. Forty-eight hours after casting the specimens were sealed in copper and then allowed to cure at 75° F for an additional 81 days (a total of 83 days of curing) at which time they were placed in the test temperature environment. Air-dried specimens were also removed from the mold 24 hours after casting and placed in the curing room for an additional 24 hours. However, rather than being sealed 48 hours after casting, the air-dried specimens were submerged in lime-saturated water for the next five days (a total of seven days of curing). At seven days, the specimens were removed from the lime-saturated water and placed in the laboratory at 75° F and 60 percent relative humidity and allowed to air-dry until 83 days after casting, at which time they were sealed in copper and placed in the test temperature environment.

State of Stress

Test specimens were loaded triaxially at five stress levels, ranging from 0 to 3600 psi for both axial stress σ_a and radial confining stress σ_r. Since the combination of stresses involved some zero stress levels, the loading conditions can be classified as uniaxial ($\sigma_r = 0$), biaxial ($\sigma_a = 0$), and triaxial. The five stress levels involved were 0, 600, 1200, 2400, and 3600 psi

nominal pressures. The accuracy of the radial stress was the indicated stress ± 5 percent. Prior to actual testing it was discovered that the actual stress in the axial direction was somewhat less than indicated, due to friction in the hydraulic-mechanical system used to load the specimens axially. Thus each loading unit was calibrated by a load cell prior to loading the creep specimens and it was found that the average initial axial stresses delivered to the specimens in all of the load cells were 0, 545, 1080, 2185, and 3460 psi. Variations of axial stress which occurred with time were monitored with mechanical dial gages attached to the loading frame and were found to be negligible. The loading system is described in more detail in the section on equipment.

TEST SPECIMENS

Description of Specimens

A total of 340 concrete specimens were cast in seven batches, designated A through G, of the same mix design. Three types of specimens were prepared, creep, shrinkage, and strength. These specimens were of two different sizes. All creep and shrinkage specimens were cast in steel molds 16 inches long by 6 inches in diameter that were designed specifically for this project (Fig 7). The strength specimens were cast in standard 6 × 12-inch molds.

The 6 × 16-inch specimens were cast against 3-inch-high end slugs through which the axial load was applied. The 6 × 16-inch molds were open on one side, as shown in Fig 7, because of the end slugs and to facilitate placing the strain gages. All creep and shrinkage specimens, therefore, were cast horizontally while the strength specimens were cast vertically.

The creep specimens were the primary test specimens in the design and were used to measure the total strains experienced by the concrete under the various combinations of the three test variables. The experimental design contained 50 such specimens.

For each environmental test condition and for each batch of concrete there was a shrinkage specimen that remained unloaded in the same test environment as its companion loaded specimen. Twenty-eight shrinkage specimens for estimating shrinkage strains were cast in order that the total time-dependent strains due to load could be estimated and in order to provide an estimate of batch-to-batch variations.

In addition, 262 strength specimens were cast, distributed among the seven batches and consisting of both as-cast and air-dried specimens as well as

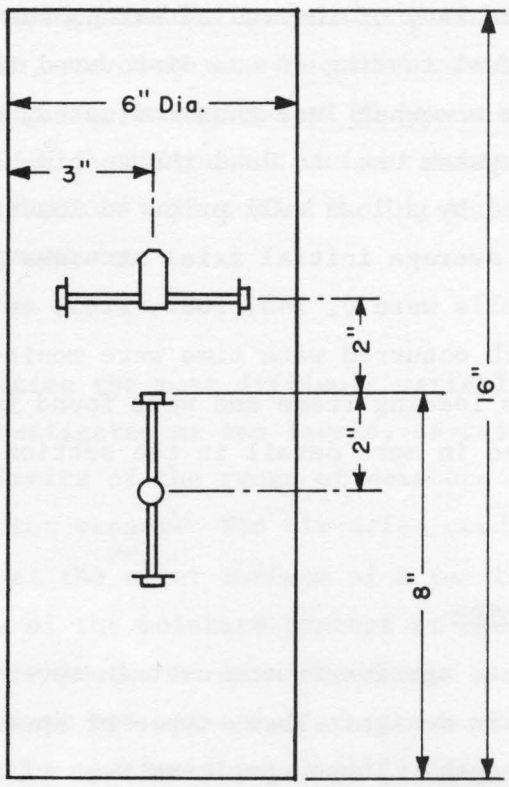

Fig 7. Mold assembly for creep and shrinkage specimens (Ref 33).

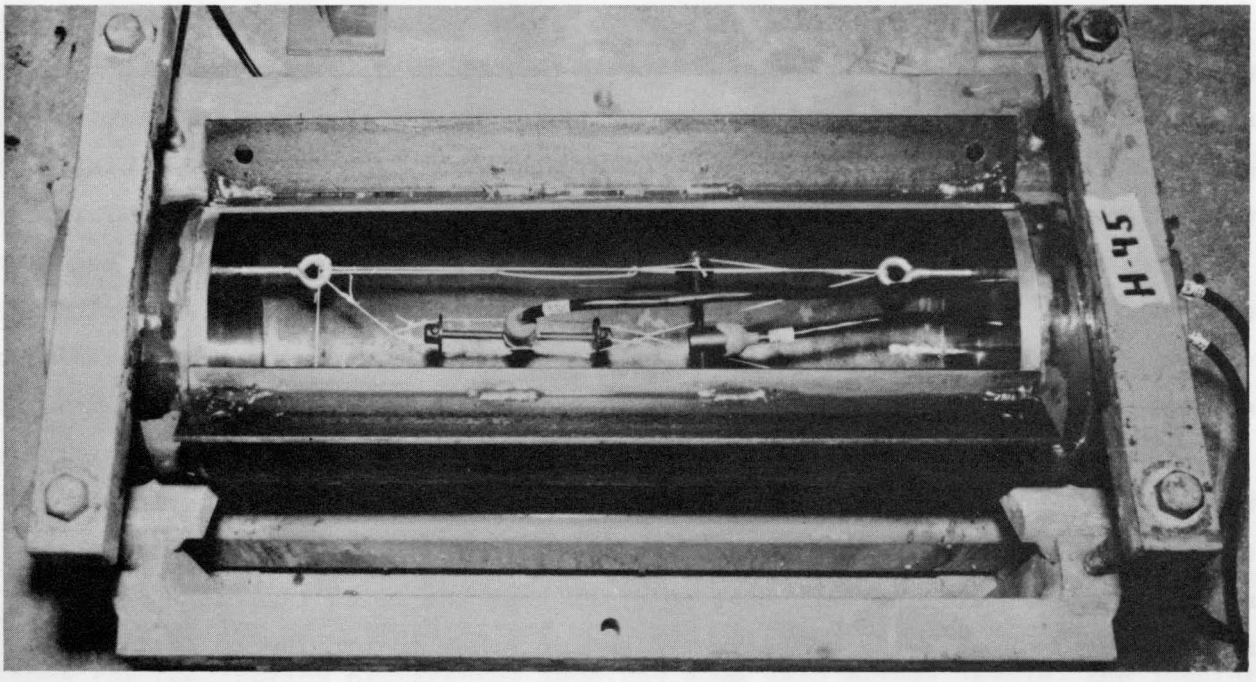

Fig 8. Location of strain gages in creep and shrinkage specimens (Ref 33).

standard cured specimens. The as-cast and air-dried specimens were subjected to the same environment conditions as the creep and shrinkage specimens. These strength specimens were prepared to evaluate the compressive and tensile strengths of the concrete for the various conditions at various times throughout the test period. In addition, they provided a means of measuring batch-to-batch variations of strength. The standard strength specimens, which were cured by submerging in lime-saturated water, were cast to compare the as-cast and air-dried concretes with concrete cured in accordance with ASTM Specification C-192 and to establish the strength according to an established procedure.

Casting and Compaction

The test specimens for the various test conditions were prepared as described in Refs 16 and 33. A brief summary of the casting and compaction operations follows:

(1) The various molds were assembled in numerical order for casting, and the strain gages were positioned (Fig 8) in the 6 × 16-inch molds by use of a wooden template and held in place with steel wire and nylon string. The 6 × 12-inch specimens were cast in standard molds, except that those for the as-cast specimens contained 0.008-inch-thick copper inserts which were used for sealing the as-cast specimens.

(2) After mixing, the concrete was placed in the molds. The 6 × 12-inch specimens were cast and compacted as prescribed by ASTM specification C-192 and then vibrated 3 seconds at a frequency of 3600 cycles per minute. The 6 × 16-inch specimens, which were cast horizontally, were compacted by approximately 200 strokes of a one-quarter-inch-diameter rod. A specially constructed curved trowel was used to finish the exposed longitudinal surface of the 6 × 16-inch specimens. The specimens were then vibrated 5 seconds on a vibrating table at a frequency of 3600 cycles per minute. The entire casting and compaction operation to this point took approximately 45 minutes.

(3) Four hours after the specimens were cast the 6 × 12-inch specimens were capped with neat cement and a glass plate was pressed and worked on the cement to form a smooth plane. The exposed side of the 6 × 16-inch specimens also received a final finishing with neat cement applied with the curved trowel.

Curing and Sealing

Immediately after casting, all specimens were completely covered with wet burlap and left in the laboratory for 24 hours. The molds were then removed

and the specimens placed in a curing room. The surfaces of the 6 × 16-inch specimens were scrubbed with a wire brush and pumice stone to remove any surface irregularities, and all surface voids were filled with a neat cement paste.

After 24 hours of curing, the curing procedures were different, depending on the type of test specimens involved. The remaining curing procedures are summarized in Table 1.

The sealing method which was used included the application of two coats of epoxy to the surface of the specimens. These coats were applied 24 hours apart and while the second coat was still wet, a 0.008-inch-thick copper jacket was wrapped around the specimen. The copper jacket was then soldered to the steel end slugs and to itself along the longitudinal seam. Just prior to assembling the specimens in the test units, the specimens were placed in a 6-inch-diameter 0.12-inch-thick neoprene sleeve which was slipped over the copper jacket as added protection against hydraulic oil. The ends of the neoprene jacket were then sealed with a liquid neoprene glue and clamped with a 1/4-inch stainless steel clamp.

CONCRETE MIX DESIGN

The concrete mix design and all materials employed in this investigation, except water, were furnished by the Waterways Experiment Station, Vicksburg, Mississippi. Prior to being shipped, the materials were proportioned in thirteen 12-cubic-foot-batch quantities and placed in sealed containers.

The materials consisted of Type II cement and crushed fine and coarse limestone aggregates with a 3/4-inch maximum size. The concrete mix was designed for a 28-day compressive strength of 6000 $\pm$ 600 psi for a standard cured specimen. Mix proportions and a summary of the results of engineering tests on the materials are contained in Refs 16 and 33. A brief summary of the concrete design characteristics is shown in Table 2.

LOADING EQUIPMENT

A general discussion and description of the equipment and instrumentation used in this investigation are presented in this section together with the loading, environmental control, instrumentation, and recording systems employed.

TABLE 1. CURING HISTORY OF SPECIMENS BEYOND 24-HOUR CONCRETE AGE (REF 33)

Specimen Type	Age	Curing/Sealing Operation
6 × 16-inch As-Cast	24 hours	First coat of epoxy applied
		Specimens placed in concrete laboratory fog room
	48 hours	Second coat of epoxy applied
		Specimens sealed in copper
		Specimens placed in test laboratory and cured at 73.4 ± 3° F
	83 days	Specimens sealed in neoprene jacket
		Specimens assembled and placed in loading rig which was at the environmental test temperature of 75° F or 150° F
	90 days	Creep specimens loaded for 12 months
		Shrinkage specimens remain unloaded in test environment
6 × 16-inch Air-Dried	24 hours	Specimens placed in concrete laboratory fog room
	48 hours	Specimens submerged and cured in lime-saturated water at 73.4 ± 3° F
	7 days	Specimens removed from lime water and placed in test laboratory at 73.4 ± 3° F and 60% relative humidity
	81 days	First coat of epoxy applied
	82 days	Second coat of epoxy applied; specimens sealed in copper
	83 days	Same as 6 × 16-inch as-cast
	90 days	Same as 6 × 16-inch as-cast

(Continued)

TABLE 1. (CONTINUED)

Specimen Type	Age	Curing/Sealing Operation
6 × 12-inch As-Cast	24 hours	Specimens placed in concrete laboratory fog room
	48 hours	Specimens sealed in copper
		Specimens placed in test laboratory and cured at 73.4 ± 3° F
	83 days	Specimens to be tested at 183 days or beyond placed in the applicable temperature test environment (75° F or 150° F)
	28, 90, 183, 365 days	Compressive and tensile strengths determined; 24 hours prior to strength test, copper seal removed and specimen placed in 73.4 ± 3° F environment
6 × 12-inch Air-Dried	24 hours	Specimens placed in concrete laboratory fog room
	48 hours	Specimens submerged and cured in lime-saturated water at 73.4 ± 3° F
	7 days	Specimens removed from lime water and placed in test laboratory at 73.4 ± 3° F and 60% relative humidity
	83 days	Specimens to be tested at 183 days or beyond sealed in copper and placed in applicable test temperature (75° F or 150° F)
	28, 90, 183, 365 days	Same as 6 × 12-inch as-cast
6 × 12-inch Standard	24 hours	Specimens placed in concrete laboratory fog room
	48 hours	Same as 6 × 12-inch air-dried
	28, 90 days	Specimens removed from lime-saturated water, compressive strength determined

TABLE 2. MIX DESIGN SUMMARY

Water-cement ratio, by weight	0.425
Cement content, sacks/cu yd	7.25
Maximum size of coarse aggregate, inches	3/4
Slump, inches	2

Material	Size Range	Mix Proportion, Percent By Volume	By Weight
Cement		15.5	17.8
Fine aggregate	Sand	37.1	35.9
Coarse aggregate (A)	No. 4	14.2	13.9
Coarse aggregate (B)	3/8 inch	16.6	16.2
Coarse aggregate (C)	1/2 inch	16.6	16.2

Loading Unit

The loading frame was designed specifically for this project; a schematic of the loading unit for the triaxially loaded case (Fig 9) illustrates all components of the loading systems. The radial load was applied directly to the sealed specimens by means of hydraulic pressure through oil, contained by a one-inch-thick steel pressure jacket, and the axial load was applied by a hydraulic ram. Thus, the triaxial loading system was made up of both an axial and a radial pressure system that could be varied independently. The same type loading frame without the pressure jackets was used for the uniaxial case. For the biaxial case, the pressure jacket system was used without the loading frames.

As noted in Fig 9, each loading frame contained two specimens from the same batch, an as-cast and an air-dried specimen, which were subjected simultaneously to the same temperature and loading conditions. Likewise, the biaxially loaded specimens were simultaneously loaded in pairs under identical test conditions.

To evaluate the shrinkage strains in the loaded specimens, unloaded shrinkage specimens were placed in the same test environment as the loaded specimens.

The loading system developed for this investigation was generally satisfactory. Nevertheless, two problems were detected. First, during preliminary testing conducted to evaluate the equipment and to familiarize project personnel with the techniques and procedures which were to be used in the investigation, it was found that the axial pressures transmitted to the specimens were significantly less than the pressure input into the system. This pressure loss was due to the friction between the piston o-rings and the hydraulic cylinder. Machine tolerances between the moving parts were very close in order to prevent oil leakage at the high pressures involved. Consequently, slight misalignment caused friction which, along with normal friction, reduced the pressures actually applied to the specimens to 3 to 10 percent below the desired pressure. The second problem involved the radial pressure system. Extreme care was required during sealing of the creep specimens; when a weak point developed in the seal, the hydraulic oil under high radial pressures broke through the sealing jackets and penetrated the specimen, which resulted in either a structural failure in the specimen or contamination of the specimen, rendering it useless for further investigation. The weakest

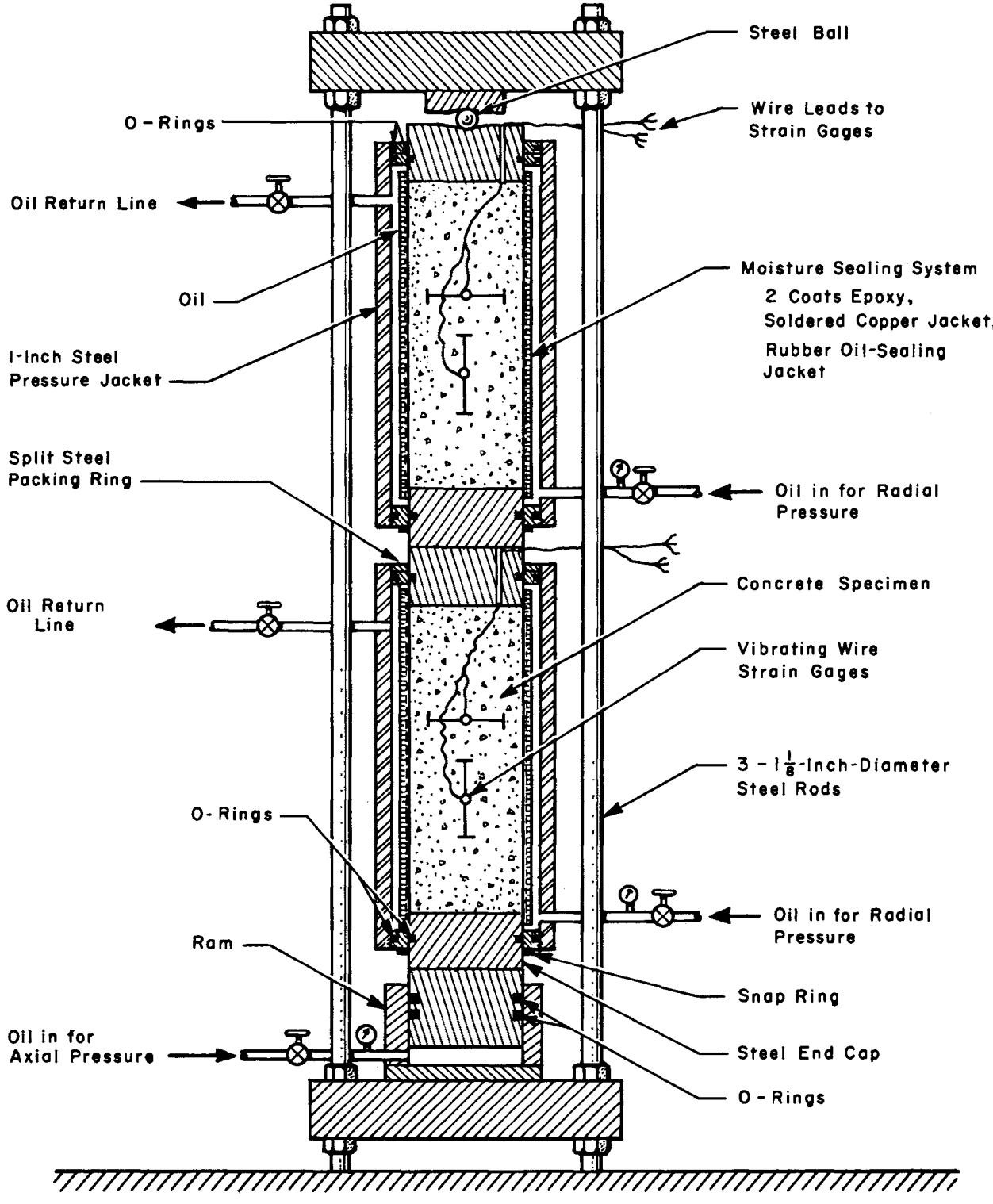

Fig 9. Schematic of triaxial test unit (Ref 16).

point was usually at the interface between the end slug and the concrete. Extreme care in sealing and the construction of an expansion bellows in the copper jacket at this interface apparently solved the problem.

Hydraulic System

Hydraulic pressure was supplied to the loading units by using the 100 psi air pressure available in the laboratory to drive oil pressure intensifiers. This type of system was adequate for creep testing since only a very small quantity of oil was necessary once the system was pressurized. A schematic of the hydraulic system is shown in Fig 10.

The hydraulic system consisted of a pressure control console and eight pressure lines to the loading units, plus return lines. The pressure control console housed the pressure control valves, pressure intensifiers, air reservoir, auxillary air compressor, and pressure gages, for the four different header pressures.

The pressure system was designed for 5000 psi pressure and consisted of hydraulic pressure pipes with flexible pressure hoses to the test units. A dual manifold system was employed for each of the four pressures, 600, 1200, 2400, and 3600 psi. One manifold system supplied pressure to the 75° F laboratory and the other to the 150° F control room. Each manifold system contained a return line which was connected to each test unit and allowed oil to circulate to the oil reservoir in the console. The primary purpose for this arrangement was to provide a way to remove air from the hydraulic system and to circulate oil to keep the valves from sticking.

The hydraulic system was designed with two back-up subsystems. An auxiliary pressure intensifier was installed which could be used to replace any of the four intensifiers that required maintenance. Also included was an auxiliary air compressor which would turn on automatically if the laboratory air pressure dropped significantly. The control system automatically regulated the pressure to within $\pm$ 5 percent of the assigned gage pressure.

Environmental Control System

To make effective creep comparisons, it was necessary to maintain a constant environment over a long period of time. Temperature and humidity conditions were effectively controlled by the systems used on the project.

The tests performed under the nominal 75° F test condition were conducted in an environmental control laboratory, and the tests performed under the

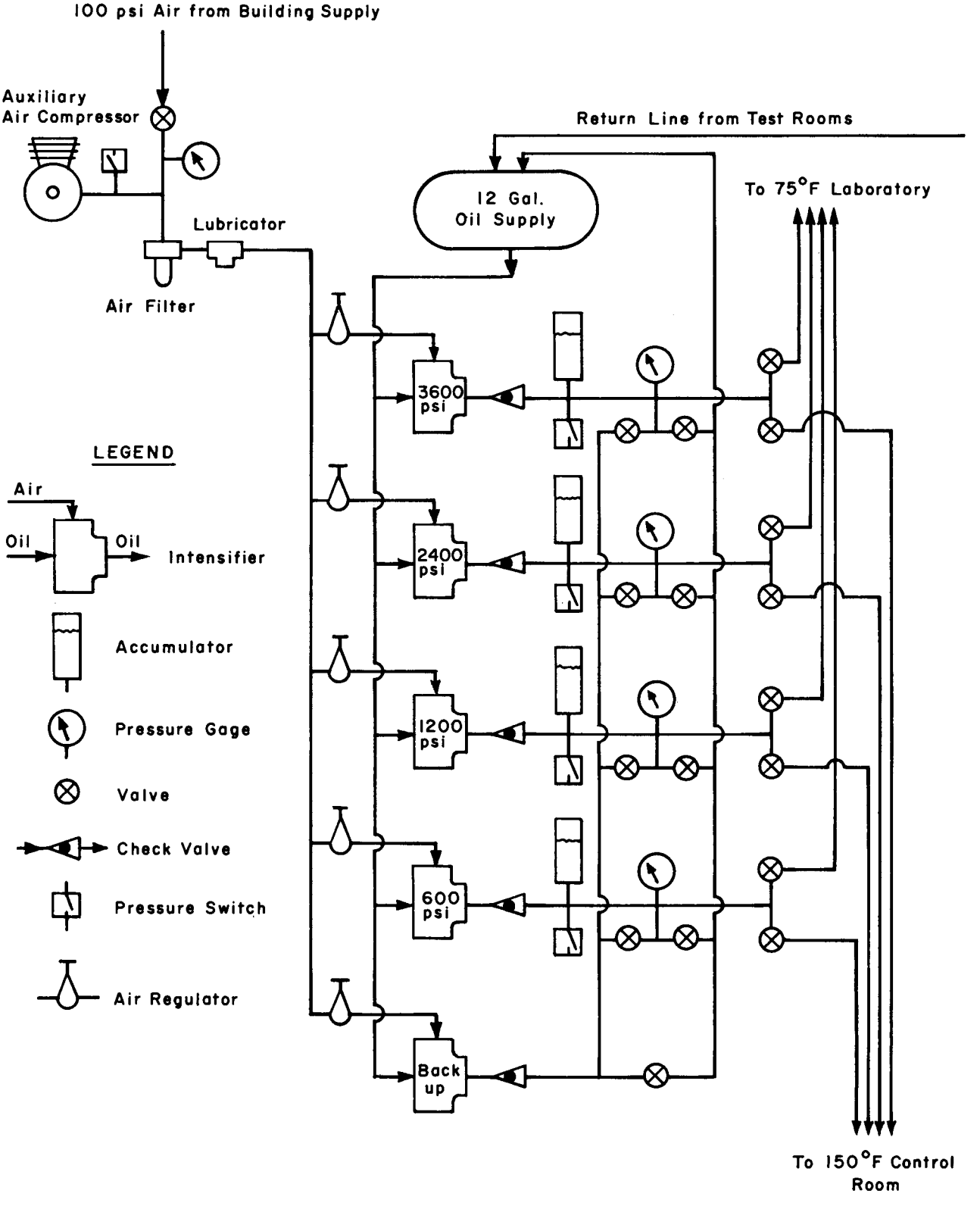

Fig 10. Flow diagram of hydraulic system (Ref 33).

nominal 150° F test condition were conducted in a special temperature control room designed to maintain a constant temperature in the range of -20 to 150° F. Records maintained throughout the investigation indicated excellent control.

Instrumentation

Vibrating Wire Strain Gage. Vibrating wire strain gages (Perivale PC 641) were selected for this investigation. They are sonic devices that operate on the principle that the frequency of a wire changes as the strain in the wire changes. The gage measured the frequency of a vibrating wire, and when its frequency changed, the change in strain was calculated using Mersonnes' and Hooke's Laws.

The change in strain $\Delta\epsilon$ was determined by the following relationships:

$$\Delta\epsilon = \epsilon_i - \epsilon_f = K(F_i^2 - F_f^2) \qquad (4.2)$$

where

ϵ_i = the initial (or reference) strain,

ϵ_f = the strain point desired,

F_i = the initial (or reference) frequency,

F_f = the frequency at the strain point desired, and

K = the gage factor.

This gage, which was primarily designed for measuring strains in concrete, when cast in concrete had a gage factor of 1.24×10^{-3}, a figure determined experimentally by the manufacturer. This particular gage had a range of ±1000 micro-units of strain and could be read to less than 1 micro-unit. A cross section of the Perivale gage is shown in Fig 11. The gage was approximately 4 inches long with a 3-1/2-inch gage length and consisted primarily of a hollow brass tube with a steel wire tensioned between the steel caps. The frequency of the wire was measured by an electronic comparator (Fig 12) which caused an electromagnet inside the gage to pluck the wire. The same magnetic coil was used to detect the vibration of the wire and the frequency was compared with a standard frequency generated in the comparator. From this comparison, the frequency of the gage wire could be determined and used to calculate change in strain (Eq 4.1). In this project, a mid-range frequency was selected for

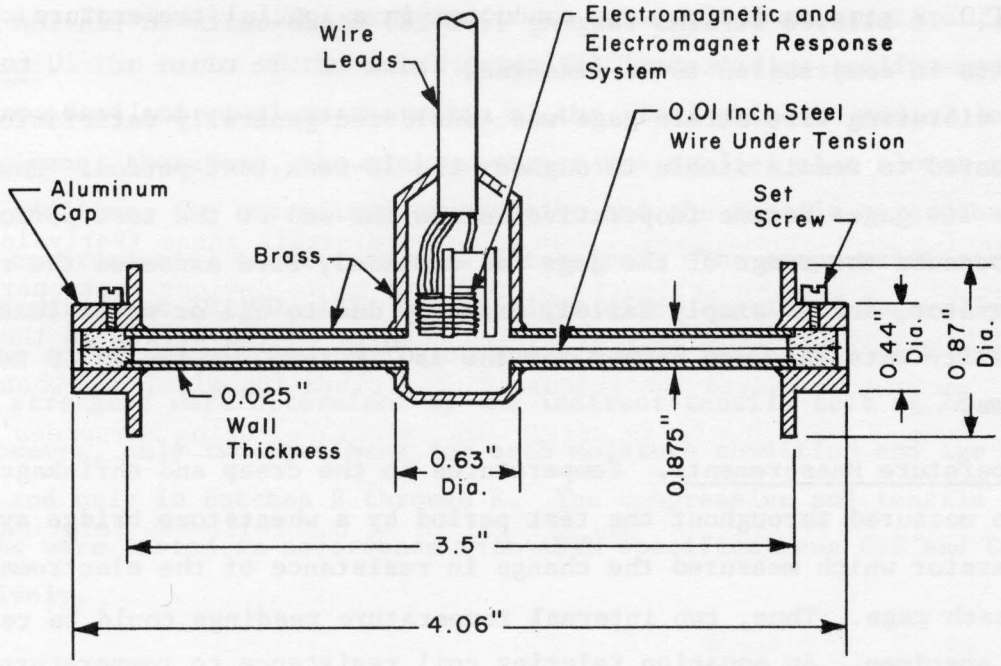

Fig 11. Cross section of a Perivale vibrating wire strain gage (Ref 33).

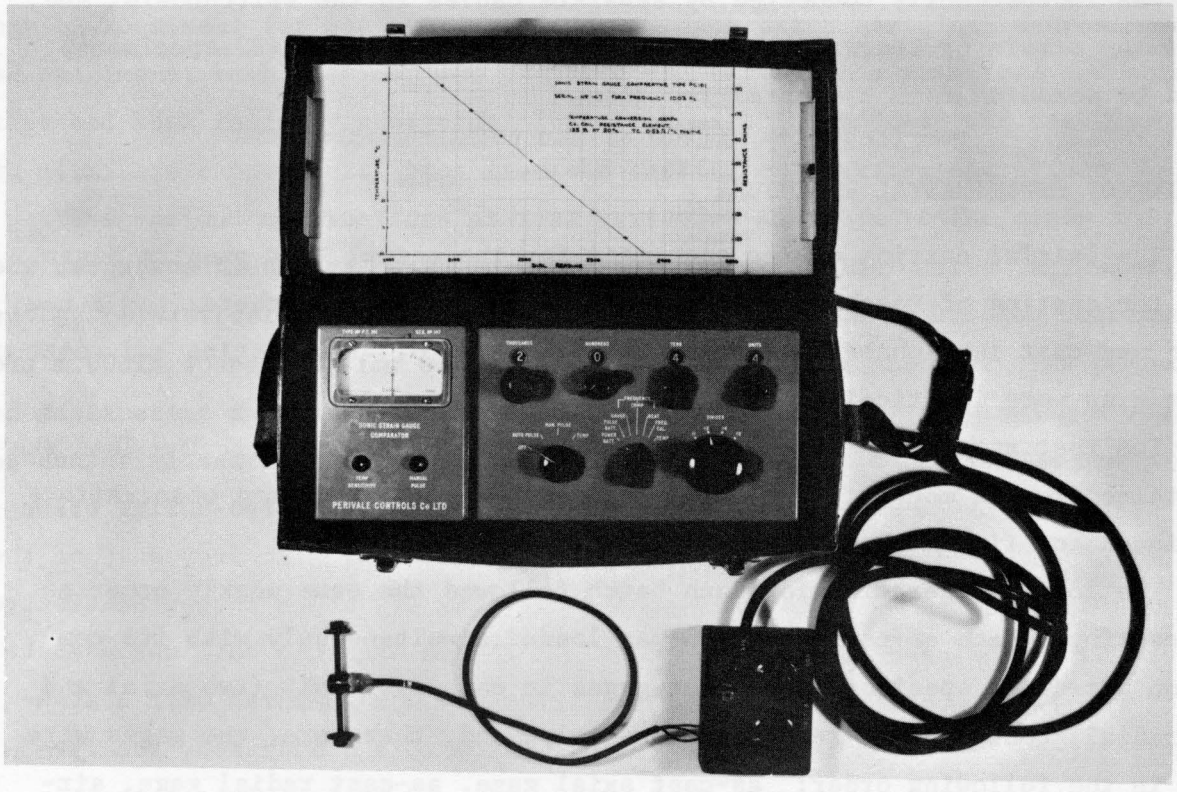

Fig 12. Electronic comparator for frequency and temperature measurement.

all gages. It allowed strains ranging from 285 micro-units in tension to 1050 micro-units in compression to be measured.

The vibrating wire strain gage was considered generally satisfactory. The gage appeared to remain stable throughout the 18-week test period. However, 35 of the 164 gages became inoperative before the end of the test period: 11 stopped because the range of the gage was exceeded, five exceeded the range of the comparator, and 19 simply failed, probably due to oil or water leakage. The mortality rate was much higher for the 150° F than for the 75° F test conditions.

Temperature Measurements. Temperatures in the creep and shrinkage specimens were measured throughout the test period by a wheatstone bridge system in the comparator which measured the change in resistance of the electromagnetic coil in each gage. Thus, two internal temperature readings could be recorded for each specimen. An equation relating coil resistance to temperature was provided by the manufacturer.

Switchboard System. For recording strain and temperature data, the comparator was connected to a switchboard that had a capacity of 180 gages. Each gage was independently connected by separate cables to the switchboard, and, thus, the strain or temperature in any one of the 164 gages (82 specimens) could be measured from a central location.

OUTLINE OF EXPERIMENTAL PROCEDURE

The initial casting of the specimens for the actual test program began with the casting of Batch A on October 29, 1968. Each week thereafter a new batch was cast in alphabetical order through Batch G. The casting and testing procedures were identical for all batches.

The test specimens were cured for 90 days and then loaded. The load was maintained for 12 months; then the specimens were unloaded, and observations continued for five more months.

The loading operation for each batch followed the same weekly order as the casting. Each as-cast specimen was loaded simultaneously with its companion air-dried specimen. The four gages in each test unit (two axial and two radial) could not be read simultaneously, and, therefore, the gages were read in the following order: as-cast axial gage, as-cast radial gage, air-dried axial gage, and air-dried radial gage. Both axial and radial loads were

applied simultaneously. The maximum stress was applied at a rate of 35 psi per second. The ratio of the axial to radial loads during loading was maintained constant and equal to the ratio of the final axial to radial loads on the specimens; therefore, the minimum stress was applied at a slower rate.

In addition, the unconfined compressive and the tensile strengths for the various environmental conditions were determined. The compressive strengths were determined at 28, 90, 183, and 365 days after casting. Generally, three specimens for each moisture condition and age were tested for each batch. The tensile strengths were determined by the indirect tensile test at 28 and 90 days; however, only two specimens for each moisture condition and age were tested, and only in Batches B through F. The compressive and tensile strength specimens were tested in accordance with ASTM specifications C39 and C496, respectively.

EXPERIMENTAL DESIGN

The various test conditions investigated in this experiment were randomly assigned to each batch. This randomization was restricted only by the condition that each batch contain specimens at both test temperatures and an equal number of specimens for each curing history. Each batch contained approximately 48 specimens; each specimen was prepared and tested in a numerical sequence that had been randomly assigned. This randomization process was used in order to eliminate experimental bias from the casting and testing operations.

The various combinations of test variables assigned to the creep and shrinkage specimens are shown in the experimental design charts in Tables 3 and 4, respectively. It should be noted (Table 3) that each batch contained one shrinkage specimen for each temperature and curing history. The purpose of duplicating the shrinkage specimens for each batch was to provide a means of measuring batch-to-batch variation and a basis for comparison of creep results if the variations were significant.

TABLE 3. EXPERIMENTAL DESIGN FOR CREEP SPECIMENS (REF 33)

Temperature, °F	Nominal Axial Load, psi	Radial Load, psi	Curing History* As-Cast	Air-Dried
75	0	600	F-13	F-42
75	0	3600	A-9f	A-12f
75	600	0	E-39	E-40
75	600	600	E-5	E-13
75	600	3600	G-35	G-30
75	1200	1200	C-16x	C-17
75	1200	2400	B-41	B-42
75	2400	0	B-7	B-19
75	2400	600	C-23	C-11
75	2400	2400	F-9	F-30
75	3600	1200	D-26	D-44
75	3600	3600	D-31	D-40
150	0	600	A-35	A-19f
150	0	1200	D-46f	D-3
150	0	2400	E-43	E-1
150	0	3600	C-34f	C-13f
150	600	0	B-4	B-1
150	1200	0	D-15	D-22
150	1200	1200	C-12	C-46x
150	1200	2400	D-2x	D-41
150	2400	0	F-33	F-34
150	2400	600	E-18	E-4
150	2400	2400	G-9	G-19
150	3600	0	B-16	B-5
150	3600	3600	F-20	F-6

* - The letter indicates the batch and the numeral the specimen number within the batch.
x - Radial pressure zero ($\sigma_r = 0$) due to oil leak in specimen.
f - Specimen failed shortly after loading.

TABLE 4. EXPERIMENTAL DESIGN FOR SHRINKAGE SPECIMENS (REF 33)

Temperature, °F	Load, psi	Curing History*	
		As-Cast	Air-Dried
75	0	A-8	A-38
75	0	B-29	B-23
75	0	C-39	C-6
75	0	D-20	D-33
75	0	E-28	E-23
75	0	F-23	F-17
75	0	G-18	G-10
150	0	A-22	A-32
150	0	B-13	B-26
150	0	C-41	C-36
150	0	D-12	D-23
150	0	E-10	E-42
150	0	F-15	F-21
150	0	G-1	G-21

* - The letter indicates the batch and the numeral the specimen number within the batch.

CHAPTER 5. EXPERIMENTAL RESULTS

A large number of tests and measurements of various kinds were made during this investigation. This chapter contains a summary of the results of these tests. A portion of this information is used in Chapter 6 to (1) develop the unit creep function and to predict creep strains for specimens subjected to multiaxial states of stress and (2) to evaluate the accuracy of these predicted creep strain values. Trends and effects observed in the data are noted; however, no attempt is made to explain their cause since this is not the intent of this report.

STRENGTH OF CONCRETE

The compressive strengths of all specimens were determined in accordance with ASTM C39-66 testing procedures, and the tensile strengths were obtained in accordance with ASTM C496-69.

The 28, 90, and 183-day strengths for the seven batches of concrete are shown in Table 5. These strength values usually represent the average of at least three tests although in some cases only two specimens were tested.

The average strength of standard cured specimens at 28 days was 6460 psi, which was higher than the design strength, 6000 psi. Of the 29 specimens tested at 28 days, only two, which had defective caps, showed strength values less than the design strength. The standard deviation was 208 psi. The average strength of standard cured specimens at 90 days was 8300 psi with a standard deviation of 309 psi.

The strengths of the as-cast and air-dried specimens were of primary interest. After two days of moist curing, the air-dried specimens were submerged in lime-saturated water for five days and then air-dried at 75^{o} F for the remainder of the 90-day curing period. This sequence of curing caused the air-dried specimens to have a higher average strength than the as-cast specimens during the first three-month period. The as-cast specimens were sealed two days after casting. This sealing reduced the degree and rate of hydration compared with efficient wet curing; consequently, the strength of as-cast specimens was the lowest among the three types of curing during the

TABLE 5. STRENGTH OF CONCRETE CYLINDERS*

Age in Days / Curing History / Batch	28			90			183			
							As-Cast		Air-Dried	
	Standard	As-Cast	Air-Dried	Standard	As-Cast	Air-Dried	75° F	150° F**	75° F	150° F**
A	6760	6580	7060	8550	6880	6960	8260	8120	7030	7760
B	6650 (630)	4710 --	6200 --	8690 (540)	6110 (550)	7790 (540)	--	--	--	--
C	6140 (580)	5700 --	6520 --	8290*** (680)	6430*** (610)	7370*** (580)	--	--	--	--
D	6200 (620)	5980 (520)	6650 (530)	8540 (510)	6500 (530)	7790 (550)	--	--	--	--
E	6520 (570)	5410 --	6540 --	8200 (710)	7290 (590)	7430 (550)	--	--	--	--
F	6510 (550)	5650 --	6680 --	8090 (690)	7410 (590)	7870 (580)	--	--	--	--
G	6440	5940	6570	7730	6460	7460	7620	8280	7310	7100
Average	6460 (590)	5710 (520)	6600 (530)	8300**** (630)	6780**** (570)	7550**** (560)	7940	8200	7170	7430

*In psi. Strength is the average of at least three specimens.

**Specimens placed in 150° F temperature environment after 83 days.

***Tested after 83 days.

****Average of batches A, B, D, E, F, and G.

Numbers in parenthesis are tensile strengths.

first three-month period. However, continuous curing at a high moisture content caused a greater rate of strength increase than dry curing so that the average strength of the as-cast specimens was higher than that of the air-dried specimens after six months of curing.

At the time of loading, the average strengths of the as-cast and air-dried specimens were 6780 psi and 7550 psi, respectively. At 183 days the as-cast concrete cylinders which were cured at 75° F temperature for the entire 183 days exhibited an average strength of 7940 psi and the average strength of specimens cured at 75° F temperature for the first 83 days and 150° F temperature for the remainder of the curing period was 8200 psi. The as-cast specimens showed a continuous gain in strength with time, but the air-dried specimens indicated a slight decrease in strength at 183 days.

INSTANTANEOUS STRAINS AND ELASTIC PROPERTIES

The instantaneous or elastic strain due to the applied load was determined by taking reading just prior to loading and another after the maximum load had been applied. Because four gages required reading, there was a delay in obtaining all of the readings, and, since the creep rate was quite rapid immediately after load application, an attempt was made to estimate the initial strain by extrapolating the strain time relationship to obtain the strain at time zero.

The Lagrangian extrapolation method (Ref 15) was used to calculate the instantaneous strains. In general, it was found that the estimated strain was from approximately 1 to 5 micro-units less than the measured value.

The elastic properties of concrete, modulus of elasticity and Poisson's ratio, were calculated from theory of elasticity. Calculated values for modulus of elasticity and Poisson's ratio are shown in Tables 6 through 9. The modulus of elasticity and Poisson's ratio of uniaxially and biaxially loaded specimens were very consistent, while values for the triaxially loaded specimens were inconsistent. This inconsistency is probably due to the fact that the relationships used to calculate the values are very sensitive when the loading conditions approach a hydrostatic state of stress. In addition, the radial and axial loads were applied at different rates, which may have caused additional errors. For this reason specimens subjected to a stress condition approaching a hydrostatic state of stress were eliminated.

Excluding hydrostatically loaded specimens, the average moduli of elasticity for the as-cast and air-dried specimens loaded at 75° F were

TABLE 6. INSTANTANEOUS STRAINS AND ELASTIC PROPERTIES OF AS-CAST SPECIMENS AT 75° F

Specimen Number	Axis	Stress and Instantaneous Strains		Elastic Properties	
		Stress, psi	Strain, micro-units	$E \times 10^6$ psi	
E-39	Axial	527	87.3	6.04	0.293
	Radial	0	-25.6		
B-7	Axial	2179	384.7	5.66	0.243
	Radial	0	-93.5		
F-13	Axial	0	-51.7	6.13	0.264
	Radial	600	72.1		
A-9*	Axial	0	-333.4	4.51	0.209
	Radial	3600	630.8		
E-5	Axial	562	37.7	2.78	0.381
	Radial	600	57.7		
C-23	Axial	2139	282.5	6.54	0.244
	Radial	600	-10.4		
C-16	Axial	1100	57.9	2.04	0.409
	Radial	1200	127.5		
D-26	Axial	3449	472.6	5.91	0.273
	Radial	1200	-11.6		
B-41	Axial	1092	- 7.9	7.14	0.239
	Radial	2400	219.2		
F-9	Axial	2147	177.6	12.55	-0.017
	Radial	2400	197.4		
G-35	Axial	536	-254.6	4.91	0.248
	Radial	3600	524.4		
D-31	Axial	3472	286.4	3.11	0.358
	Radial	3600	342.2		

* Original specimen failed and was replaced.

TABLE 7. INSTANTANEOUS STRAINS AND ELASTIC PROPERTIES OF AIR-DRIED SPECIMENS AT 75° F

Specimen Number	Axis	Stress and Instantaneous Strains		Elastic Properties	
		Stress, psi	Strain, micro-units	$E \times 10^6$ psi	ν
E-40	Axial	527	93.4	5.64	0.279
	Radial	0	-26.1		
B-19	Axial	2179	378.6	5.76	0.274
	Radial	0	-103.6		
F-42	Axial	0	-51.8	5.98	0.258
	Radial	600	74.4		
A-12*	Axial	0	-340.1	4.85	0.229
	Radial	3600	571.7		
E-13	Axial	562	32.1	2.84	0.392
	Radial	600	50.7		
C-11	Axial	2139	331.5	5.51	0.261
	Radial	600	-21.0		
C-17	Axial	1101	74.6	4.92	0.306
	Radial	1200	100.9		
D-44	Axial	3449	532.7	5.23	0.276
	Radial	1200	-15.7		
B-42	Axial	1092	- 4.3	6.05	0.233
	Radial	2400	262.2		
F-30	Axial	2147	170.7	6.30	0.223
	Radial	2400	219.8		
G-30	Axial	536	-239.7	4.99	0.241
	Radial	3600	522.0		
D-40	Axial	3472	298.4	2.97	0.359
	Radial	3600	357.0		

* Original specimen failed and was replaced.

TABLE 8. INSTANTANEOUS STRAINS AND ELASTIC PROPERTIES OF AS-CAST SPECIMENS AT 150° F

Specimen Number	Axis	Stress and Instantaneous Strains		Elastic Properties	
		Stress, psi	Strain, micro-units	$E \times 10^6$ psi	ν
B-4	Axial	561	94.4	5.94	0.235
	Radial	0	-22.2		
D-15	Axial	1102	202.6	5.44	0.259
	Radial	0	-52.6		
F-33	Axial	2123	411.9	5.15	0.265
	Radial	0	-109.1		
B-16	Axial	3450	537.6	6.42	0.280
	Radial	0	-150.3		
A-35	Axial	0	-47.9	6.35	0.254
	Radial	600	70.6		
D-46*	Axial	0	-100.9	6.08	0.256
	Radial	1200	147.0		
E-43	Axial	0	-220.7	5.56	0.256
	Radial	2400	321.1		
C-34*	Axial	0	-350.6	4.97	0.242
	Radial	3600	549.7		
E-18	Axial	2259	322.3	6.19	0.219
	Radial	600	-4.2		
C-12	Axial	1032	77.4	10.36	0.096
	Radial	1200	95.2		
D-2	Axial	1086	-53.6	5.28	0.285
	Radial	2400	266.4		
G-9	Axial	2268	181.4	3.12	0.355
	Radial	2400	238.7		
F-20	Axial	3474	308.7	1.56	0.416
	Radial	3600	423.2		

* Original specimen failed and was replaced.

TABLE 9. INSTANTANEOUS STRAINS AND ELASTIC PROPERTIES OF AIR-DRIED SPECIMENS AT 150° F

Specimen Number	Axis	Stress and Instantaneous Strains		Elastic Properties	
		Stress, psi	Strain, micro-units	$E \times 10^6$ psi	ν
B-1	Axial	561	102.2	5.49	0.249
	Radial	0	-25.4		
D-22	Axial	1102	254.9	4.32	0.210
	Radial	0	-53.5		
F-34	Axial	2123	468.8	4.53	0.262
	Radial	0	-122.7		
B-5	Axial	3450	758.7	4.58	0.231
	Radial	0	-174.0		
A-19*	Axial	0	-53.4	5.29	0.234
	Radial	600	86.8		
D-3	Axial	0	-86.3	5.91	0.212
	Radial	1200	160.1		
E-1	Axial	0	-233.7	4.93	0.240
	Radial	2400	369.7		
C-13*	Axial	0	-376.7	4.40	0.250
	Radial	3600	631.2		
E-4	Axial	2259	377.6	5.23	0.237
	Radial	600	-14.7		
C-46	Axial	1032	101.0	10.28	-.003
	Radial	1200	117.3		
D-41	Axial	1086	-23.2	4.04	0.246
	Radial	2400	382.1		
G-19	Axial	2268	189.7	2.82	0.361
	Radial	2400	253.4		
F-6	Axial	3474	386.9	3.80	0.278
	Radial	3600	429.3		

* Original specimen failed and was replaced.

5.86×10^6 and 5.50×10^6 psi, respectively. Specimens loaded at 150° F had lower modulus values, with the average values for the as-cast and air-dried specimens being 5.74×10^6 psi and 4.87×10^6 psi, respectively.

SHRINKAGE STRAINS

To estimate creep strains it was necessary to measure shrinkage strains during the testing period and in order to interpret these shrinkage strains it was necessary to measure shrinkage strains during the curing period.

During the Curing Period

Specimen handling and environment change were unavoidable during the first seven days after casting; therefore, the initial reference reading for calculating shrinkage strain during the curing period was the reading seven days after casting. All subsequent shrinkage strains are based on an assumed zero strain on the seventh day. The shrinkage strains during the curing period were classified as air-dried or as-cast.

The radial and axial shrinkage strains for as-cast specimens are shown in Figs 13 and 14 and for air-dried specimens in Figs 15 and 16, respectively. The average strain is shown as a solid line with broken lines delineating the limits of variation. For both the as-cast and air-dried conditions, it can be seen that the radial and axial shrinkage strains followed the same trends.

The average radial and axial shrinkage strains for the as-cast specimens increased to approximately 16 micro-units 28 days after casting and then decreased to approximately zero on about the 82nd day. In the air-dried specimens shrinkage strains continued to increase throughout the test period until 82 days after casting. The radial and axial shrinkage strains of air-dried specimens were approximately 180 and 250 micro-units, respectively.

Since shrinkage of the air-dried specimens was expected, each specimen was weighed periodically throughout the curing period in order to determine the amount of water loss. This loss of water with time is shown in Fig 17, which indicates that the air-dried specimens lost between 8 and 11 ounces of water during the 82-day curing period.

During the Testing Period

Shrinkage strains were measured during the loading period in order to estimate creep strain, i.e., that portion of the time-dependent strain which

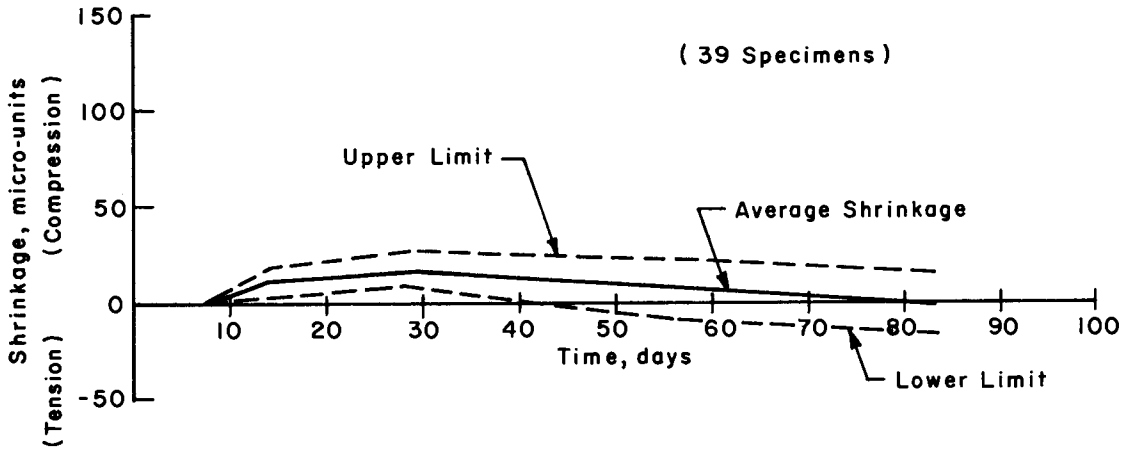

Fig 13. Average radial shrinkage strains for as-cast specimens during the curing period.

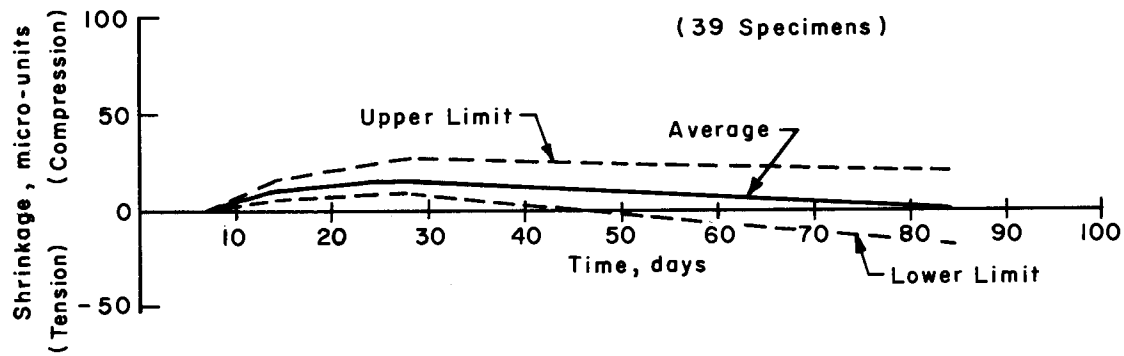

Fig 14. Average axial shrinkage strains for as-cast specimens during the curing period.

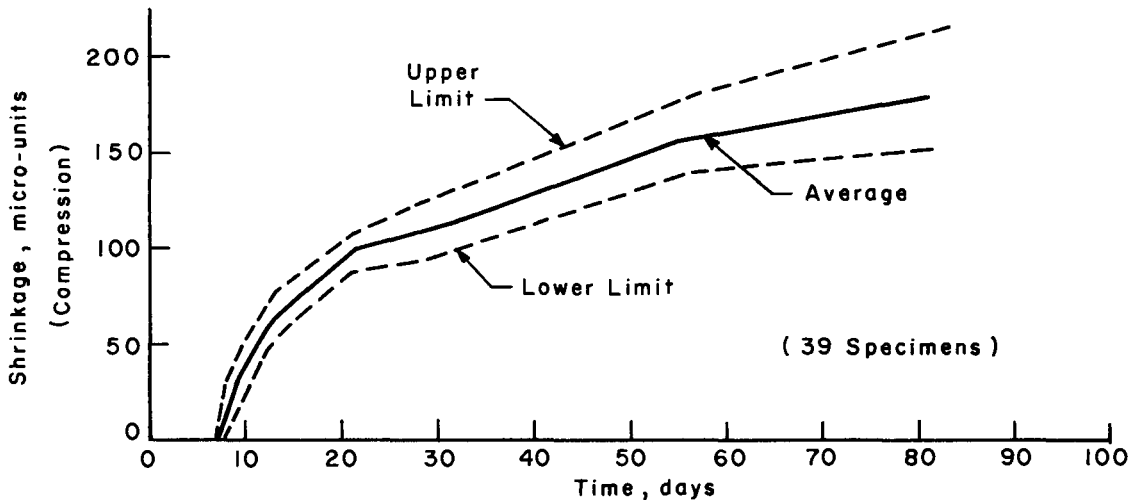

Fig 15. Average radial shrinkage strains for air-dried specimens during the curing period.

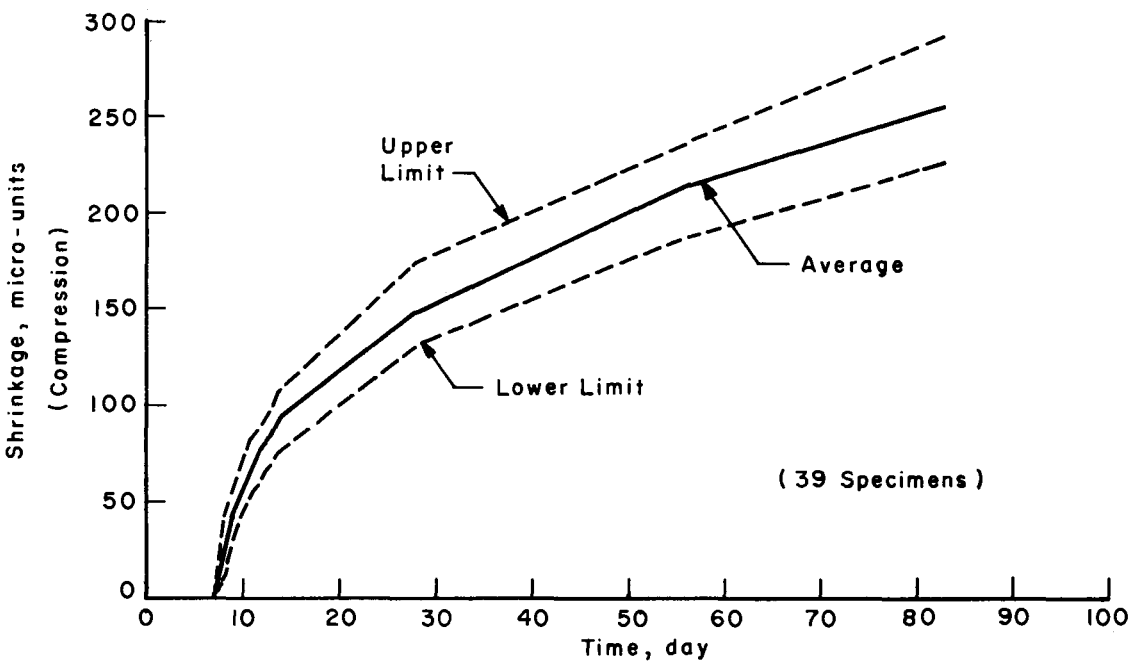

Fig 16. Average axial shrinkage strains for air-dried specimens during the curing period.

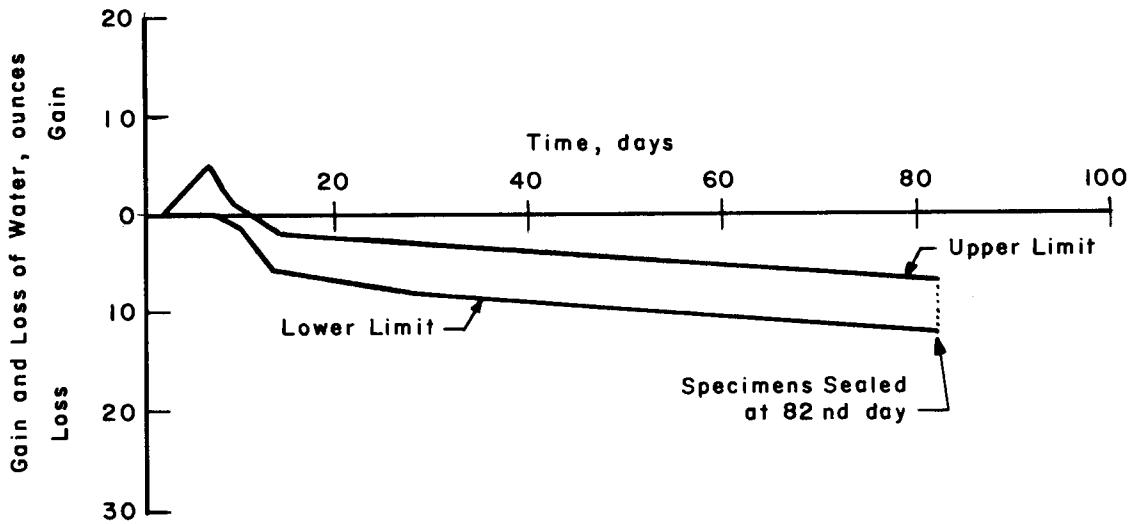

Fig 17. Moisture change for air-dried specimens during the curing period.

was due to load only. Throughout the 12-month loading period shrinkage specimens were subjected to the same environmental condition as the creep specimens. Average shrinkage curves for the as-cast and air-dried specimens during the loading period are shown in Figs 18 and 19, respectively.

Essentially no shrinkage occurred in the as-cast specimens (Fig 19) at 75° F; however, at 150° F the specimens exhibited expansion rather than shrinkage. Most of this expansion occurred during the first 84 days of the loading period, at which time the axial and radial gages indicated tensile strains of 29 and 37 micro-units, respectively. During the remainder of the loading period very little additional strain was detected.

The shrinkage behavior associated with specimens subjected to the 150° F temperature can probably be attributed to an interaction effect involving temperature change, the concrete, and the gage. This effect is believed to be due primarily to the fact that the gage and the concrete are not compatible when subjected to a temperature change. When the temperature was raised from 75 to 150° F the gage tended to expand more than the concrete, and the gage was prevented from expanding by the concrete. Nevertheless, localized stresses were produced in the concrete, and as these stresses were relieved by localized creep of the concrete, the gage was allowed to expand producing increased tension in the gage wire. This increasing tension during the first 84 days after loading accounts for the apparent expansion of the concrete. This effect is discussed in detail in Ref 33.

The axial and radial shrinkage strains in the air-dried specimens at 75° F (Fig 18) increased at a decreasing rate throughout the entire loading period. However, the radial strains were compressive (shrinkage) while the axial strains were tensile (expansion). Nevertheless, the magnitudes of the strains after 12 months were relatively small, with the axial gage indicating 34 micro-units (tension) and the radial gage 18 micro-units (compression).

The strains in the air-dried specimens at 150° F were similar to, although somewhat larger than, those of the as-cast specimens at the same temperature. These specimens expanded continuously at a decreasing rate. At the end of the 12-month loading period the axial and radial strains were 67 and 53 micro-units (expansion), respectively.

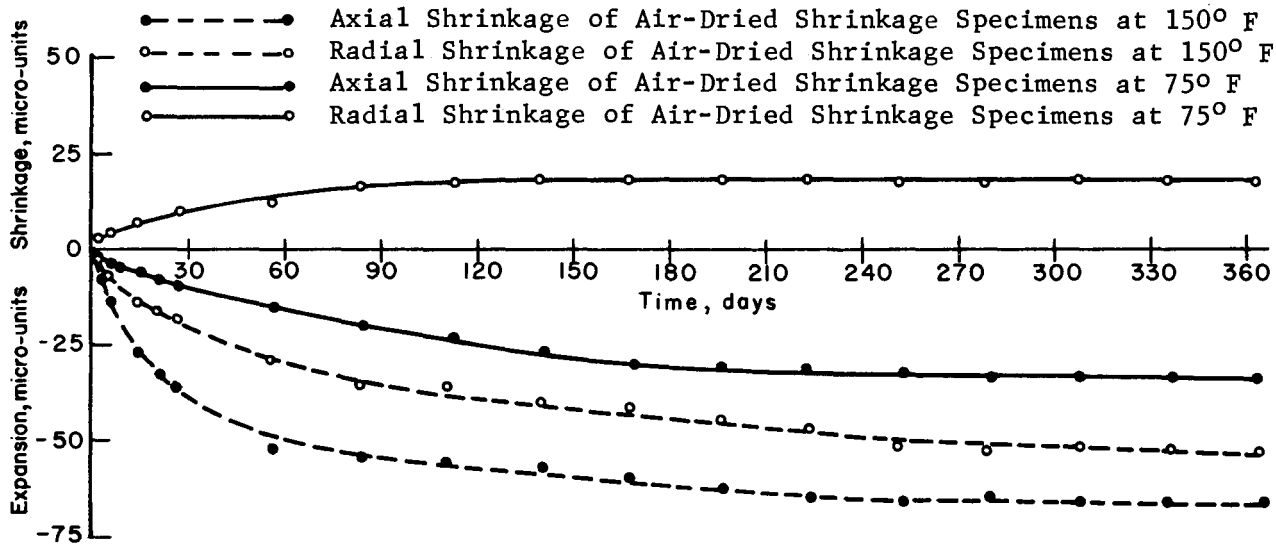

Fig 18. Average axial and radial shrinkage strains for air-dried shrinkage specimens during the loading period.

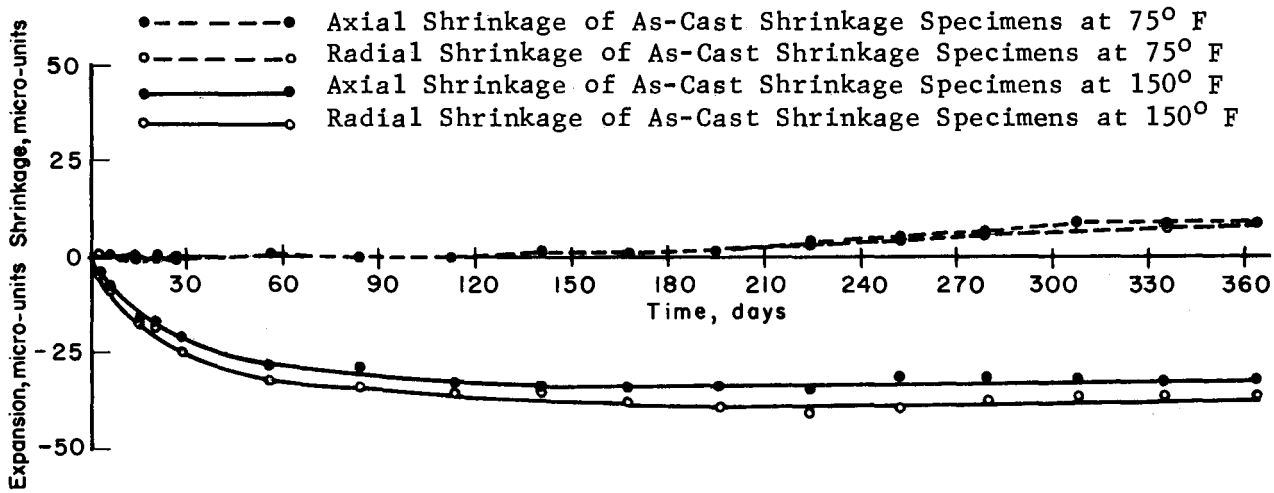

Fig 19. Average axial and radial shrinkage strains for as-cast shrinkage specimens during the loading period.

CREEP STRAINS

Creep strains were estimated by subtracting the instantaneous strains and shrinkage strains from the total strains. In doing this it was assumed that the instantaneous (elastic) strain was constant and, thus, did not vary with time and that the time-dependent strains, shrinkage and creep, were not interrelated. The creep strain-time relationships for the various specimens are shown in Figs A1 through A19 in the appendix.

Uniaxially Loaded Specimens

Twelve specimens were loaded uniaxially. These specimens were loaded in pairs, one as-cast and one air-dried, under six different loading conditions, two at 75° F and four at 150° F. However, a number of gages in these uniaxially loaded specimens at 150° F failed during the tests.

The axial strains in the as-cast and air-dried specimens loaded at a nominal stress of 3600 psi exceeded the strain limits of the gage 112 days after loading and during the actual loading. In addition, the strain gages in as-cast specimens loaded at 600 and 2400 psi stopped functioning 308 days after loading.

The creep strain-time relationships for the as-cast and air-dried specimens at 75° F are shown in Figs A1 and A2, respectively. At the lower stress levels, there was very little difference between the radial strains for the air-dried and as-cast specimens or the axial strains for the air-dried and as-cast specimens at the lower stress level. However, at the higher stress level, the axial creep strains recorded for the air-dried specimens were much larger than for the as-cast specimens.

The creep strain-time relationships for the as-cast and air-dried specimens subjected to four different stress levels at 150° F are shown in Figs A3 and A4. The radial creep strains increased until approximately three months after loading at which time they began to decrease.

Multiaxially Loaded Specimens

Thirty-eight specimens were loaded multiaxially. These specimens were also loaded in pairs, one as-cast and one air-dried, under 19 different loading conditions, ten at 75° F and 9 at 150° F. Six pairs of specimens were loaded biaxially and 13 were loaded triaxially. The resulting creep strain-time relationships have been grouped according to confining pressure under the appropriate temperature and curing condition.

75° F Temperature. Six different loading conditions involved specimens at 75° F. The results of the test at 75° F for the as-cast specimens with confining pressures of 600, 1200, 2400, and 3600 psi are shown in Figs A5 through A8. These results indicate that the creep strains in the radial and axial directions were reduced by the application of stresses in the perpendicular direction.

Results for the air-dried specimens at 75° F are shown in Figs A9 through A12. Creep strains in the loaded direction were larger than those of the as-cast specimens.

150° F Temperature. Nine different loading conditions were tested at 150° F. Four of these conditions were biaxial and five were triaxial. Of the eight biaxial specimens, five either failed or had strain gage failures. Thus the results of only three biaxial specimens were included.

The creep strain-time relationships for the as-cast specimens are presented in Figs A13 through A16. The results indicate that under comparable conditions the creep strains of the as-cast specimens at 150° F were higher than those at 75° F.

The relationships for air-dried specimens are shown in Figs A17 through A19. These results indicate that the creep strains of air-dried specimens at 150° F were higher than of as-cast and air-dried specimens at 75° F.

Summary of Creep Strains

A more comprehensive evaluation of the effects of moisture condition and testing temperature is contained in Ref 33. Nevertheless, the results discussed above can generally be summarized as follows:

(1) At a constant temperature, air-dried specimens had higher creep strains than as-cast specimens.

(2) Both as-cast and air-dried specimens tested at 150° F exhibited higher creep strains than those tested at 75° F.

(3) In uniaxially and biaxially loaded specimens at both temperatures, creep strains occurred in the direction perpendicular to the direction of the applied stress. Thus, a creep Poisson's effect apparently occurred.

CREEP POISSON'S RATIO

Although the existence of a creep Poisson's ratio has been questioned (Chapter 2), the results from this investigation definitely indicate a creep Poisson's effect. Thus, an estimate of creep Poisson's ratio is required in order to predict creep behavior under a multiaxial state of stress.

The following expression, based on the derivation made in Chapter 3, was used to calculate the creep Poisson's ratio for cylindrical specimens subjected to sustained uniaxial and biaxial states of stress at stress levels less than the creep proportional limit.

$$\nu_c = \frac{\sigma_a(\epsilon_c)_r - \sigma_r(\epsilon_c)_a}{2\sigma_r(\epsilon_c)_r - (\epsilon_c)_a(\sigma_r + \sigma_a)}$$

where

ν_c = creep Poisson's ratio;

σ_a = axial stress, psi;

σ_r = radial stress, psi;

$(\epsilon_c)_a$ = creep strain in axial direction;

$(\epsilon_c)_r$ = creep strain in radial direction.

Creep Poisson's ratios calculated from as-cast and air-dried specimens tested at 75° F are shown in Figs 20 and 21. The ratios for both as-cast and air-dried specimens increased slightly with time. The overall average of creep Poisson's ratios for as-cast specimens was 0.150, and for air-dried specimens this value was 0.108.

The results of creep Poisson's ratio calculated from specimens tested at 150° F are shown in Figs 22 and 23. As indicated, the creep Poisson's ratio decreased rapidly during the first week under load. For as-cast specimens, the average creep Poisson's ratio decreased from 0.30 at three hours after loading to 0.142 at the end of the first week and then fluctuated around 0.165. For air-dried specimens, the average creep Poisson's ratio decreased from 0.27 at three hours after loading to 0.17 at the end of the first week and then fluctuated around 0.14. The overall average of Poisson's ratio for creep during the first month's period was 0.149 for as-cast specimens and 0.140 for air-dried specimens.

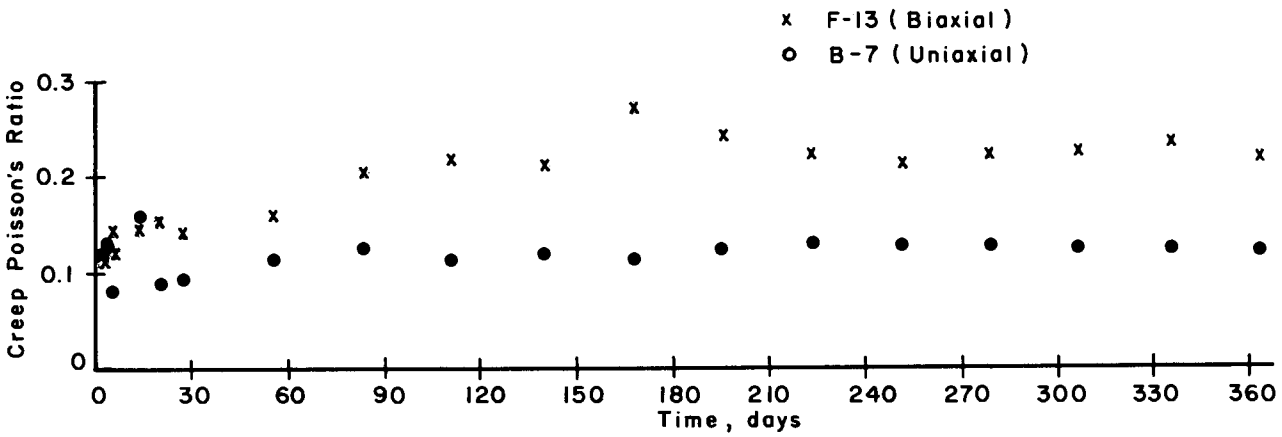

Fig 20. Creep Poisson's ratio for as-cast specimens at 75° F.

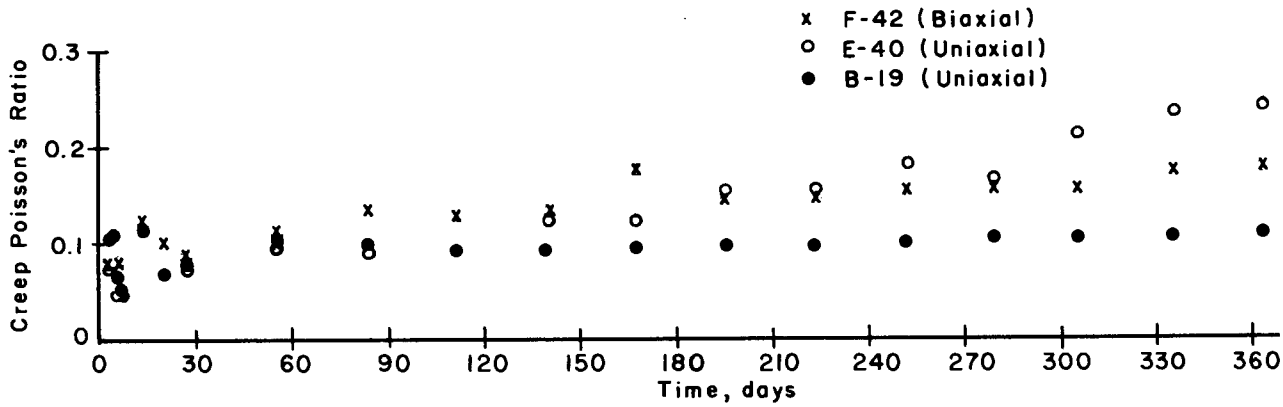

Fig 21. Creep Poisson's ratio for air-dried specimens at 75° F.

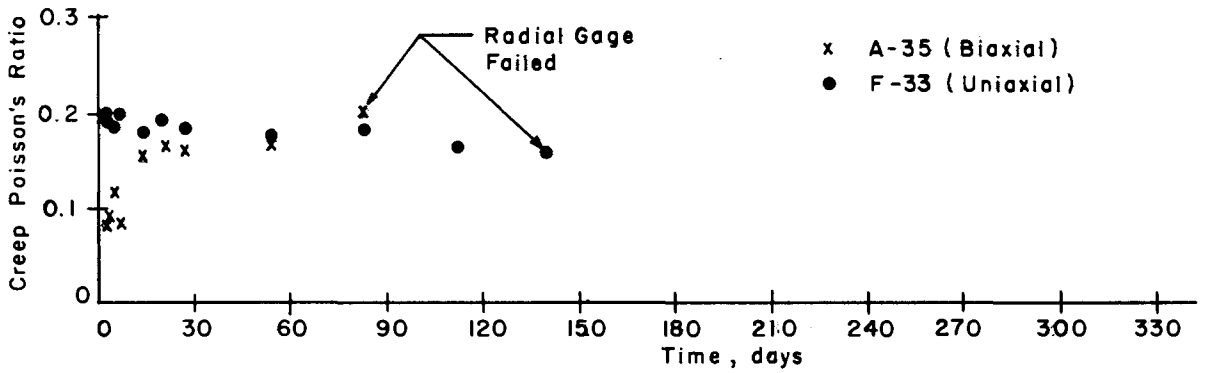

Fig 22. Creep Poisson's ratio for as-cast specimens at 150° F.

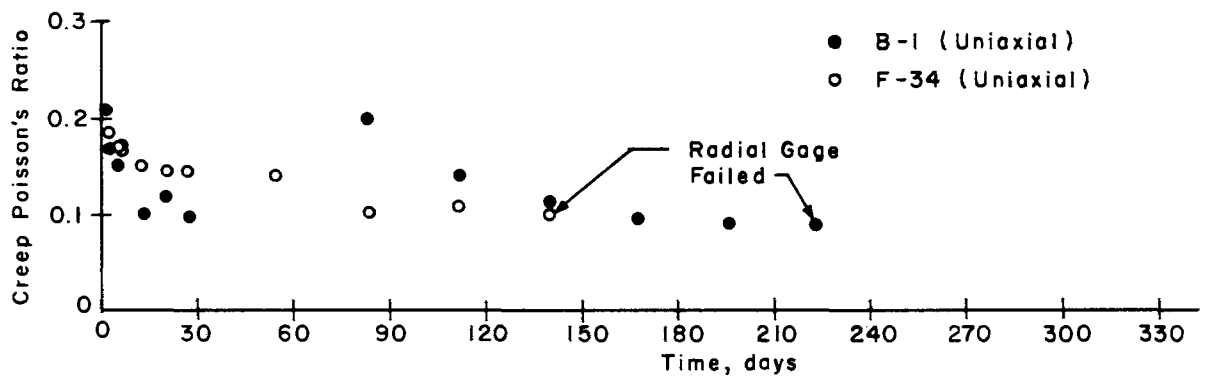

Fig 23. Creep Poisson's ratio for air-dried specimens at 150° F.

CHAPTER 6. DISCUSSION AND EVALUATION OF RESULTS

The purpose of this chapter is to evaluate the constants in the unit creep function and to evaluate the accuracy of the resulting unit creep predictive equations. Thus, the chapter is subdivided into two parts. The first part is concerned with the evaluation of constants in terms of the uniaxial data obtained in the experimental portion of this investigation. The second part compares the predicted results obtained from the unit creep function with the actual observed data.

EVALUATION OF THE UNIT CREEP FUNCTION

The concept and development of unit creep predictive relationships was discussed in Chapter 3. It was hypothesized that creep strains resulting from multiaxial states of stress could be predicted from uniaxial creep data by utilizing Eqs 3.10, 3.11, and 3.12. For the loading conditions in the experimental portion of this investigation in which $\sigma_y = \sigma_z = \sigma_r$, $\sigma_x = \sigma_a$ these three equations reduce to

$$(\varepsilon_c)_a = [F(t,\tau)]\,[\sigma_a - 2\nu_c\sigma_r] \tag{6.1}$$

$$(\varepsilon_c)_r = [F(t,\tau)]\,[\sigma_r - \nu_c(\sigma_a + \sigma_r)] \tag{6.2}$$

where

σ_a = axial stress,

σ_r = radial stress,

ν_c = creep Poisson's ratio,

τ = age at loading,

t = time after loading,

$F(t,\tau)$ = unit creep function.

$(\varepsilon_c)_a$ = creep strain in axial direction,

$(\varepsilon_c)_r$ = creep strain in radial direction.

The unit creep function is expressed in the form

$$F(t,\tau) = K(1 - e^{-\alpha t^{\beta}})$$

where K, α, and β are constants.

In order that these relationships can be used for prediction purposes, it is necessary to evaluate the constants K, α, and β in the unit creep function and to estimate a value for creep Poisson's ratio ν_c from uniaxial test results (Chapter 5). Once the unit creep function and creep Poisson's ratio are determined, creep strains at a later age and creep strains resulting from multiaxial states of stress can be predicted.

Unit Creep Function

The specimen conditions studied were as-cast and air-dried, both at 75° F and 150° F. All specimens were loaded at the age of 90 days, and therefore, the effect of the age at loading τ on creep strains could not be included and was considered constant. Thus, the unit creep function becomes $F(t,90)$.

Prior to the determination of creep strain per unit stress, the stress-creep strain-time relationships obtained from uniaxial tests were established, to determine the creep proportional limit. The assumption of linearity between stress and creep strain is valid only at stress levels less than the creep proportional limit; therefore, only creep strains resulting from these stress levels were used for unit creep function evaluation. The constants in the unit creep function were determined by fitting the creep strains per unit stress to the unit creep function in the general form of Eq 3.2. This was accomplished by a nonlinear curve-fitting technique, using a computer program.

The stress-creep strain-time relationships for the as-cast and air-dried specimens are shown in Figs 24 through 27, respectively. The linearity of the stress-creep strain relationships for the as-cast specimens at 75° F (Fig 24) indicates the maximum stress level of approximately 2200 psi was less than the proportional limit. For the as-cast specimens at 150° F (Fig 25) and the air-dried specimens at 75° F (Fig 26) the creep proportional limit was judged also to be approximately 2200 psi. In contrast the creep proportional limit for the

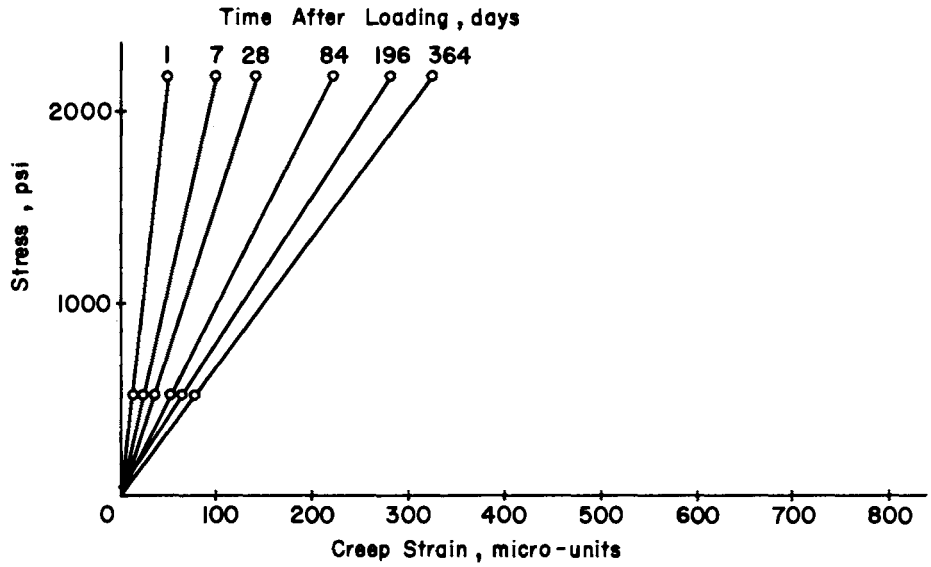

Fig 24. Stress-creep strain-time relationships for as-cast specimens at 75° F.

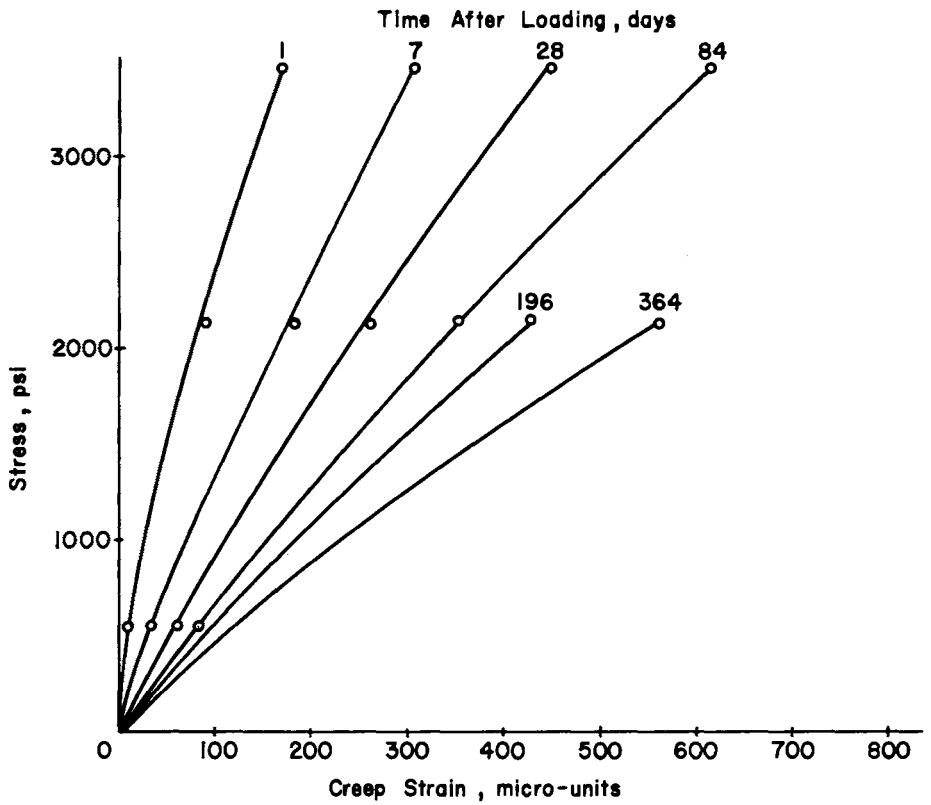

Fig 25. Stress-creep strain-time relationships for as-cast specimens at 150° F.

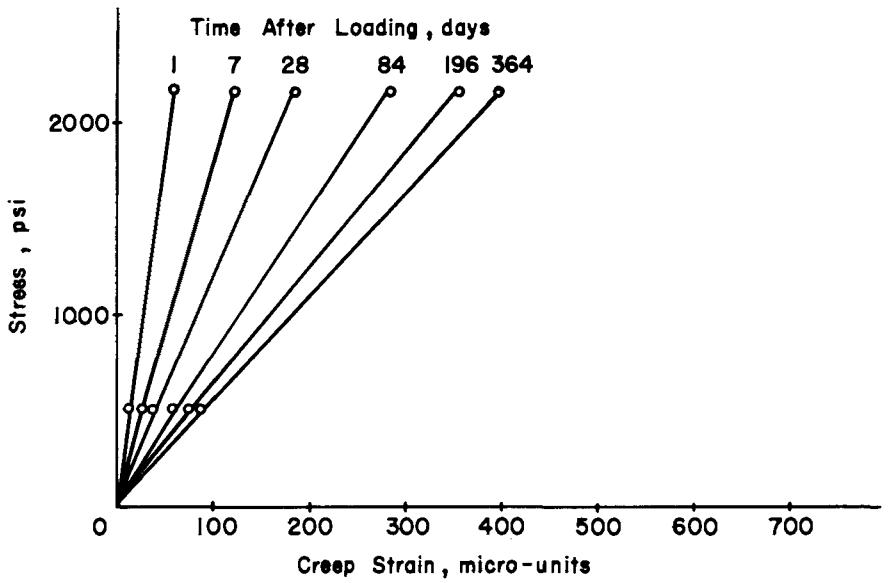

Fig 26. Stress-creep strain-time relationships for air-dried specimens at 75° F.

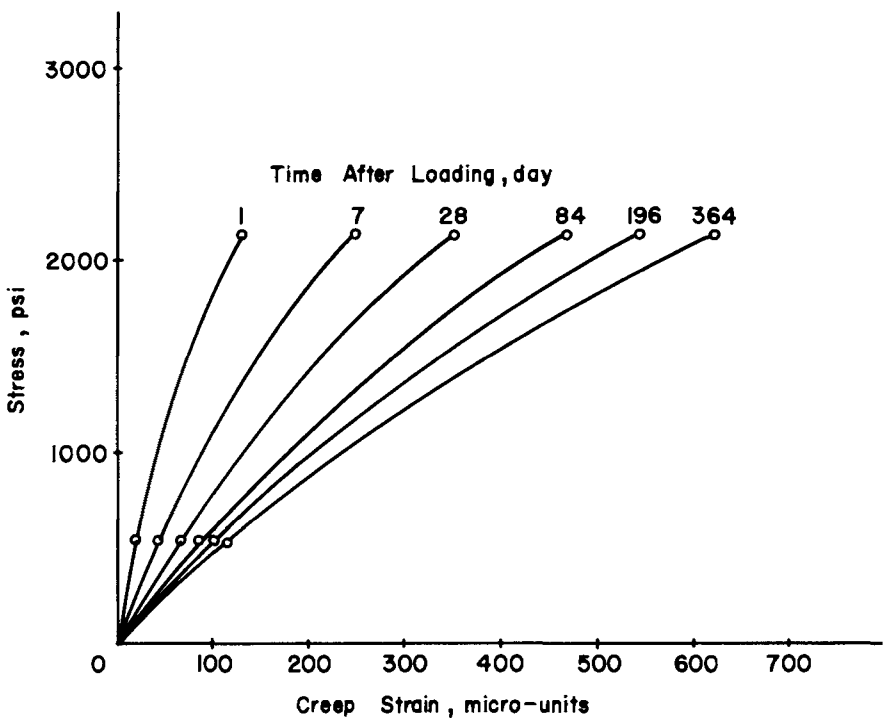

Fig 27. Stress-creep strain-time relationships for air-dried specimens at 150° F.

air-dried specimens at 150° F appeared to be lower at a stress level of 1500 psi, which was approximately 23 percent of the 28-day unconfined compressive strength. In the latter case, however, data were available for only two stress levels (561 and 2123 psi) since the data from the two specimens loaded at 1102 and 3450 psi were inconclusive due to equipment malfunction.

The unit creep function relationships for the four conditions are summarized in Table 10, and the unit creep function-time relationships are illustrated in Fig 28. In addition, Table 10 contains an estimate of the ultimate unit creep, which was assumed to occur at an infinite time after loading. It may be noted that in Fig 28 the unit creep strains for loading periods less than a year were larger for 150° F than for 75° F and for the air-dried condition than for the as-cast.

Creep Poisson's Ratio

In order to predict multiaxial creep strains, creep Poisson's ratios should be estimated from uniaxial tests. However, due to the fact that the number of uniaxial specimens was limited, values from biaxially loaded specimens were included. Creep Poisson's ratios for the various uniaxial tests conducted in this study were summarized in Figs 20 through 23 in Chapter 5. The average values for the various test conditions are 0.150 and 0.149 for as-cast specimens at 75° F and 150° F, respectively, and 0.108 and 0.140 for air-dried specimens at 75° F and 150° F, respectively.

Inserting the appropriate creep Poisson's ratios and the relationships for the unit creep function into Eqs 6.1 and 6.2 yields predictive equations for axial and radial creep strains for the four test conditions. These predictive equations are summarized in Table 11.

EVALUATION OF CREEP PREDICTIVE EQUATIONS

In order to evaluate the accuracy of these predictive equations (Table 11), it was necessary to compare predicted creep strains with actual creep strains measured experimentally. This was done in two parts. First, creep strains resulting from loading times in excess of those associated with the data used in developing the equations were compared with predicted strains. Secondly, creep strains resulting from multiaxial states of stress were compared with predicted values.

TABLE 10. UNIT CREEP FUNCTIONS AND ULTIMATE UNIT CREEP OBTAINED FROM UNIAXIALLY LOADED SPECIMENS UNDER VARIOUS TEST CONDITIONS

Test Conditions	Unit Creep Function, F(t,90), micro-units/psi	Ultimate Unit Creep Strain, micro-units/psi
As-Cast 75° F	$0.277(1 - e^{-0.091t^{0.358}})$	0.277
As-Cast 150° F	$0.358(1 - e^{-0.110t^{0.385}})$	0.358
Air-Dried 75° F	$0.282(1 - e^{-0.098t^{0.407}})$	0.282
Air-Dried 150° F	$0.276(1 - e^{-0.208t^{0.399}})$	0.276

t = time after loading, days

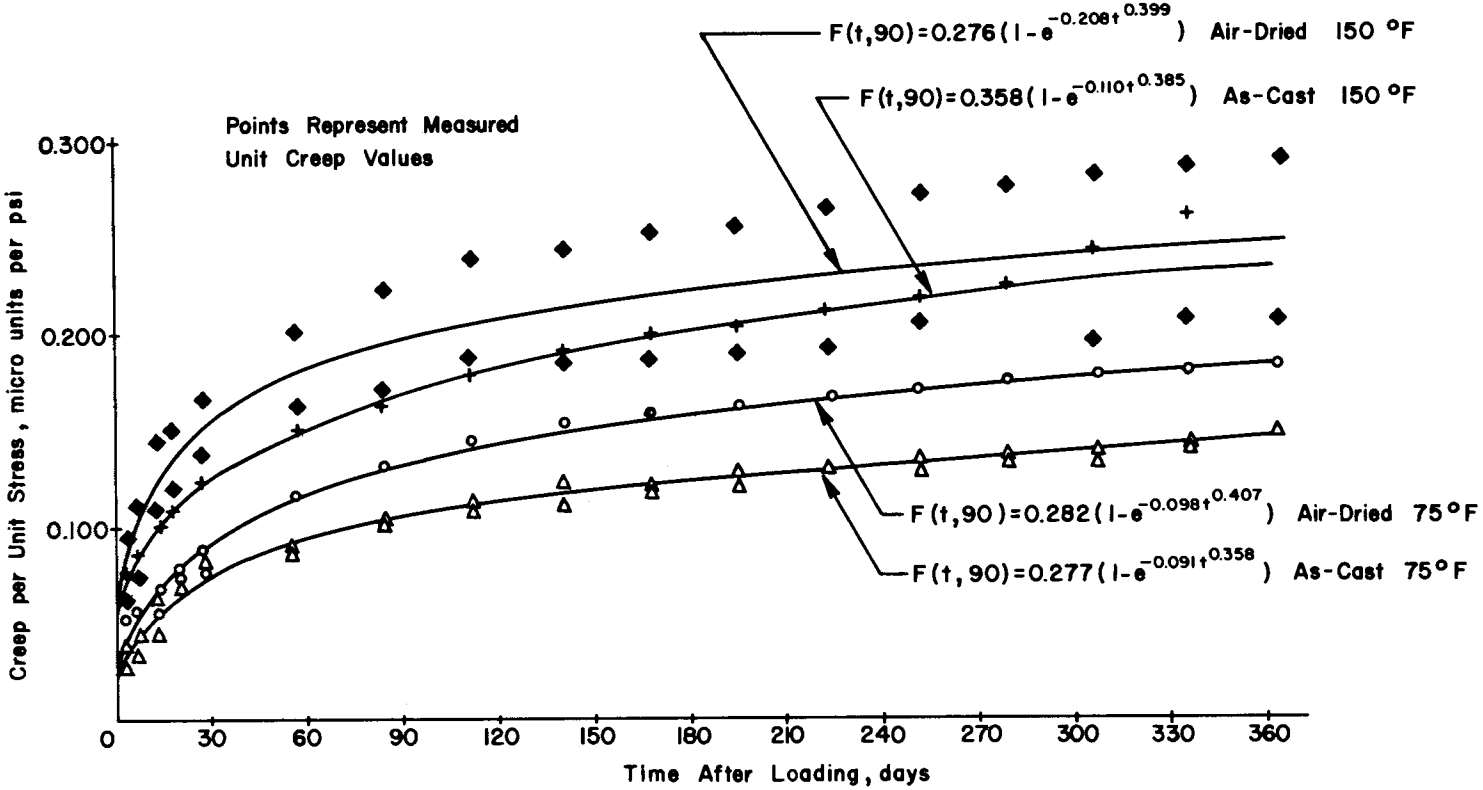

Fig 28. Unit creep functions for various test conditions.

TABLE 11. UNIT CREEP PREDICTIVE EQUATIONS

	At 75° F
Air-Dried	$(\varepsilon_c)_a = 0.282 \left[1 - e^{-0.098t^{0.407}}\right] \left[\sigma_a - 0.216\sigma_r\right]$
	$(\varepsilon_c)_r = 0.282 \left[1 - e^{-0.098t^{0.407}}\right] \left[\sigma_r - 0.108(\sigma_r + \sigma_a)\right]$
As-Cast	$(\varepsilon_c)_a = 0.277 \left[1 - e^{-0.091t^{0.358}}\right] \left[\sigma_a - 0.300\sigma_r\right]$
	$(\varepsilon_c)_r = 0.277 \left[1 - e^{-0.091t^{0.358}}\right] \left[\sigma_r - 0.150(\sigma_r + \sigma_a)\right]$
	At 150° F
Air-Dried	$(\varepsilon_c)_a = 0.276 \left[1 - e^{-0.208t^{0.399}}\right] \left[\sigma_a - 0.280\sigma_r\right]$
	$(\varepsilon_c)_r = 0.276 \left[1 - e^{-0.208t^{0.399}}\right] \left[\sigma_r - 0.140(\sigma_r + \sigma_a)\right]$
As-Cast	$(\varepsilon_c)_a = 0.358 \left[1 - e^{-0.110t^{0.385}}\right] \left[\sigma_a - 0.298\sigma_r\right]$
	$(\varepsilon_c)_r = 0.358 \left[1 - e^{-0.110t^{0.385}}\right] \left[\sigma_r - 0.149(\sigma_r + \sigma_a)\right]$

σ_a = axial stress, psi

σ_r = radial stress, psi

t = time after loading, days

$(\varepsilon_c)_a$ = creep strain in axial direction, micro-units

$(\varepsilon_c)_r$ = creep strain in radial direction, micro-units

Prediction of Long-Term Uniaxial Creep Strains

Since time under load in this investigation did not exceed 12 months, it was necessary to compare predicted creep strains with data obtained by other investigators. Creep strains for test conditions similar to conditions in this investigation have been summarized and reported by Neville (Ref 23). Creep strains after two years and five years under load were reported to be approximately 14 and 20 percent larger than the creep strains after one year. Assuming the creep strains at one year to be unity the predicted creep strains for uniaxially loaded specimens yield the results shown in Table 12. Examination of these results indicates a favorable comparison with those reported by Neville.

As shown in Table 12, most of the creep strains for air-dried specimens and as-cast specimens loaded at 150° F occurred within the first year while only about 50 percent of the ultimate creep strains associated with the as-cast specimens at 75° F occurred in the first year.

Prediction of Creep Strains Resulting from Multiaxial Stress

The accuracy and validity of the prediction equations were also evaluated by comparing predicted creep strains with experimentally measured results. Creep strains were predicted by the equations summarized in Table 11 for the test conditions and stress levels utilized in the experimental portion of this investigation. The predicted creep strains are compared with measured strains in Figs 29 through 65. Figures 29 through 32 compare the predicted and measured radial and axial creep strains at 1, 7, 14, 28, 84, 168, and 364 days after loading for the four combinations of curing history and testing temperature while Figs 33 through 65 compare the predicted and measured creep strain-time relationships for individual specimens.

Comparisons have been grouped according to the four test conditions and then by increasing radial and axial stress within each test condition.

As-Cast Specimens at 75° F

The predicted creep strain-time relationships of eight specimens, along with the measured relationships, are shown in Figs 33 through 40. The results for the uniaxial loading condition (σ_a = 2179 psi) are shown in Fig 33. As would be expected, the predicted and measured results were in excellent agreement. Likewise, for biaxial loading (Fig 34), the predicted and

TABLE 12. RATIO OF LONG-TERM AND ONE-YEAR CREEP STRAINS

Time after Loading, years	75° F		150° F		Neville* (Ref 18)
	As-Cast	Air-Dried	As-Cast	Air-Dried	
1	1.00	1.00	1.00	1.00	1.00
2	1.17	1.15	1.15	1.06	1.14
5	1.40	1.32	1.31	1.11	1.20
Infinite	1.89	1.51	1.52	1.13	--

*70° F and 50 percent relative humidity

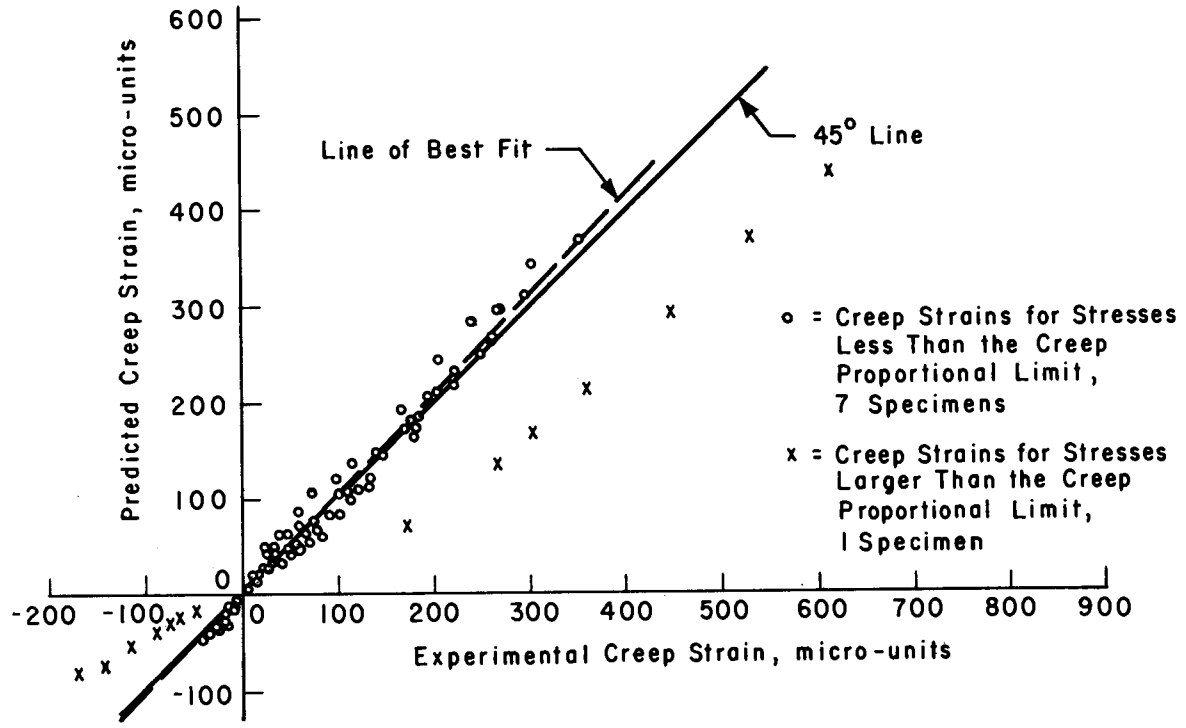

Fig 29. Predicted and experimental creep strains for triaxially loaded as-cast specimens at 75° F.

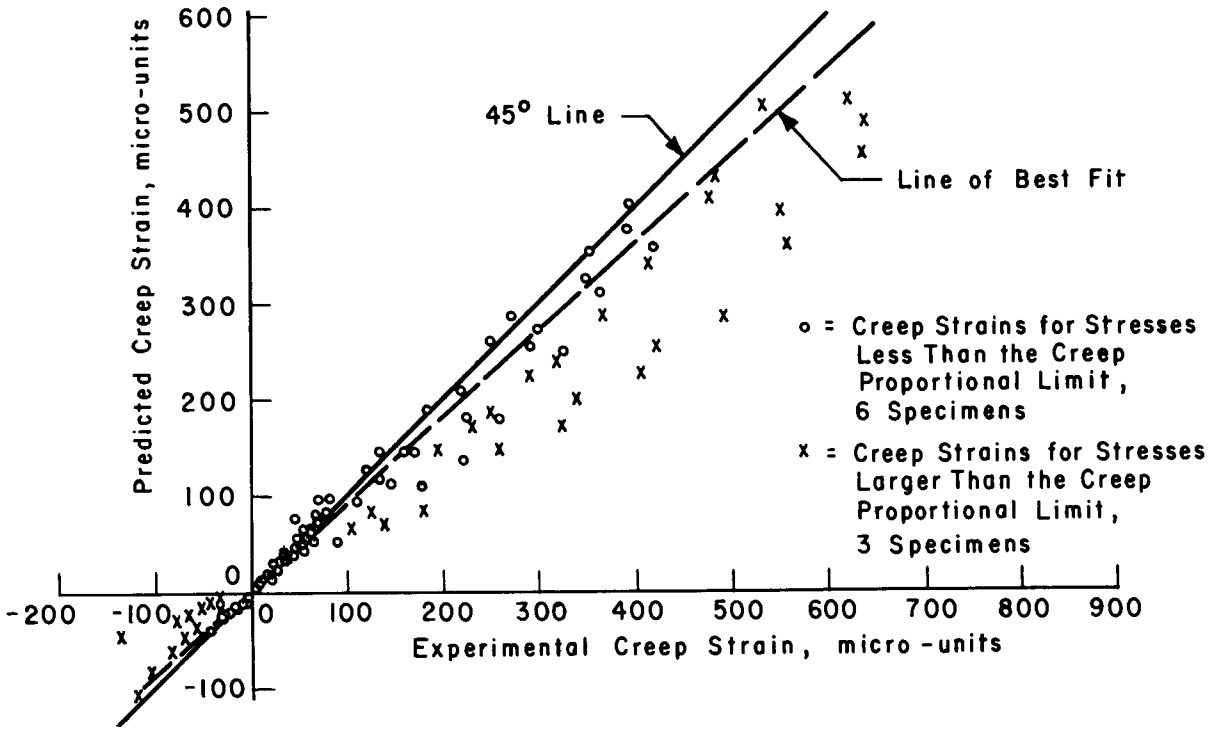

Fig 30. Predicted and experimental creep strains for triaxially loaded air-dried specimens at 75° F.

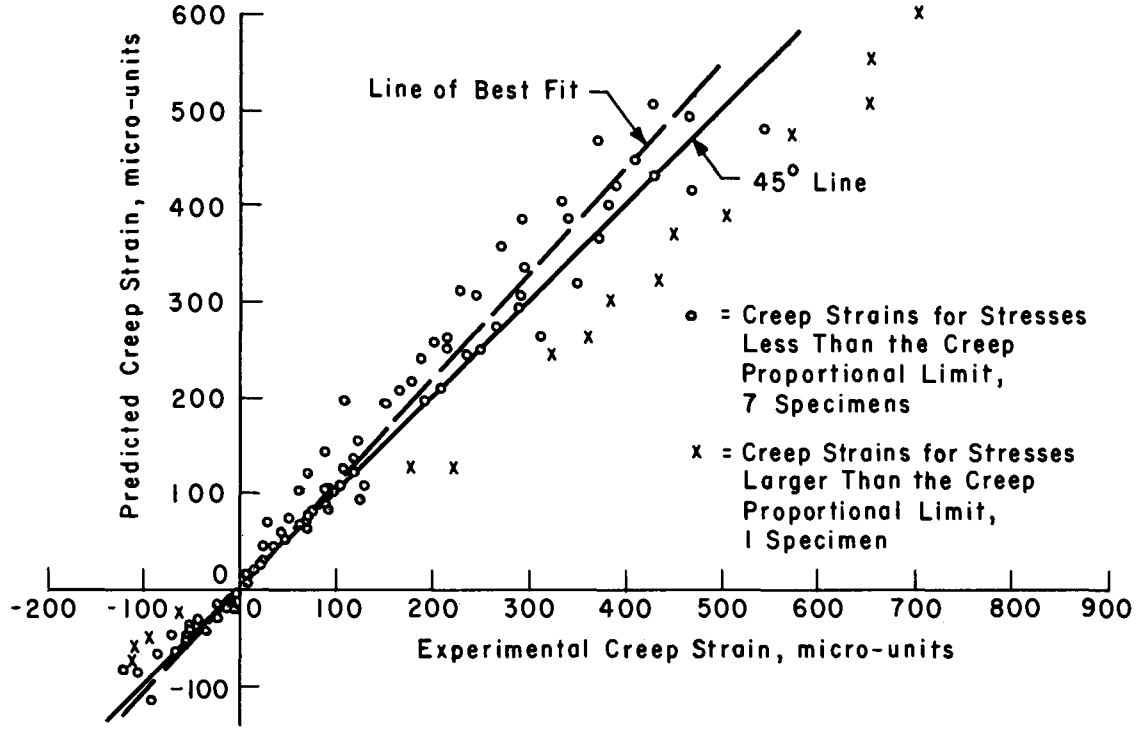

Fig 31. Predicted and experimental creep strains for triaxially loaded as-cast specimens at 150° F.

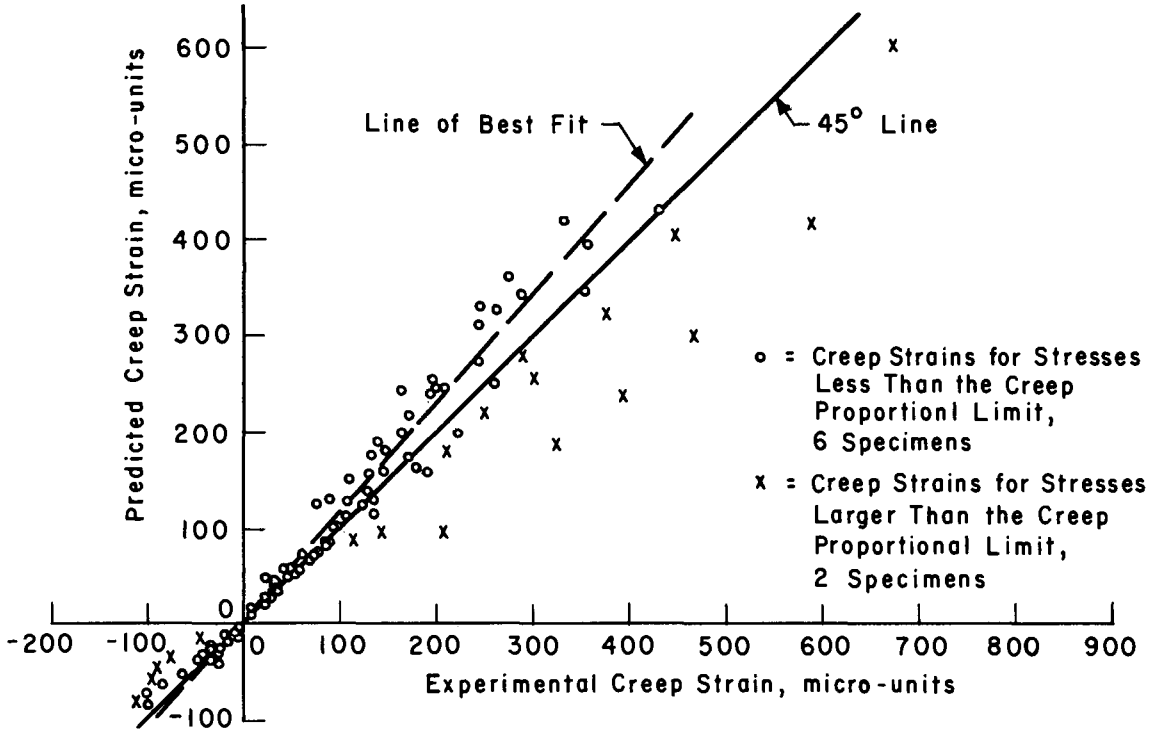

Fig 32. Predicted and experimental creep strains for triaxially loaded air-dried specimens at 150° F.

experimental creep strains for both the axial and the radial directions were very close throughout the loading period. For triaxial loading conditions (Figs 35 through 40), however, the agreement was not as good and in cases where the stresses were less than the creep proportional limit, the predicted creep strains generally were larger than the experimentally measured creep strains, while the reverse was true for specimens loaded at the higher stress levels.

A comparison between predicted creep strains and experimentally measured creep strains for all conditions at various times after loading is shown in Fig 29, which indicates that the unit-creep prediction equation for as-cast concrete tested at 75° F temperature provided a satisfactory estimate of creep strains for all stress levels less than the creep proportional limit. The dashed line is the line of best fit for specimens loaded below the creep proportional limit. The standard error of the estimate of the creep strains for the seven specimens loaded at stresses less than the creep proportional limit was 16 micro-units.

Air-Dried Specimens at 75° F

Predicted and measured creep strain-time relationships for air-dried specimens are shown in Figs 41 through 49. The results for the uniaxial loading condition (Figs 41 and 42) indicate excellent agreement between predicted and measured strains in both the axial and radial directions. The predicted creep strain-time curves were also very close to the experimental results for the biaxial loading condition (Fig 43). The results for triaxial loadings with stress levels less than the creep proportional limit, 2200 psi, are shown in Figs 44 and 45; the results for stress levels larger than the creep proportional limit are presented in Figs 46 through 49. These relationships indicate that for stress levels below the creep proportional limit, the predicted creep strains were very close to the measured creep strains. For stresses higher than the creep proportional limit, the differences between predicted and experimental results were relatively large and became larger with time and increased stress levels. These differences are due to the fact that at these higher stresses the relationship between stress and creep strain is not linear, which causes the actual creep strains to exceed the predicted values. The excellent agreement for all test conditions (6 specimens) with stresses below the creep proportional limit and the deviation between predicted and measured creep strains for test conditions (3 specimens) with stress level above the creep

proportional limit are graphically illustrated in Fig 30. The standard error of estimate of creep strains for stress levels less than the creep proportional limit was 27 micro-units.

As-Cast Specimens at 150° F

Comparisons between the predicted and measured creep strain-time curves are shown in Figs 50 through 57. As previously observed, there was satisfactory agreement for the uniaxial loading conditions (Figs 50 through 52) and in addition, the agreement was fairly satisfactory for the triaxial loading conditions for low stresses (Fig 54). However, the predicted creep strains for some other triaxial loading conditions were substantially higher than the measured values. In explanation, it should be noted that the unit creep function was derived from data obtained from a stress level of 2123 psi which was very close to the creep proportional limit (2200 psi). This in itself could produce high predicted strain values. In addition, it is possible that at 150° F, the uniaxially loaded specimens lost moisture resulting in larger creep strains and thus higher predicted creep strains. For the condition of stresses larger than the creep proportional limit, the measured strains were larger (Fig 57). In order to more fully evaluate this condition, additional tests should be conducted. The standard error of the estimate for creep strains resulting from stresses less than the creep proportional limit was 33 micro-units (Fig 31).

Air-Dried Specimens at 150° F

Comparisons between predicted and measured creep strain-time curves are shown in Figs 58 through 65. These relationships indicate that for stresses less than 2400 psi, the unit creep predictive equations generally overestimated the creep strains. The results again indicate that at the higher stresses the measured creep strains were larger than the predicted creep strains, due to the fact that these stress levels exceeded the creep proportional limit, which for the conditions of these tests was very low (1500 psi). At the lower stress levels, this was probably because the unit creep function could not be adequately defined because of lack of data and possibly because of moisture loss during the loading period. The relationship between predicted and measured creep strains for eight specimens at various times after loading is shown in Fig 32. The standard error of the estimate for creep strains resulting from stresses less than the creep proportional limit was 40 micro-units.

(text continued on page 107)

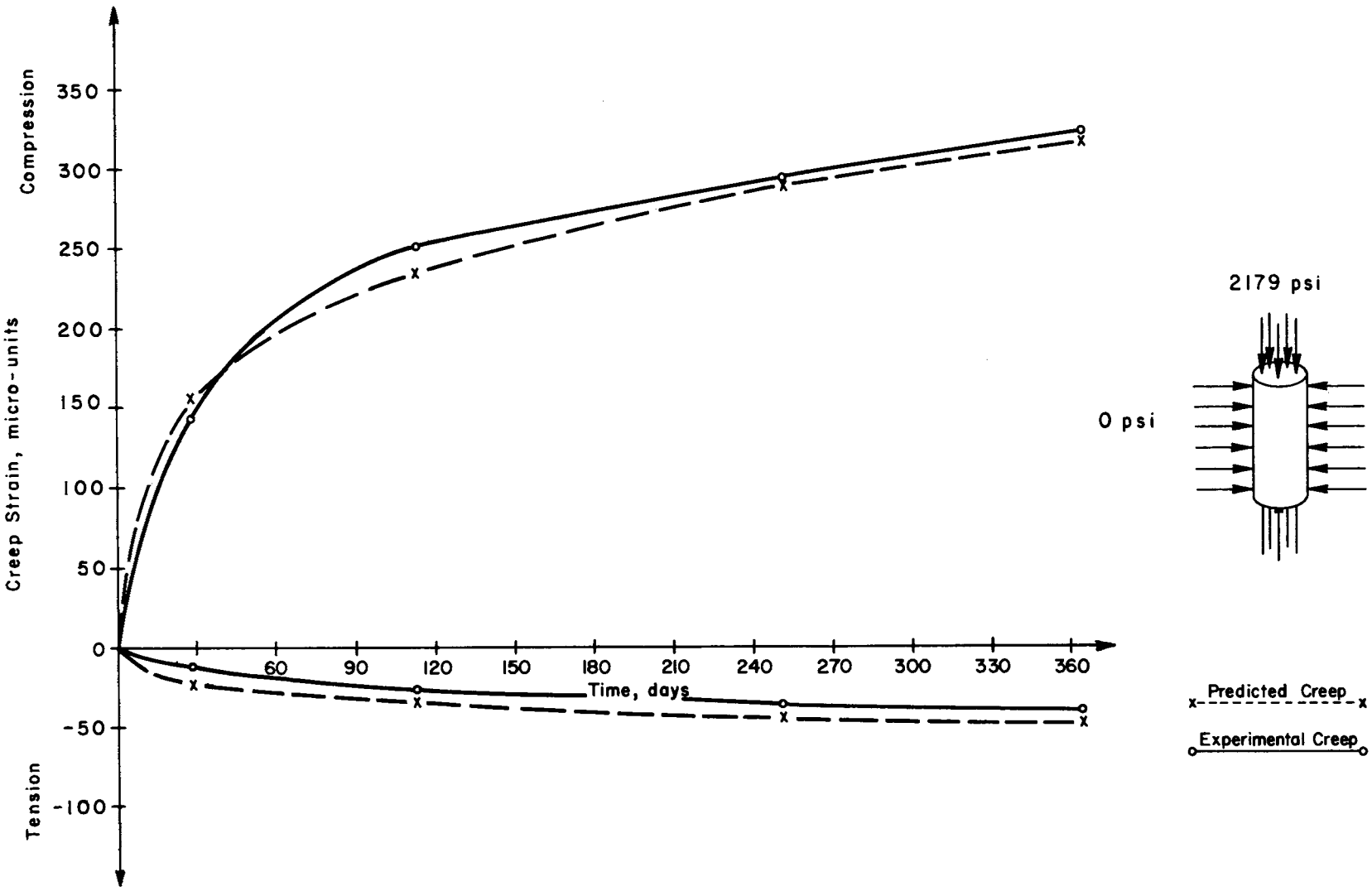

Fig 33. Predicted and experimental creep strain-time relationships for uniaxially loaded as-cast specimen (B-7) at 75° F.

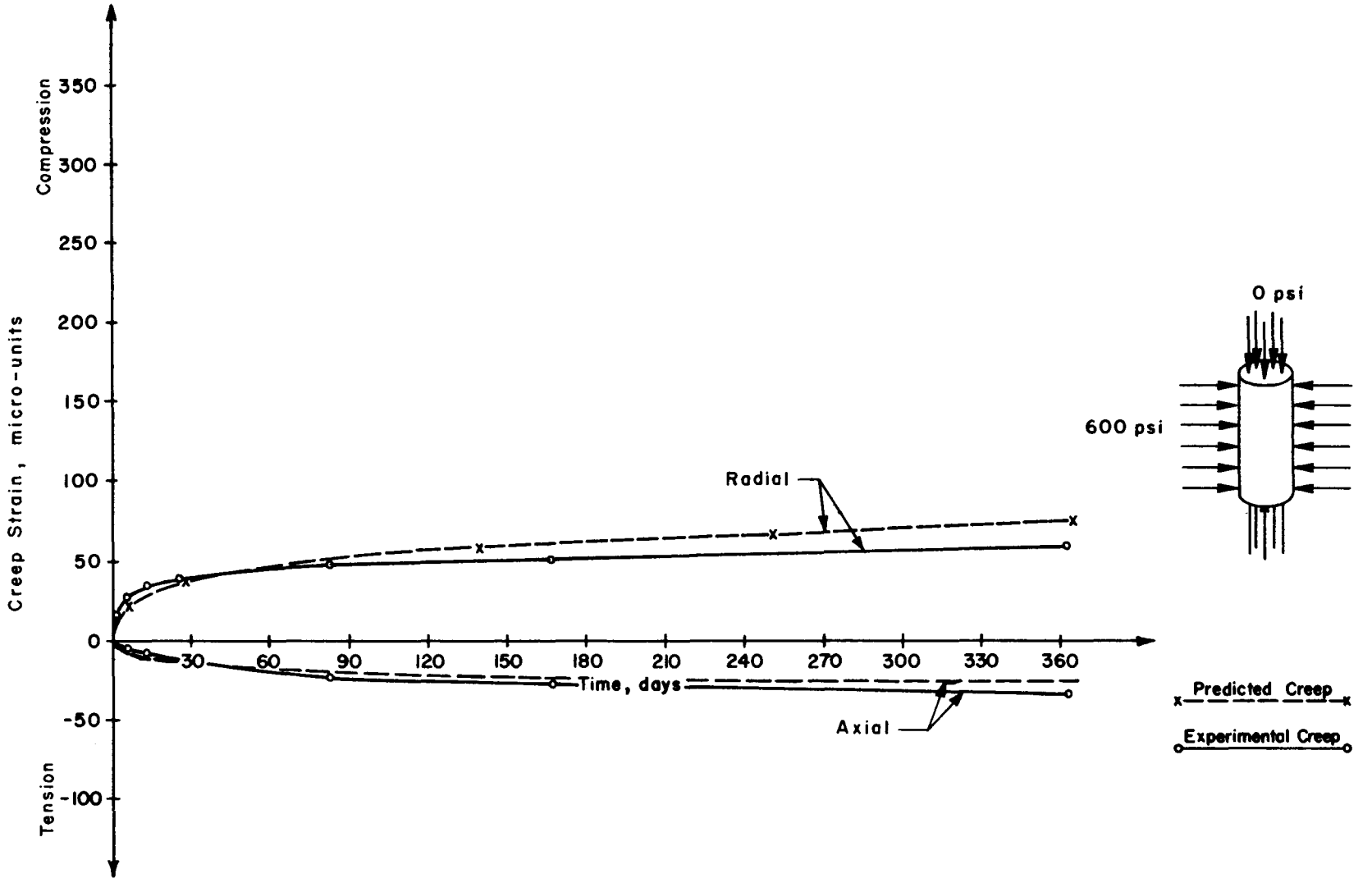

Fig 34. Predicted and experimental creep strain-time relationships for biaxially loaded as-cast specimen (F-13) at 75° F.

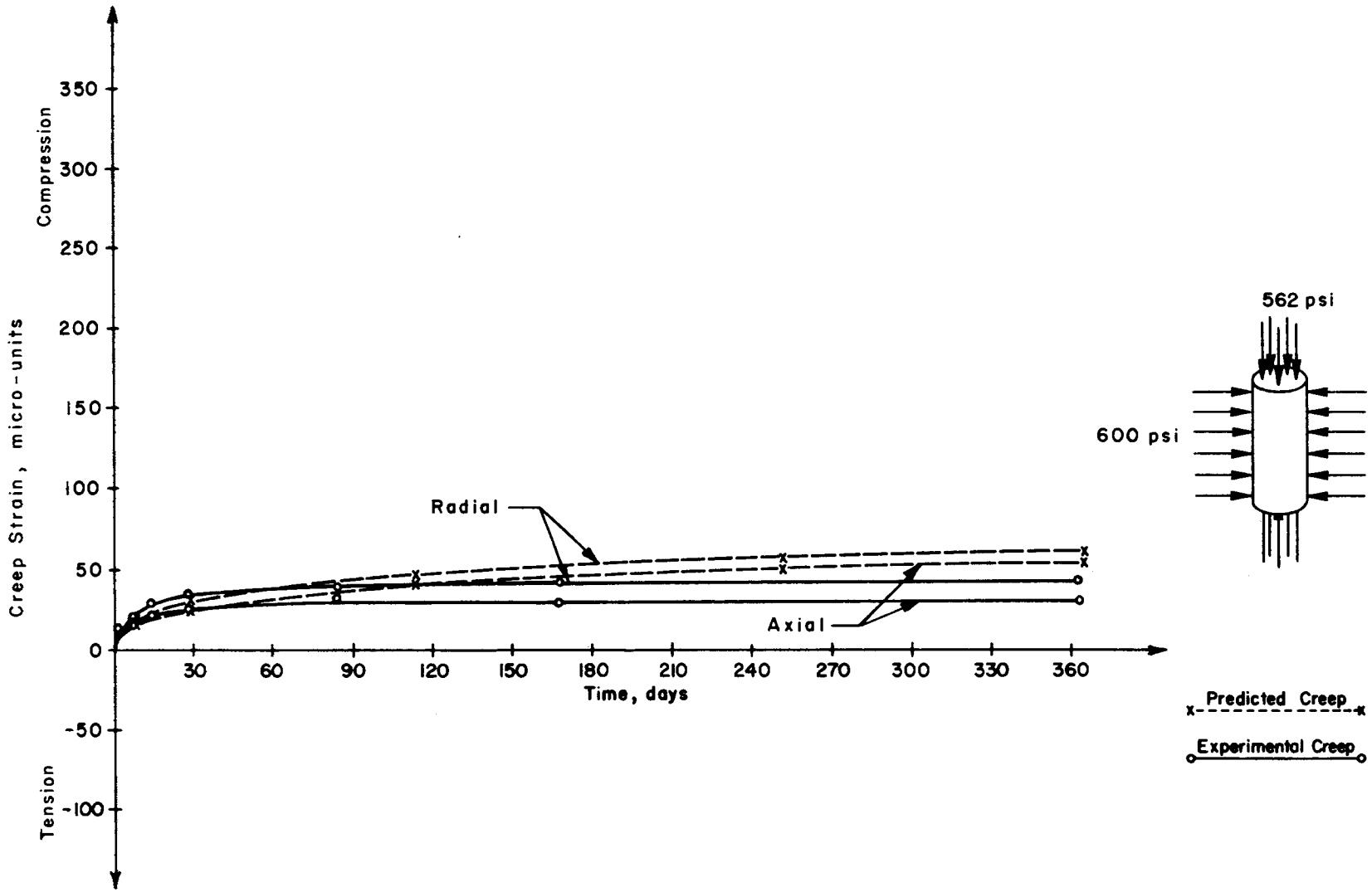

Fig 35. Predicted and experimental creep strain-time relationships for triaxially loaded as-cast specimen (E-5) at 75° F.

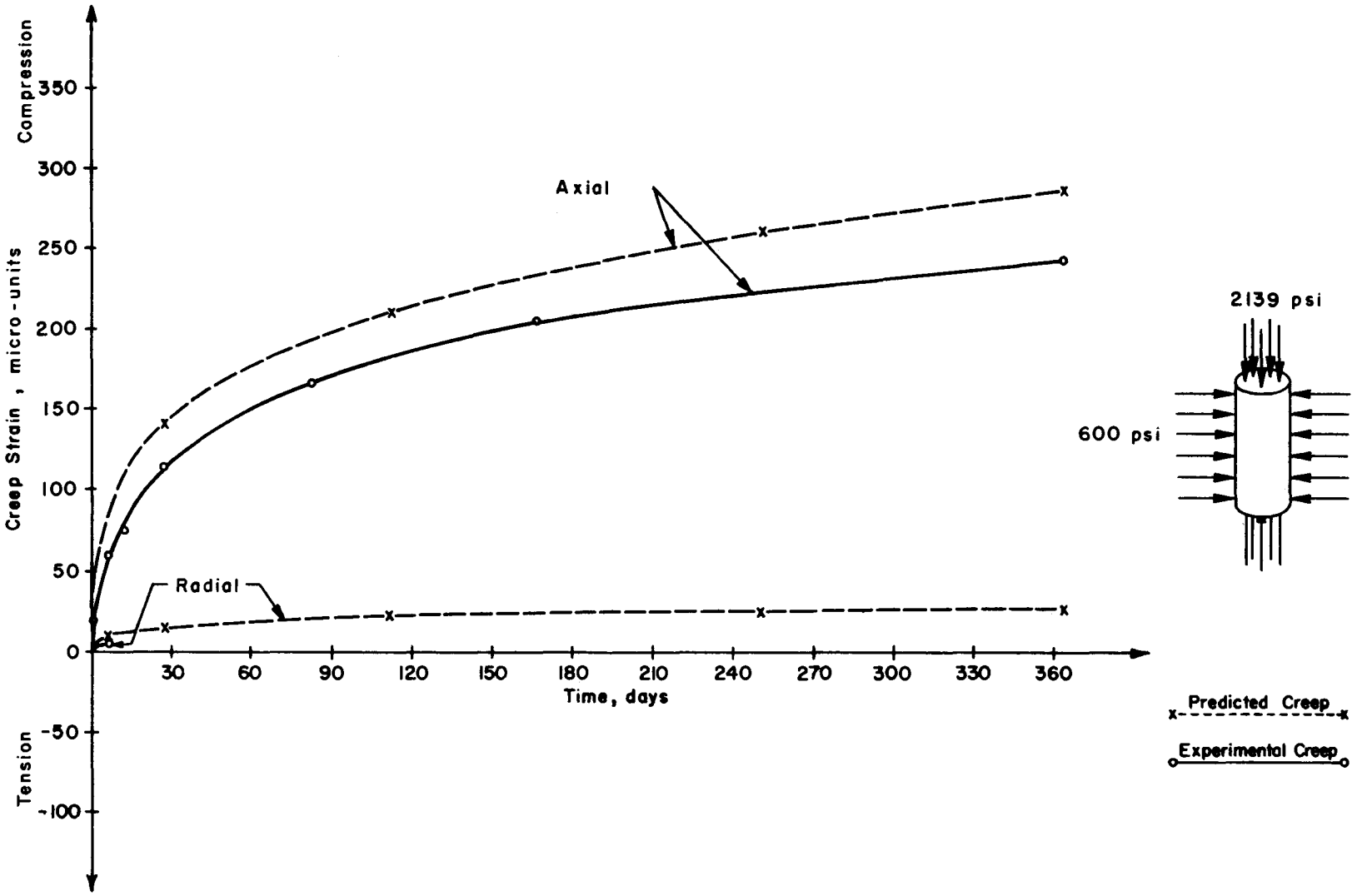

Fig 36. Predicted and experimental creep strain-time relationships for triaxially loaded as-cast specimen (C-23) at 75° F.

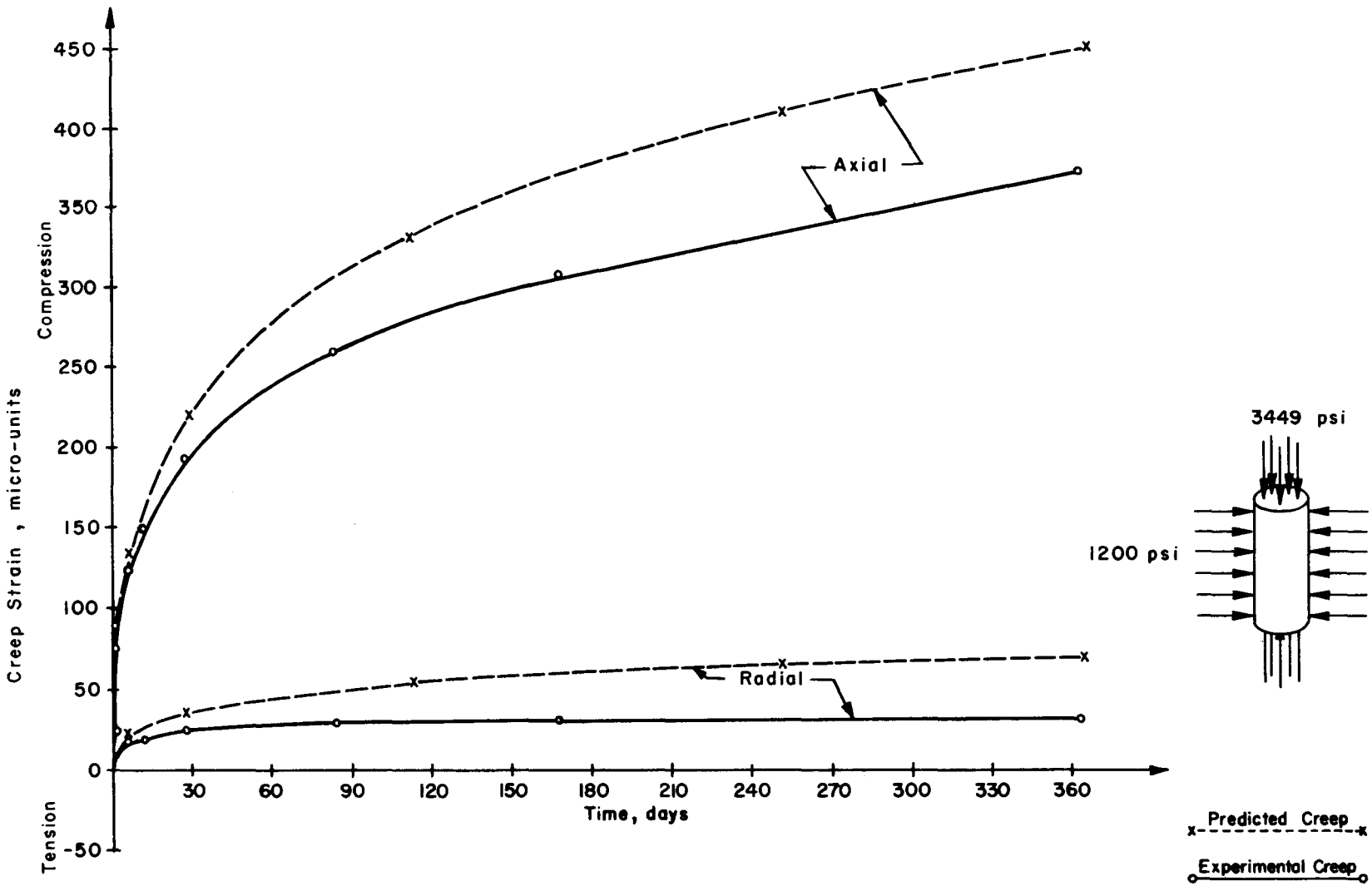

Fig 37. Predicted and experimental creep strain-time relationships for triaxially loaded as-cast specimen (D-26) at 75° F.

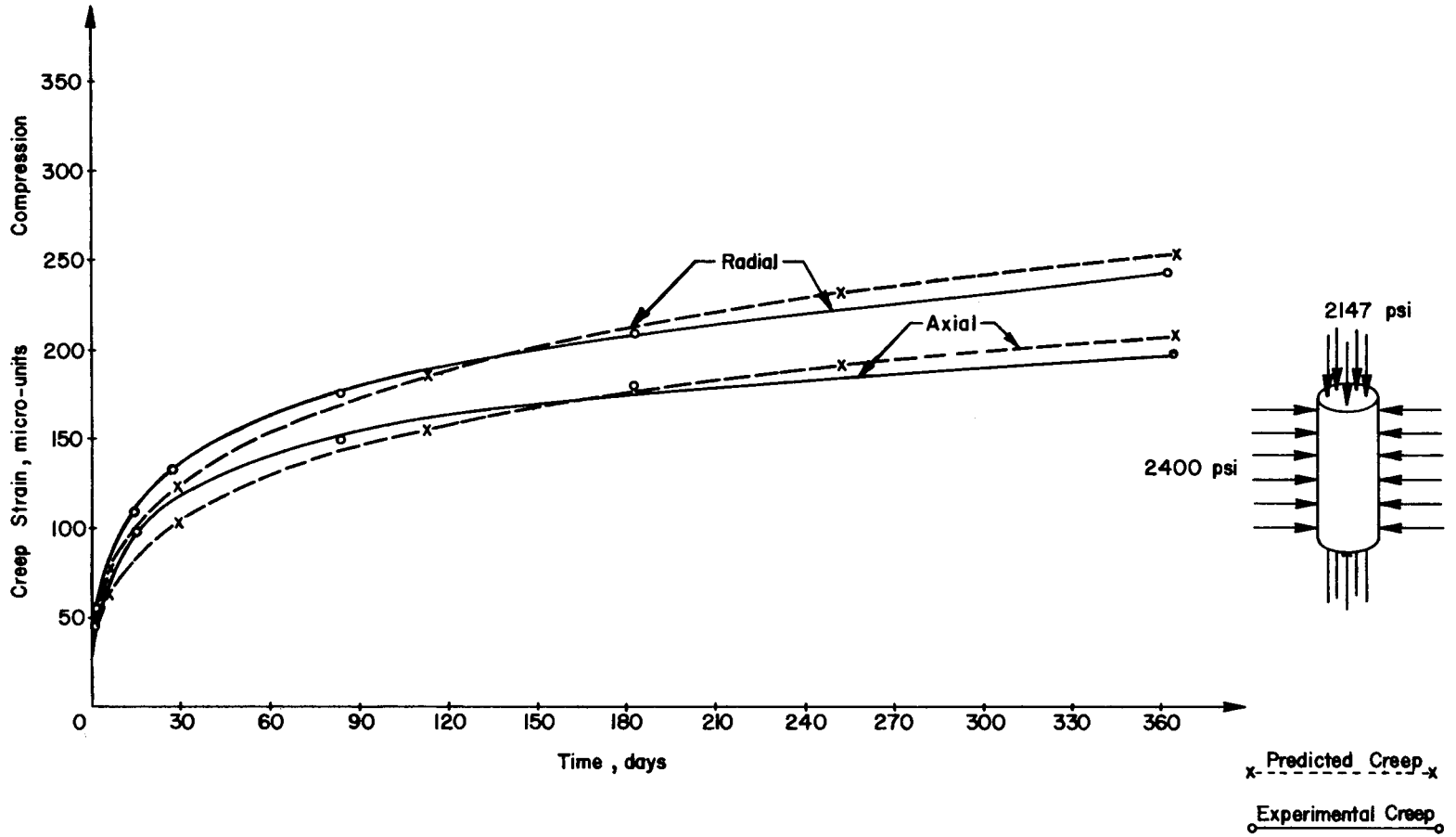

Fig 38. Predicted and experimental creep strain-time relationships for triaxially loaded as-cast specimen (F-9) at 75° F.

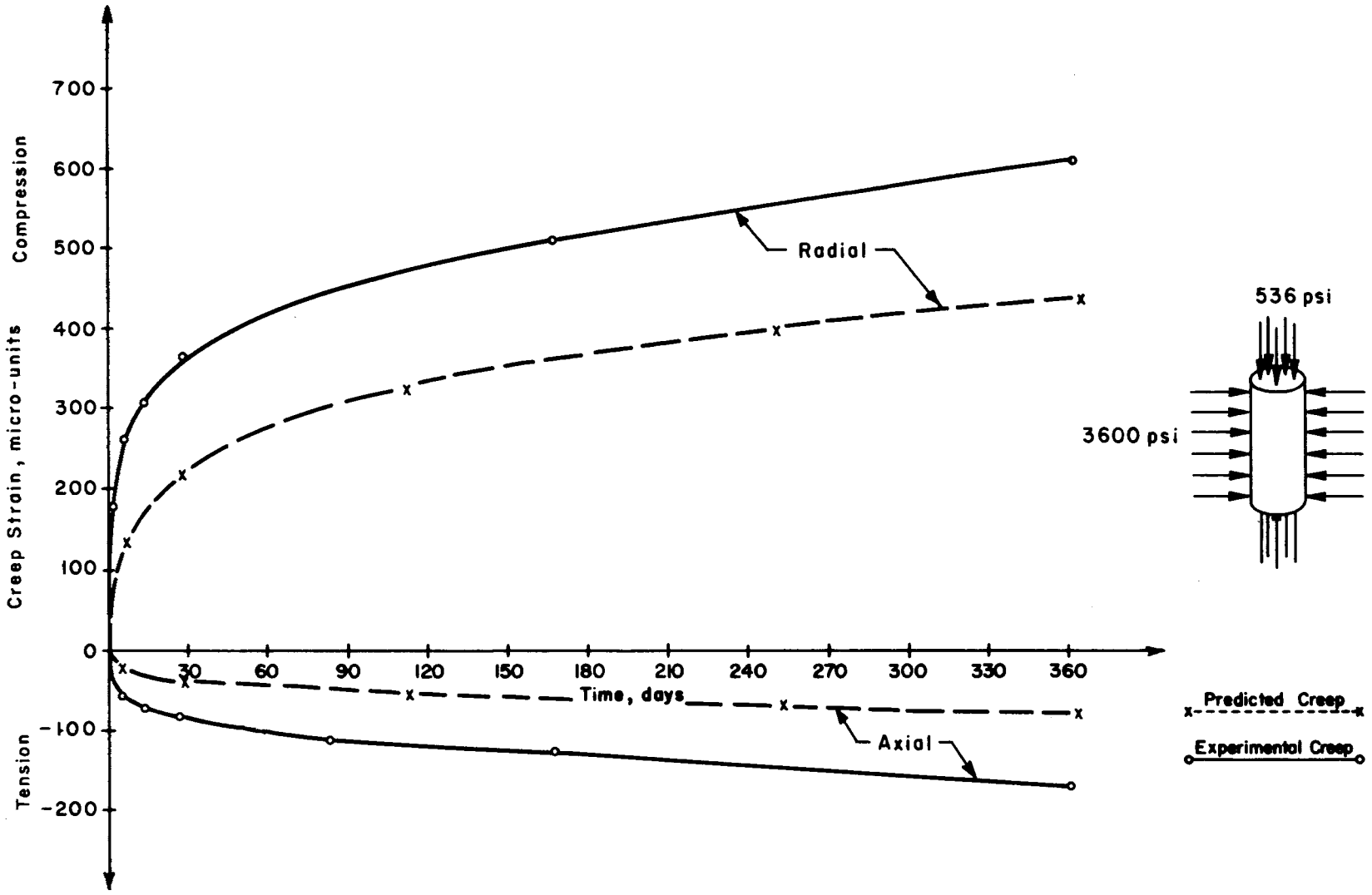

Fig 39. Predicted and experimental creep strain-time relationships for triaxially loaded as-cast specimen (G-35) at 75° F.

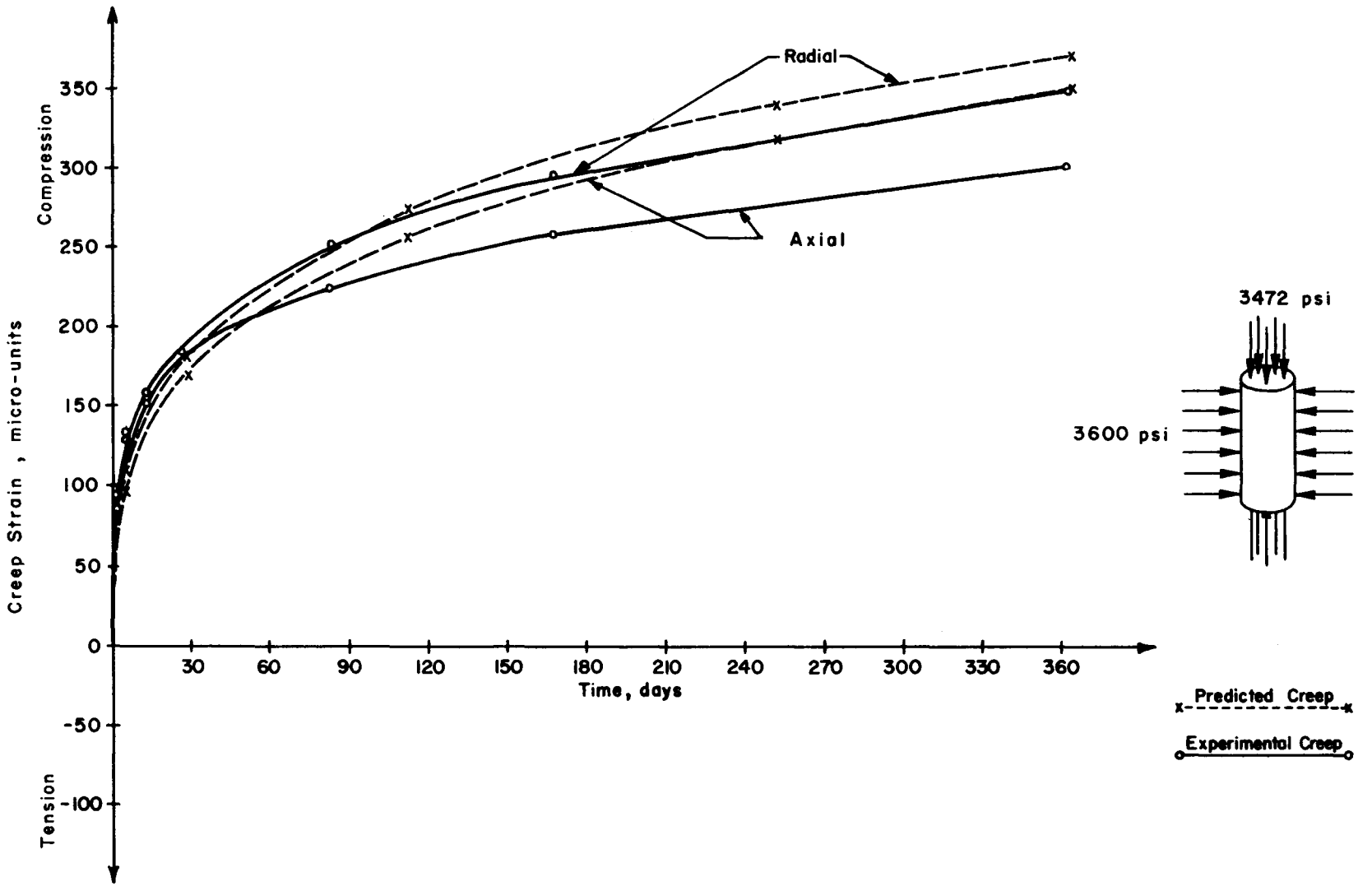

Fig 40. Predicted and experimental creep strain-time relationships for triaxially loaded as-cast specimen (D-31) at 75° F.

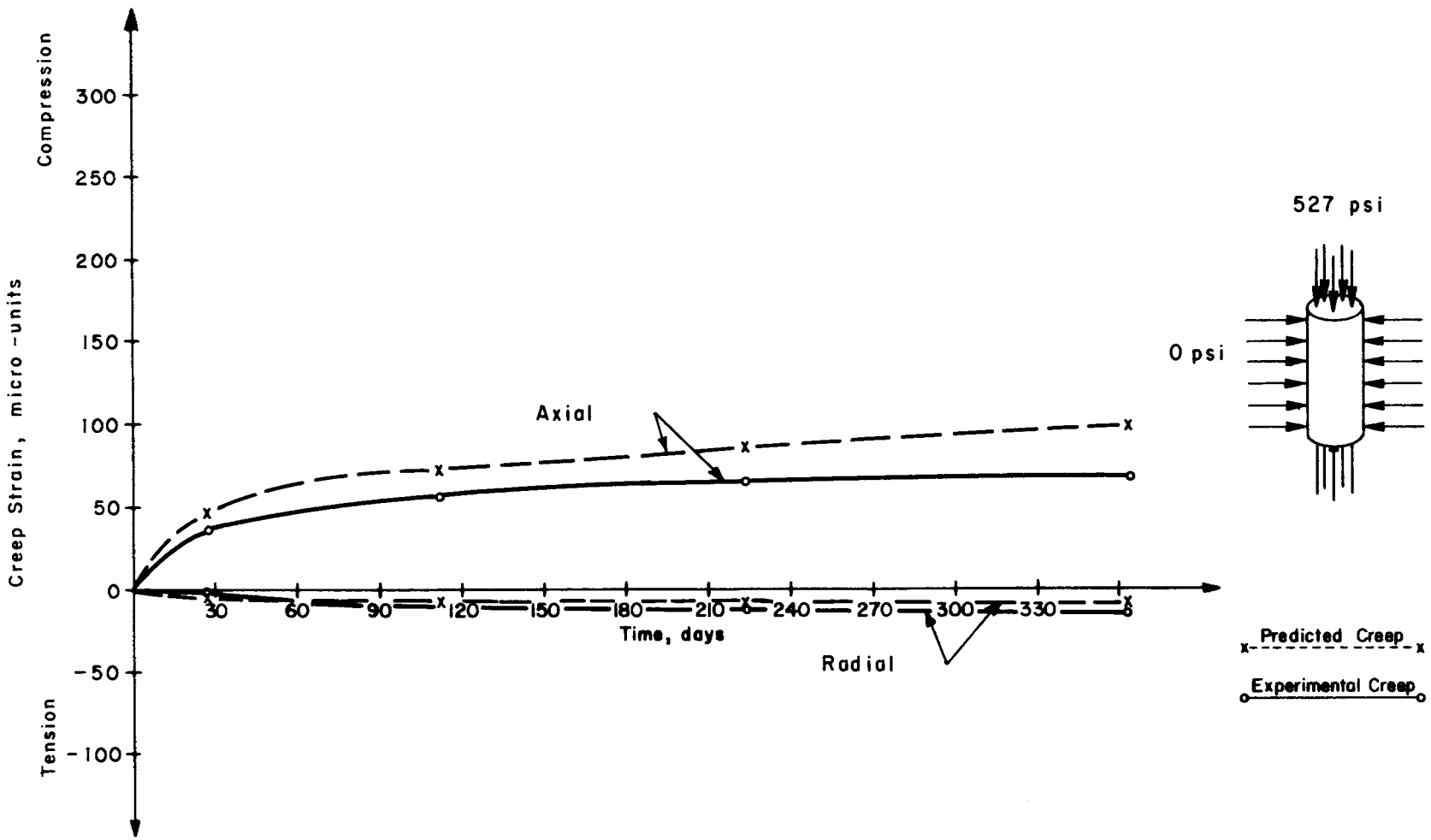

Fig 41. Predicted and experimental creep strain-time relationships for uniaxially loaded air-dried specimen (E-40) at 75° F.

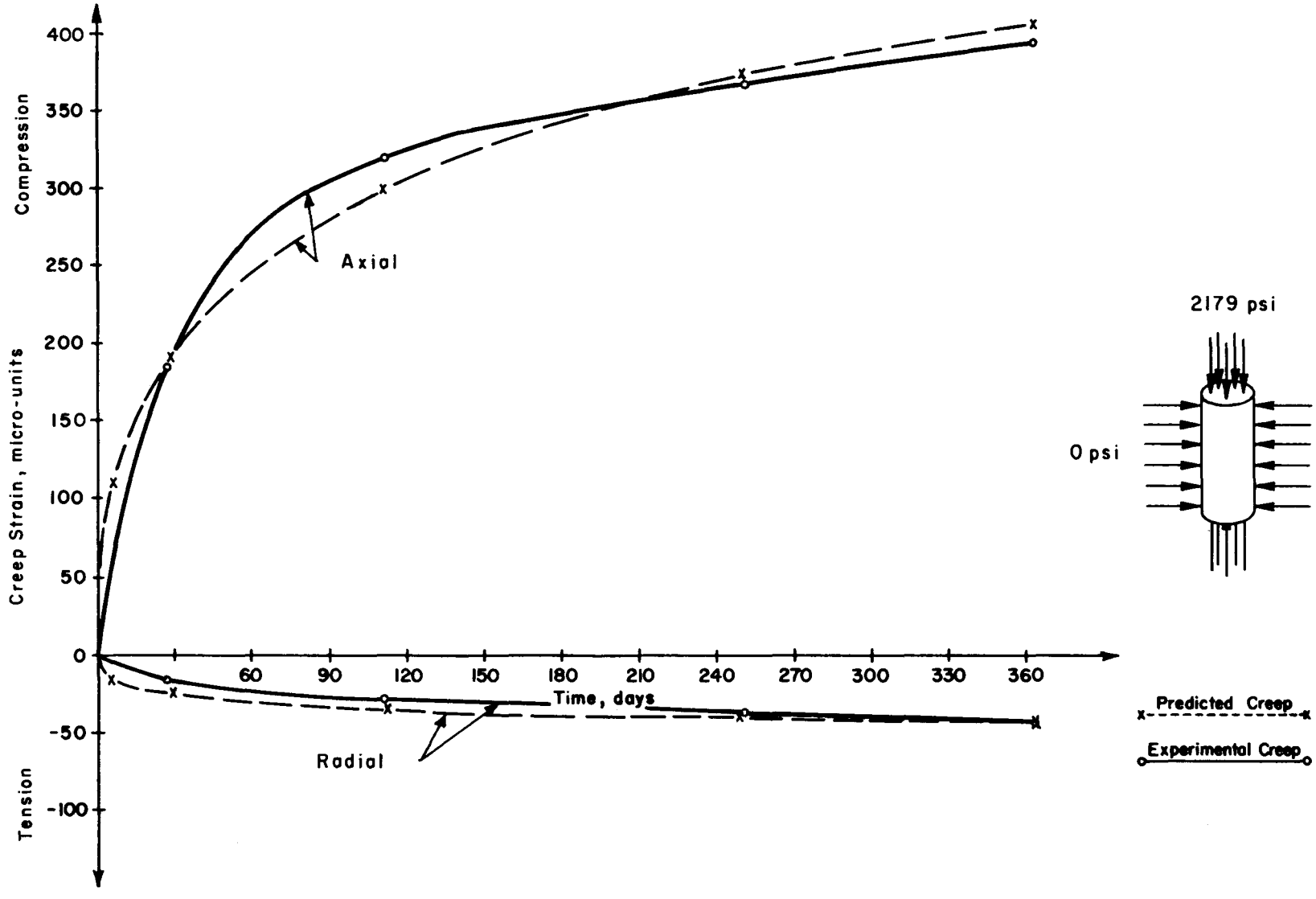

Fig 42. Predicted and experimental creep strain-time relationships for uniaxially loaded air-dried specimen (B-19) at 75° F.

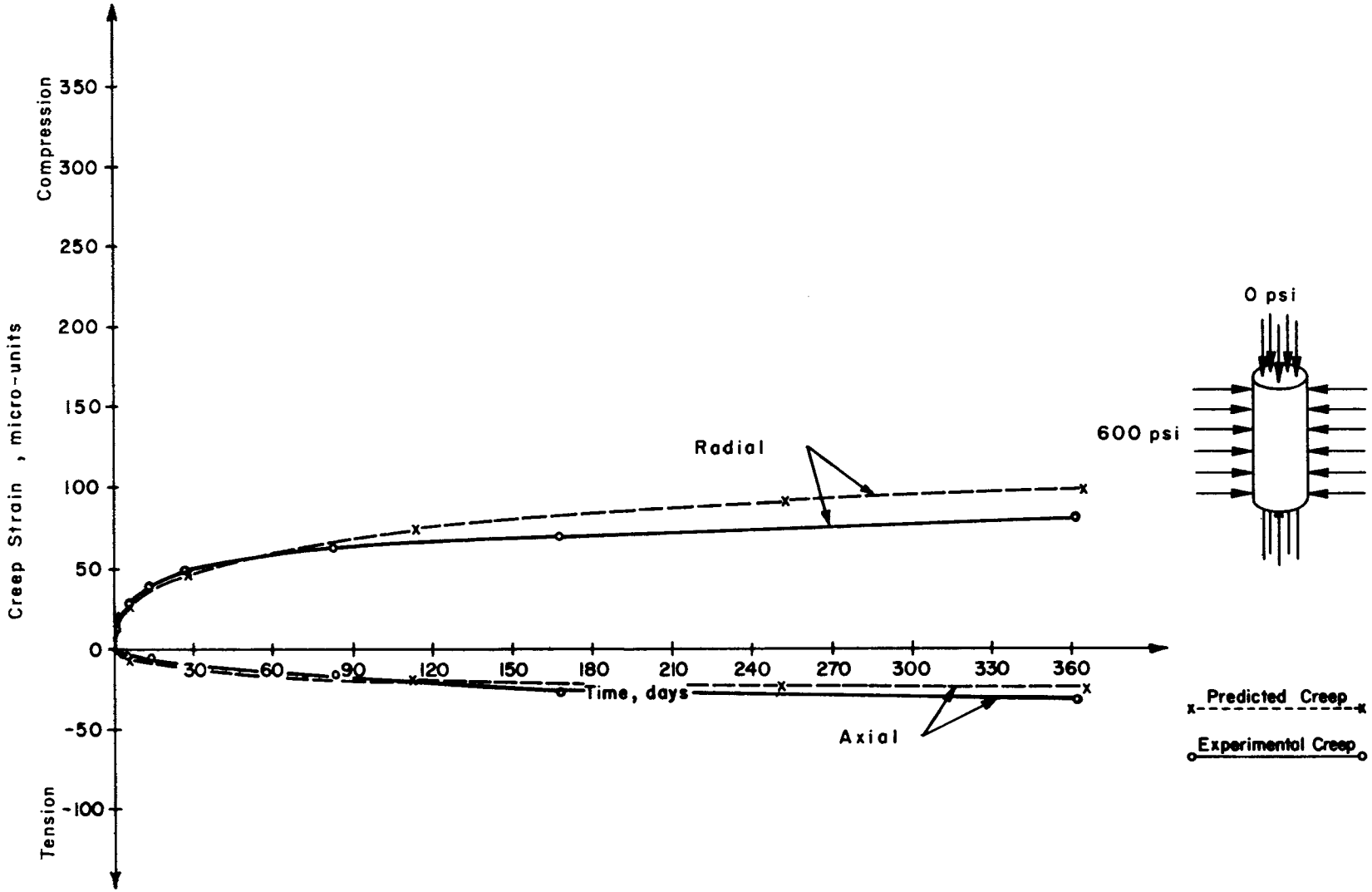

Fig 43. Predicted and experimental creep strain-time relationships for biaxially loaded air-dried specimen (F-42) at 75° F.

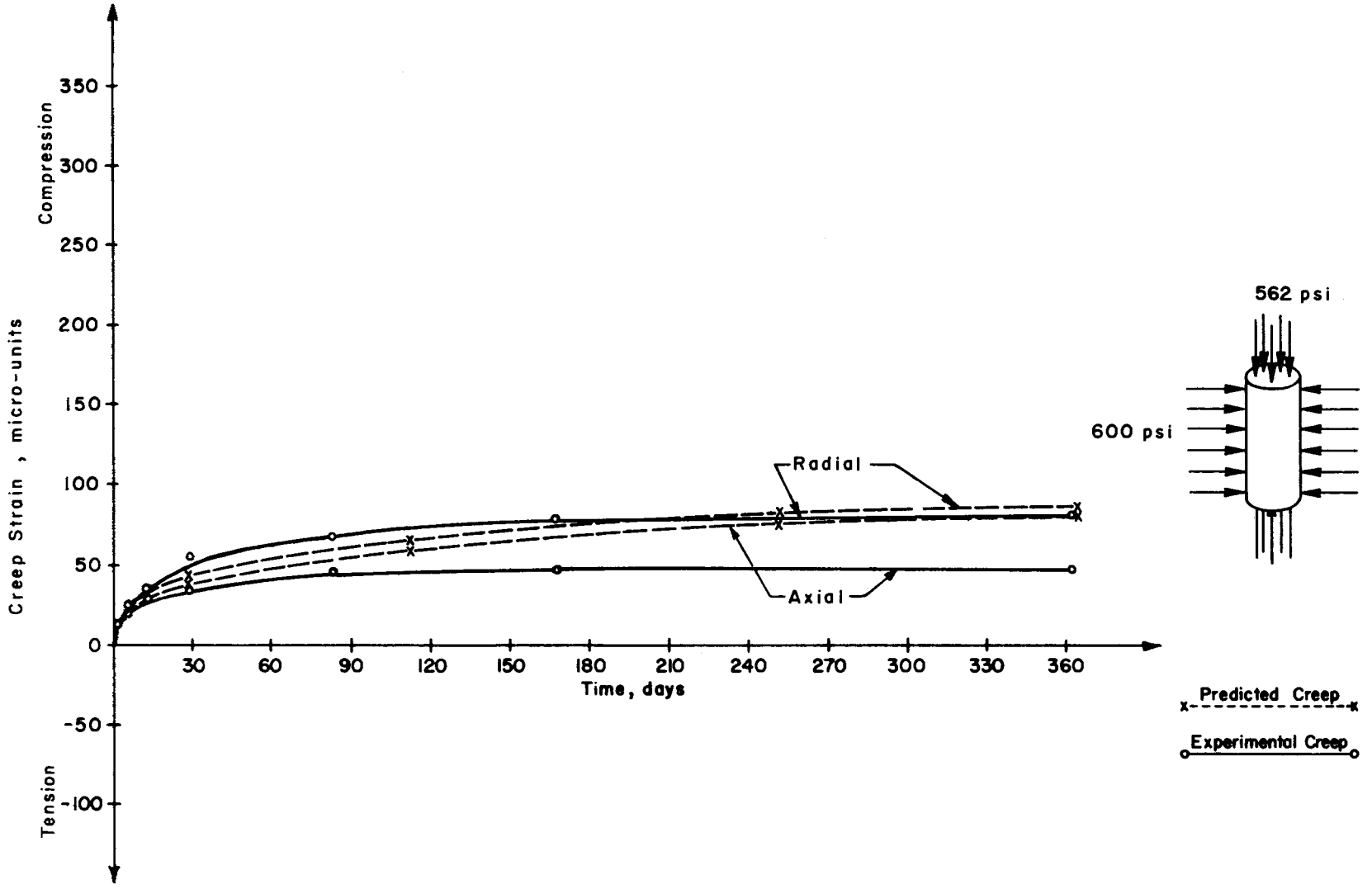

Fig 44. Predicted and experimental creep strain-time relationships for triaxially loaded air-dried specimen (E-13) at 75° F.

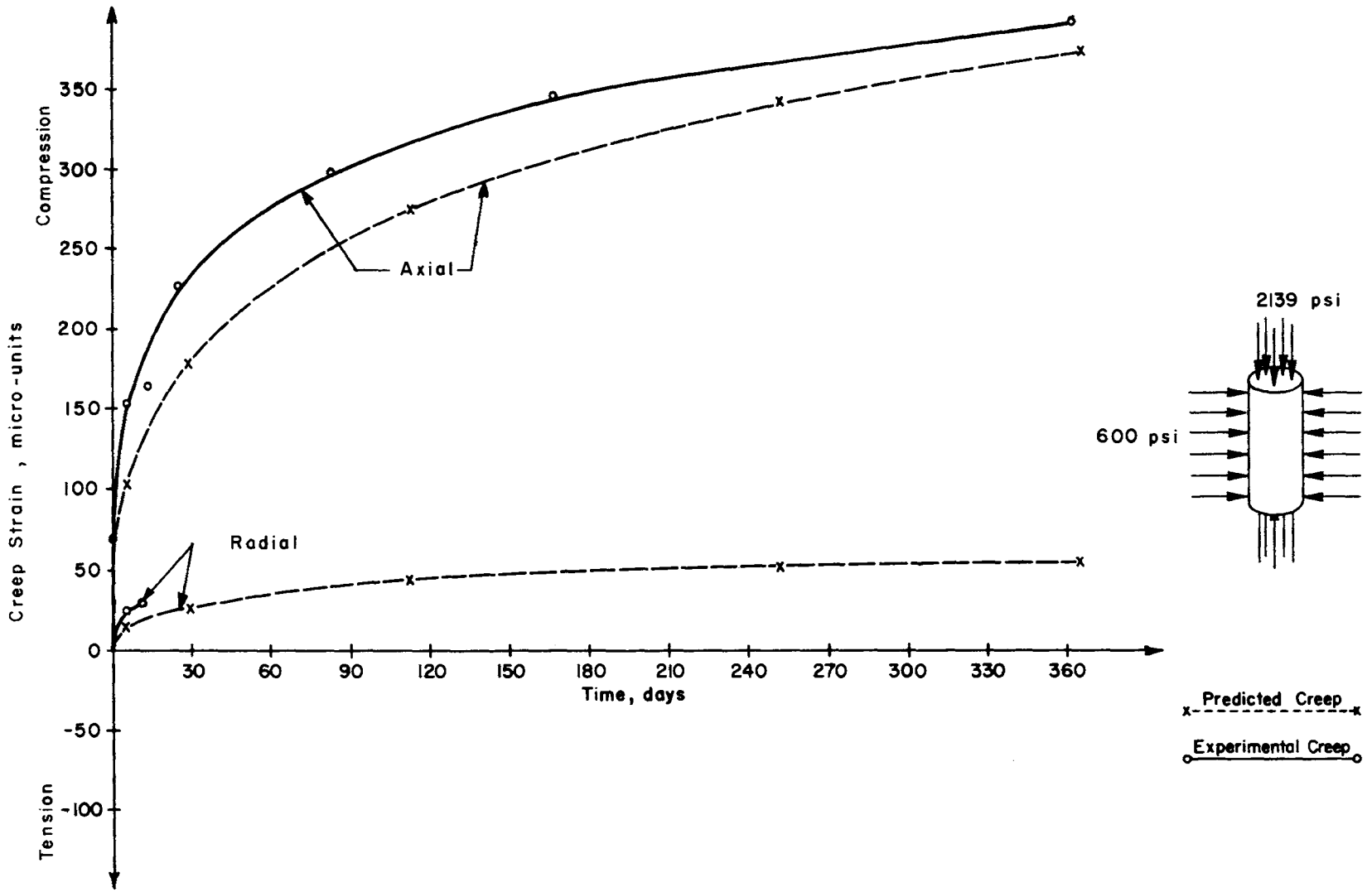

Fig 45. Predicted and experimental creep strain-time relationships for triaxially loaded air-dried specimen (C-11) at 75° F.

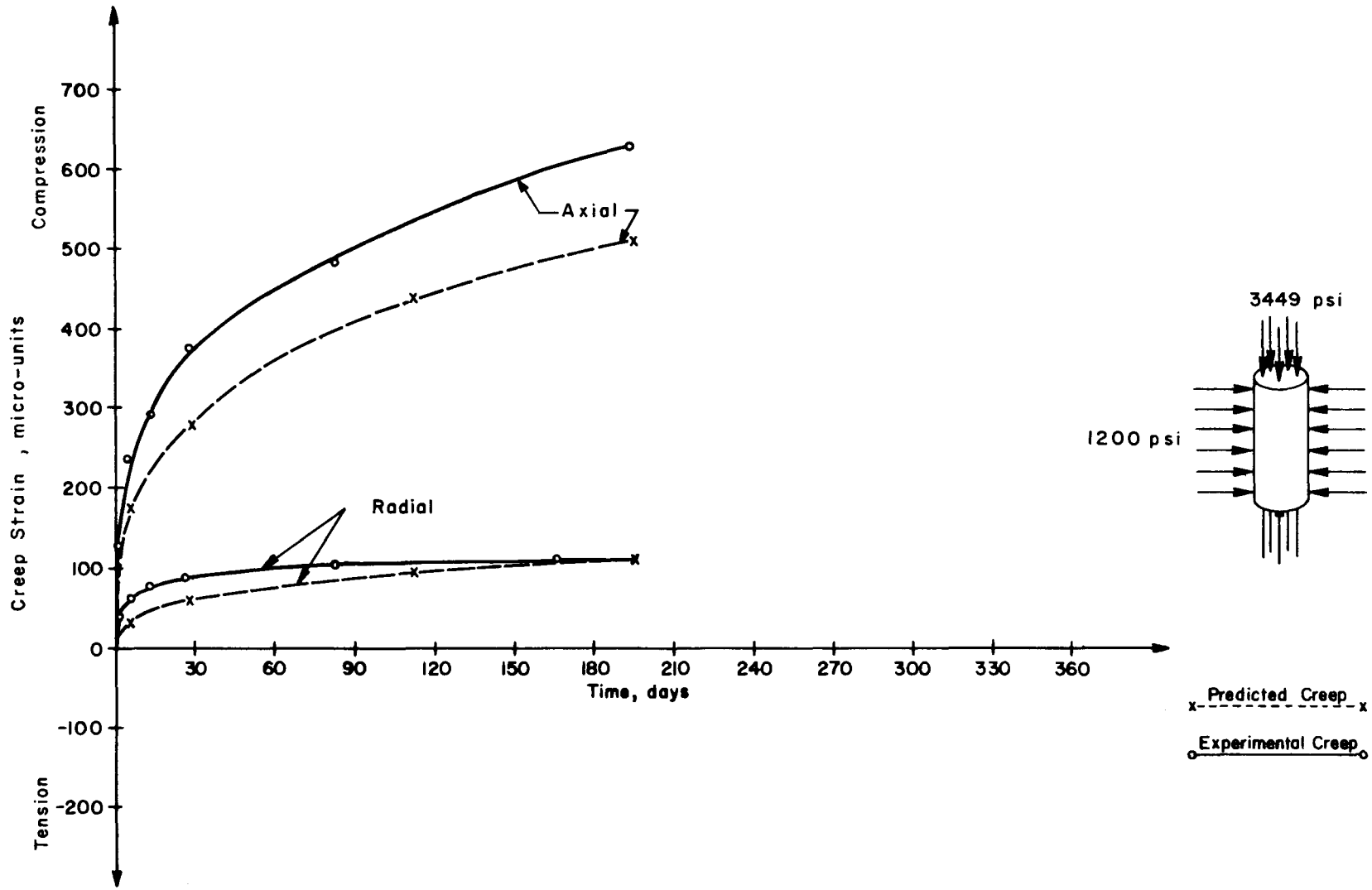

Fig 46. Predicted and experimental creep strain-time relationships for triaxially loaded air-dried specimen (D-44) at 75° F.

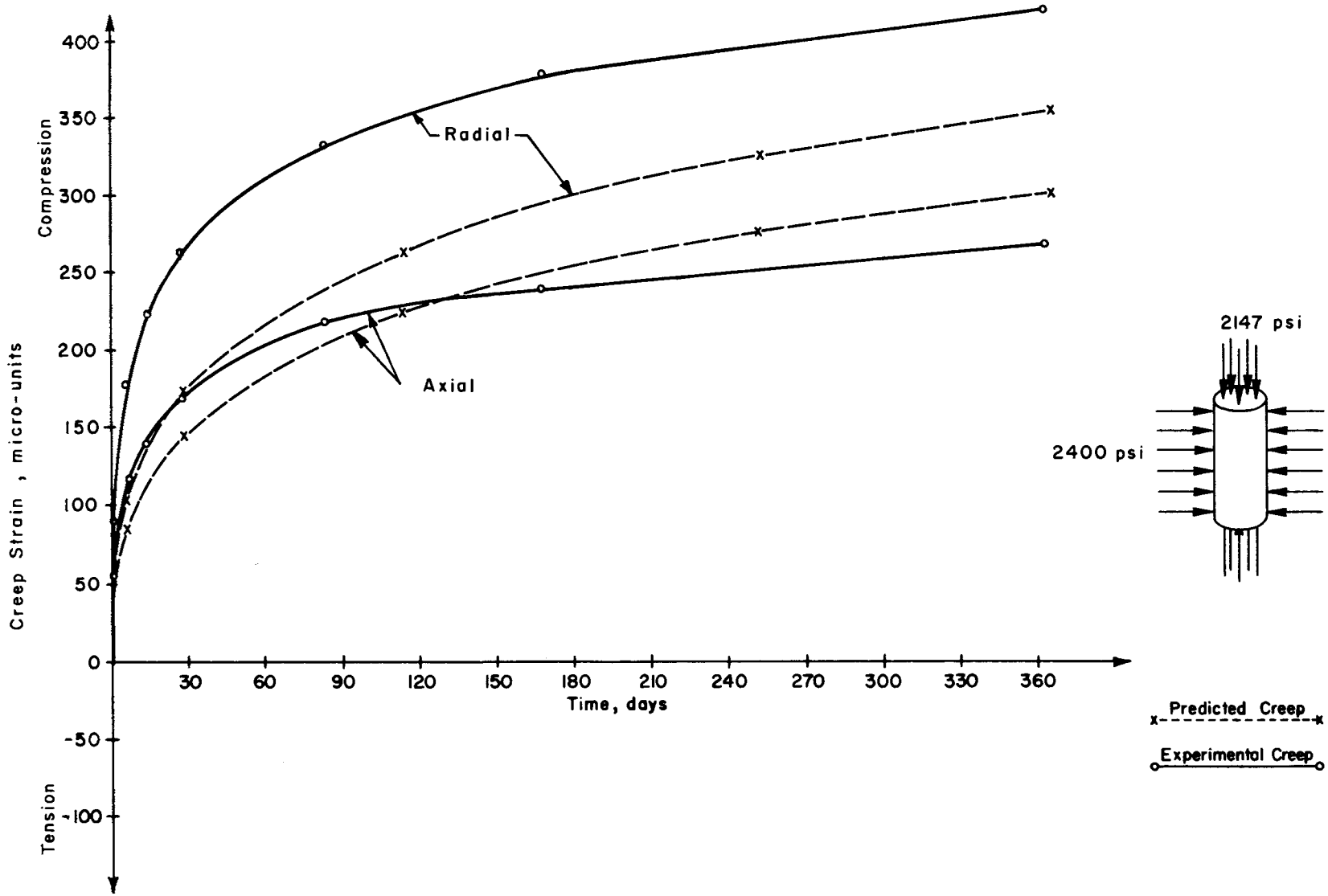

Fig 47. Predicted and experimental creep strain-time relationships for triaxially loaded air-dried specimen (F-30) at 75° F.

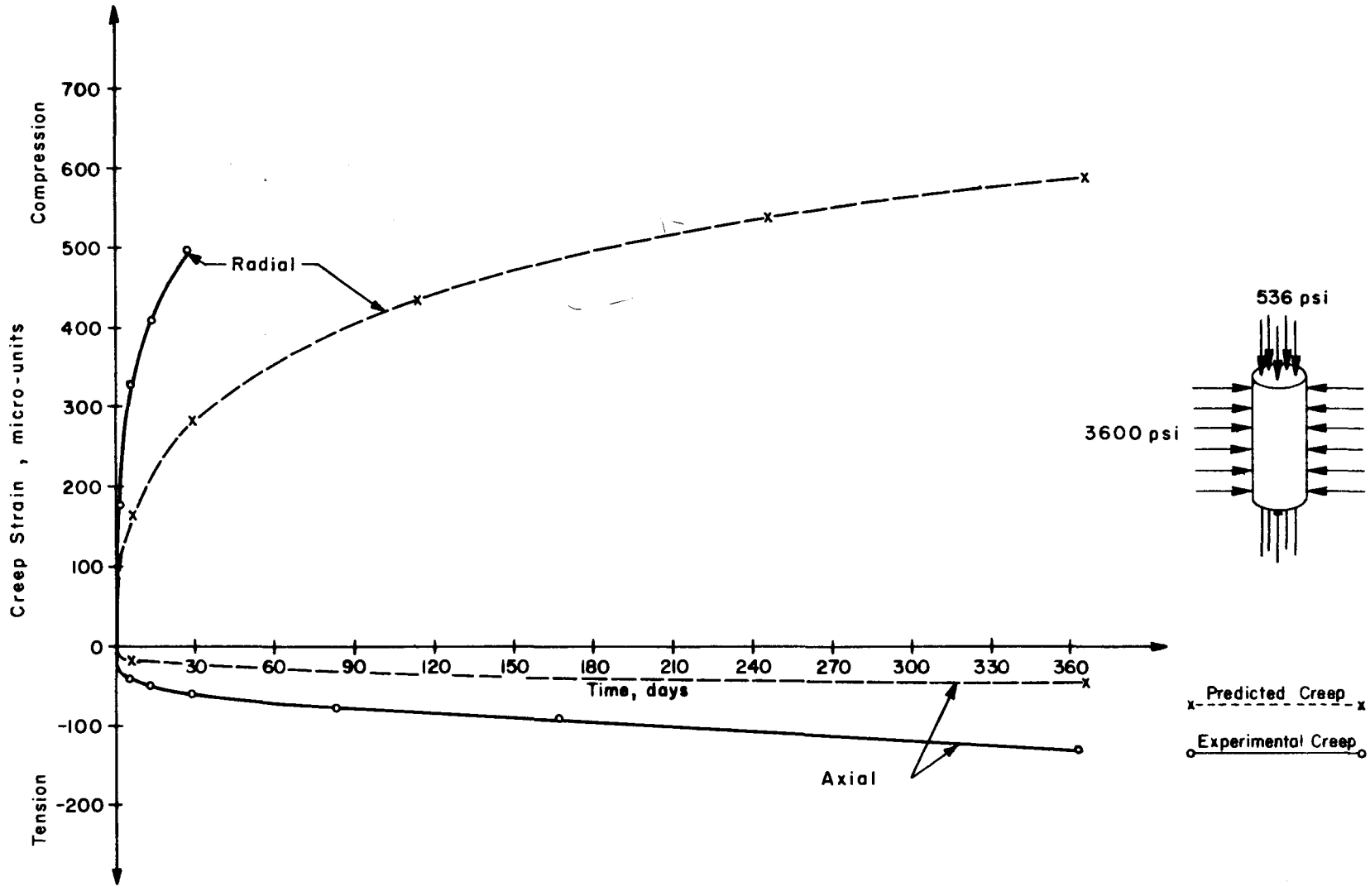

Fig 48. Predicted and experimental creep strain-time relationships for triaxially loaded air-dried specimen (G-30) at 75° F.

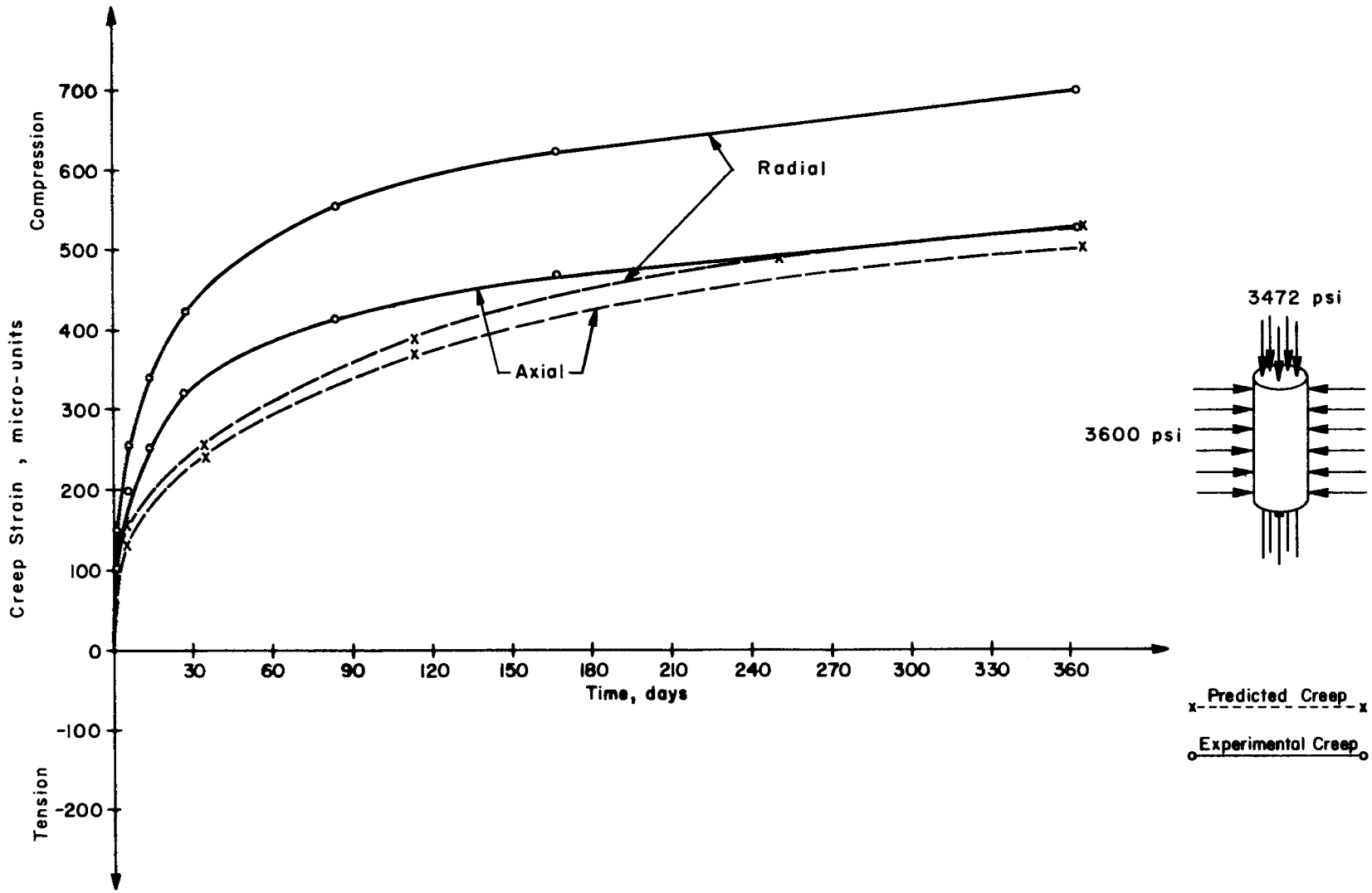

Fig 49. Predicted and experimental creep strain-time relationships for triaxially loaded air-dried specimen (D-40) at 75° F.

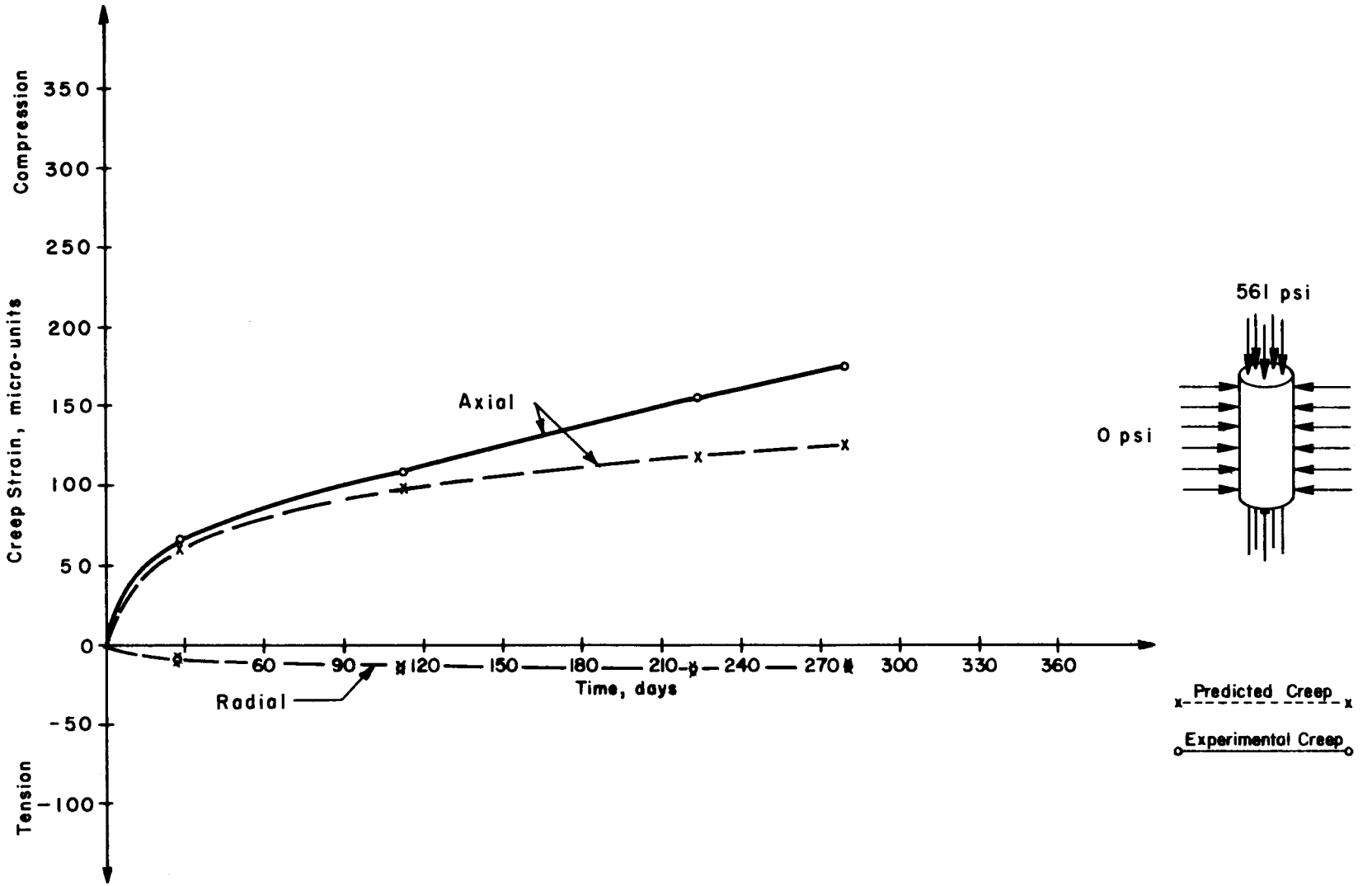

Fig 50. Predicted and experimental creep strain-time relationships for uniaxially loaded as-cast specimen (B-4) at 150° F.

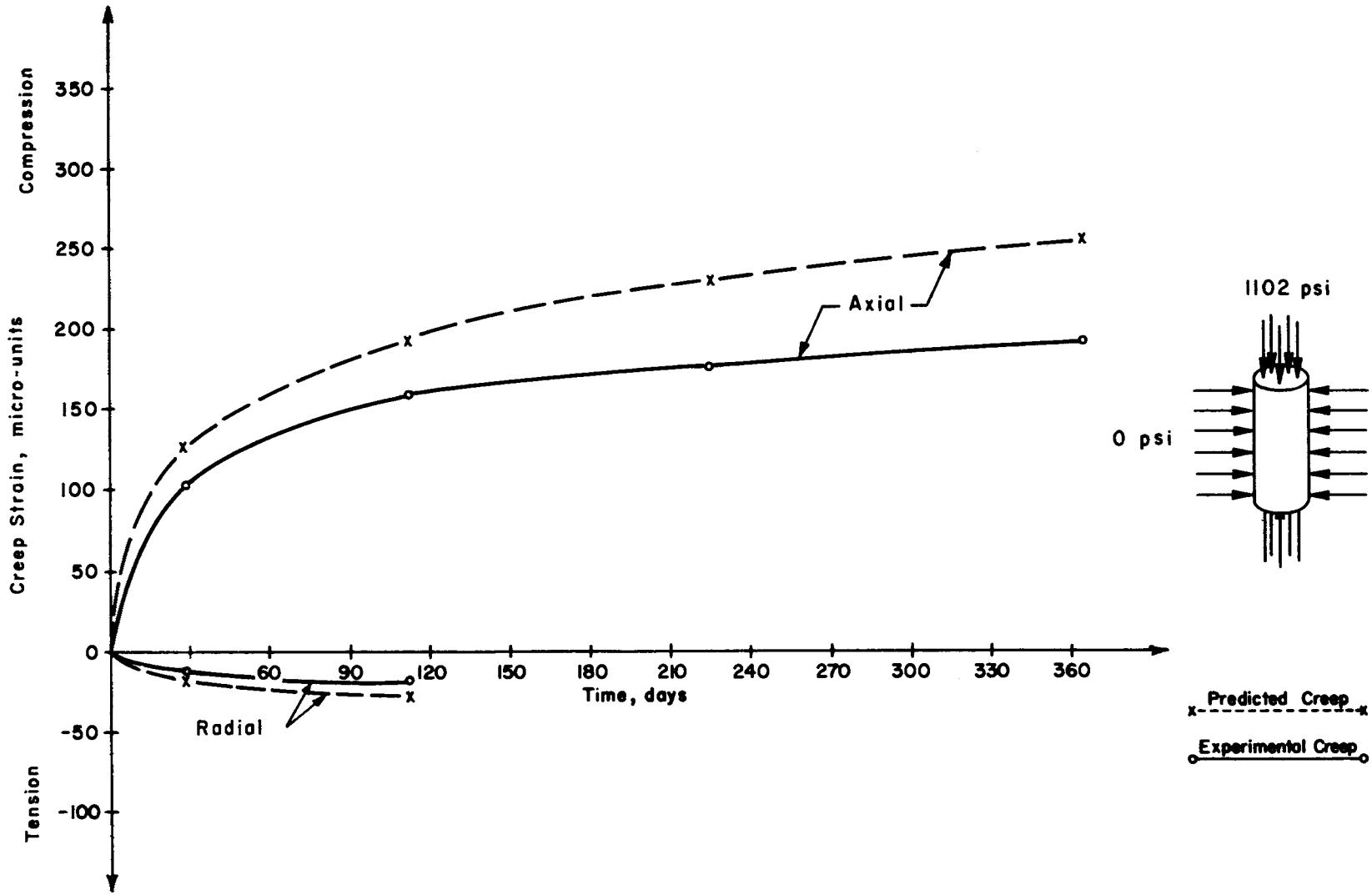

Fig 51. Predicted and experimental creep strain-time relationships for uniaxially loaded as-cast specimen (B-15) at 150° F.

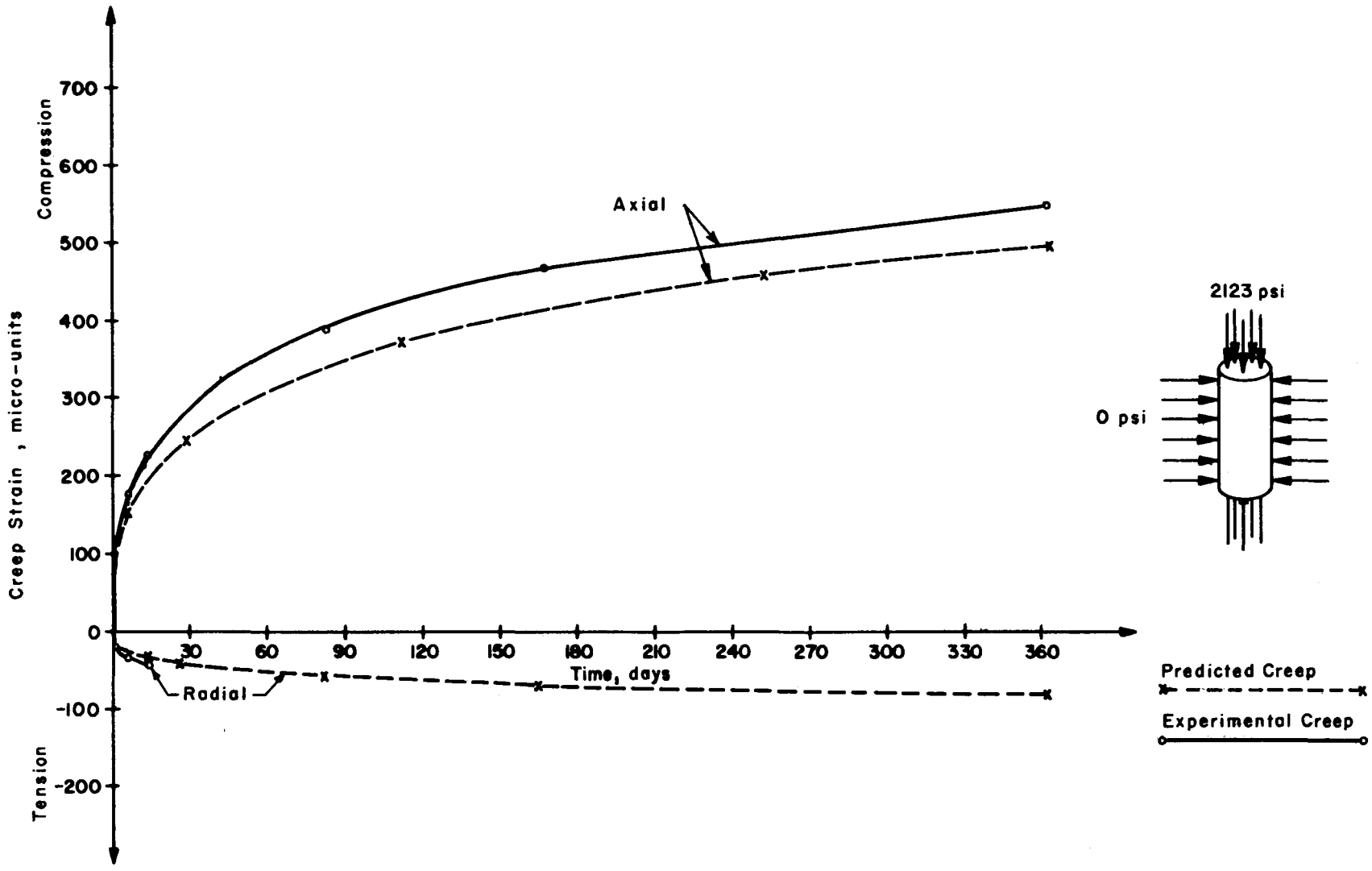

Fig 52. Predicted and experimental creep strain-time relationships for uniaxially loaded as-cast specimen (F-33) at 150° F.

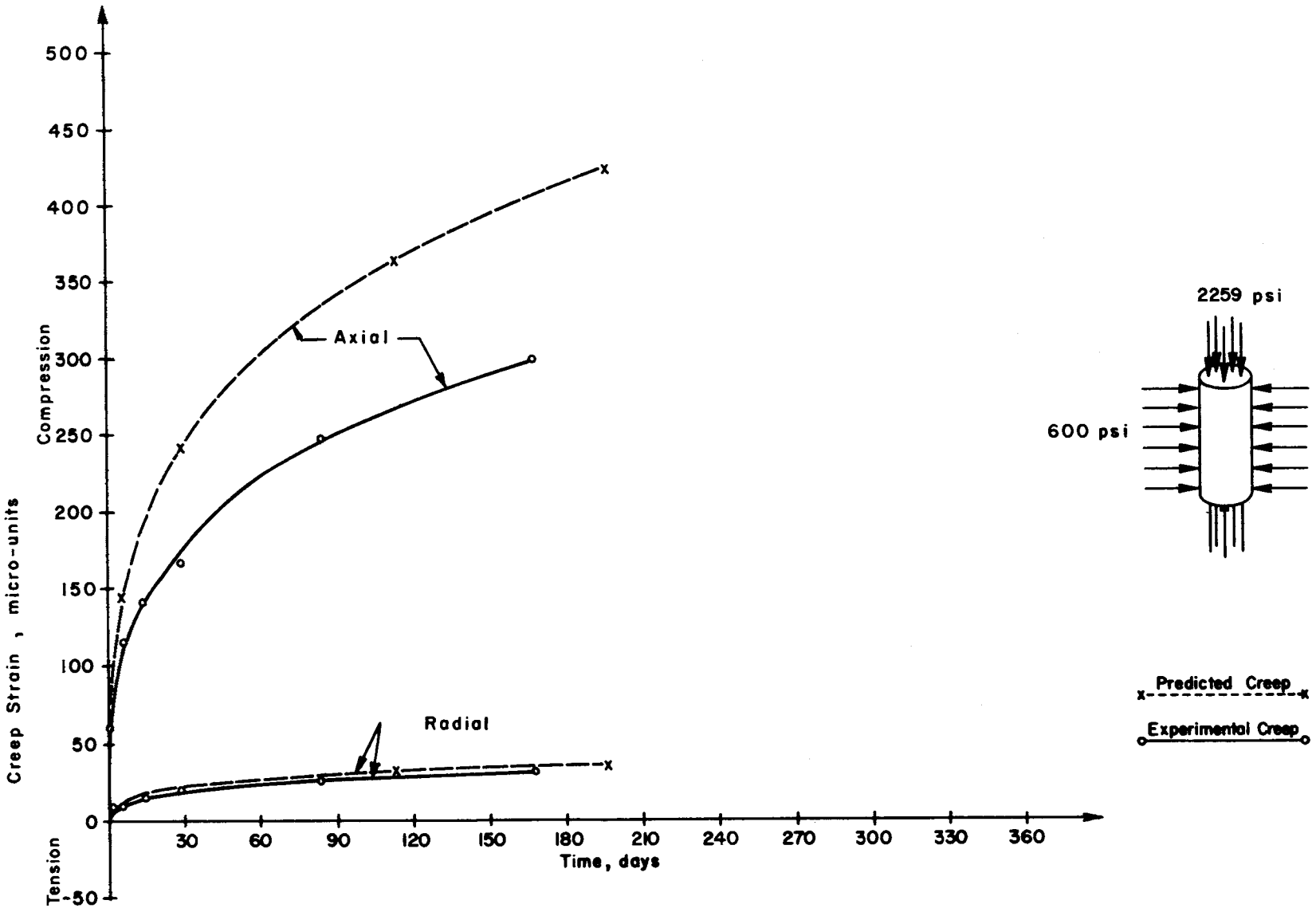

Fig 53. Predicted and experimental creep strain-time relationships for triaxially loaded as-cast specimen (E-18) at 150° F.

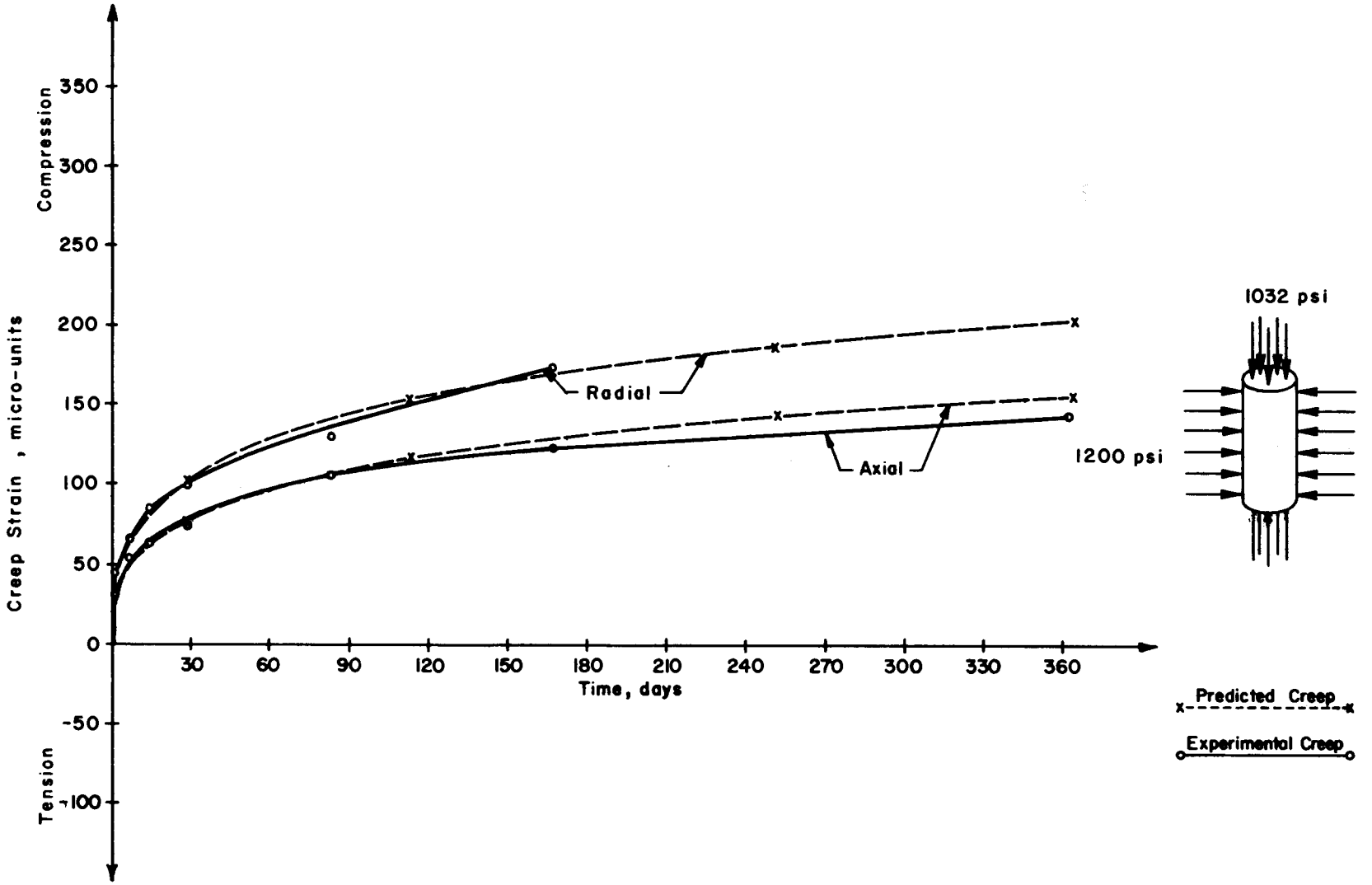

Fig 54. Predicted and experimental creep strain-time relationships for triaxially loaded as-cast specimen (C-12) at 150° F.

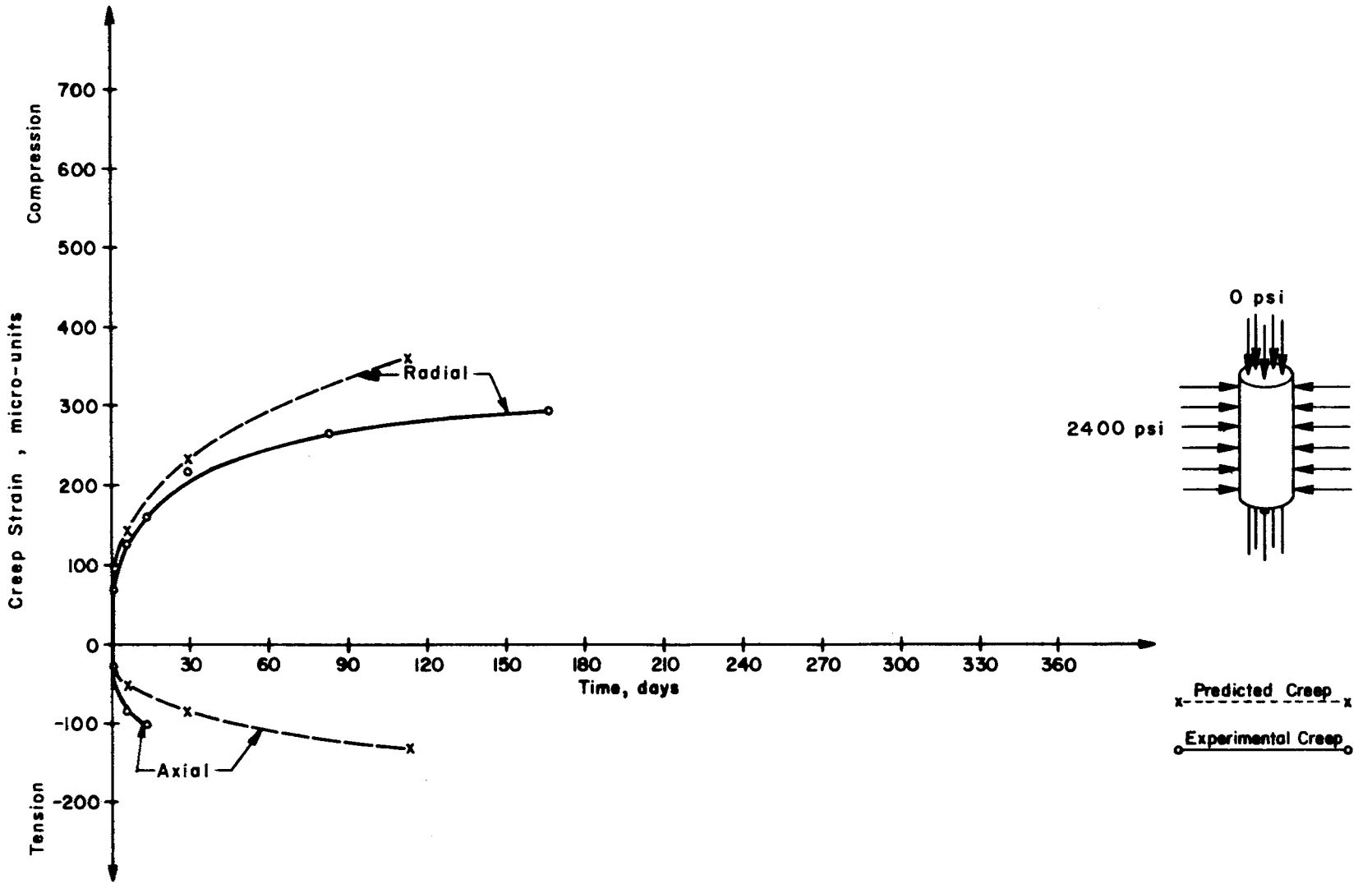

Fig 55. Predicted and experimental creep strain-time relationships for biaxially loaded as-cast specimen (E-43) at 150° F.

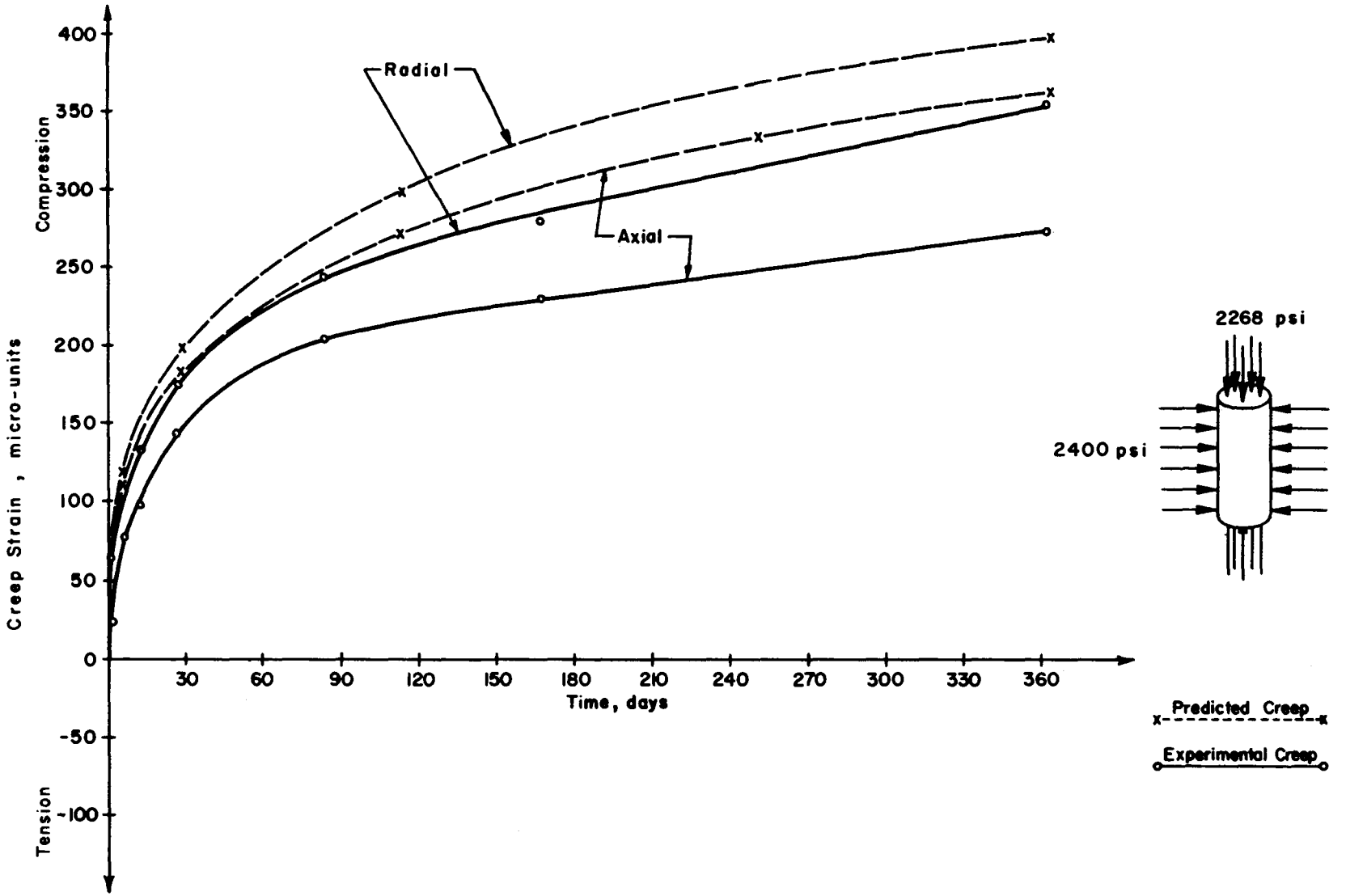

Fig 56. Predicted and experimental creep strain-time relationships for triaxially loaded as-cast specimen (G-9) at 150° F.

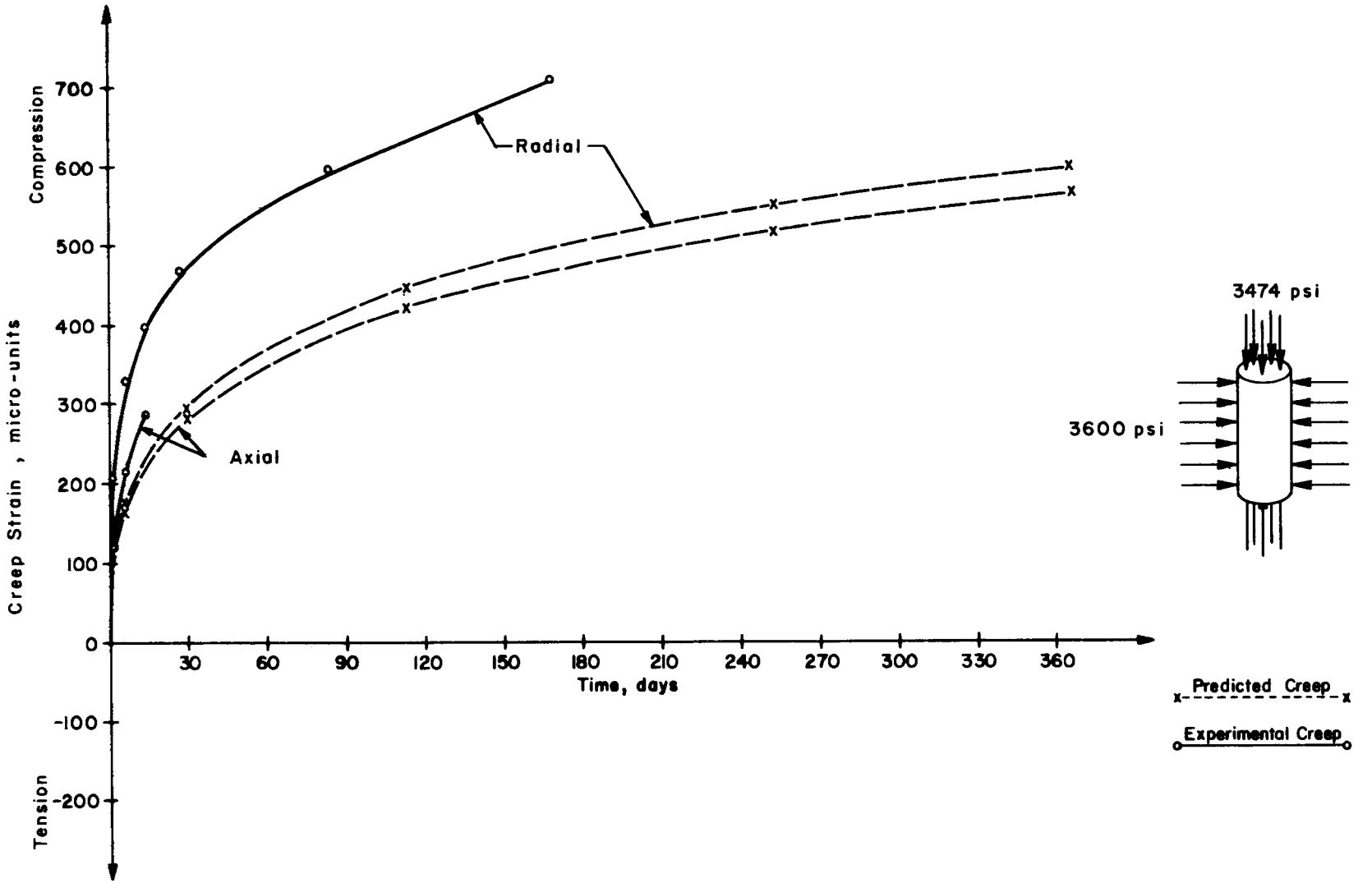

Fig 57. Predicted and experimental creep strain-time relationships for triaxially loaded as-cast specimen (F-20) at 150° F.

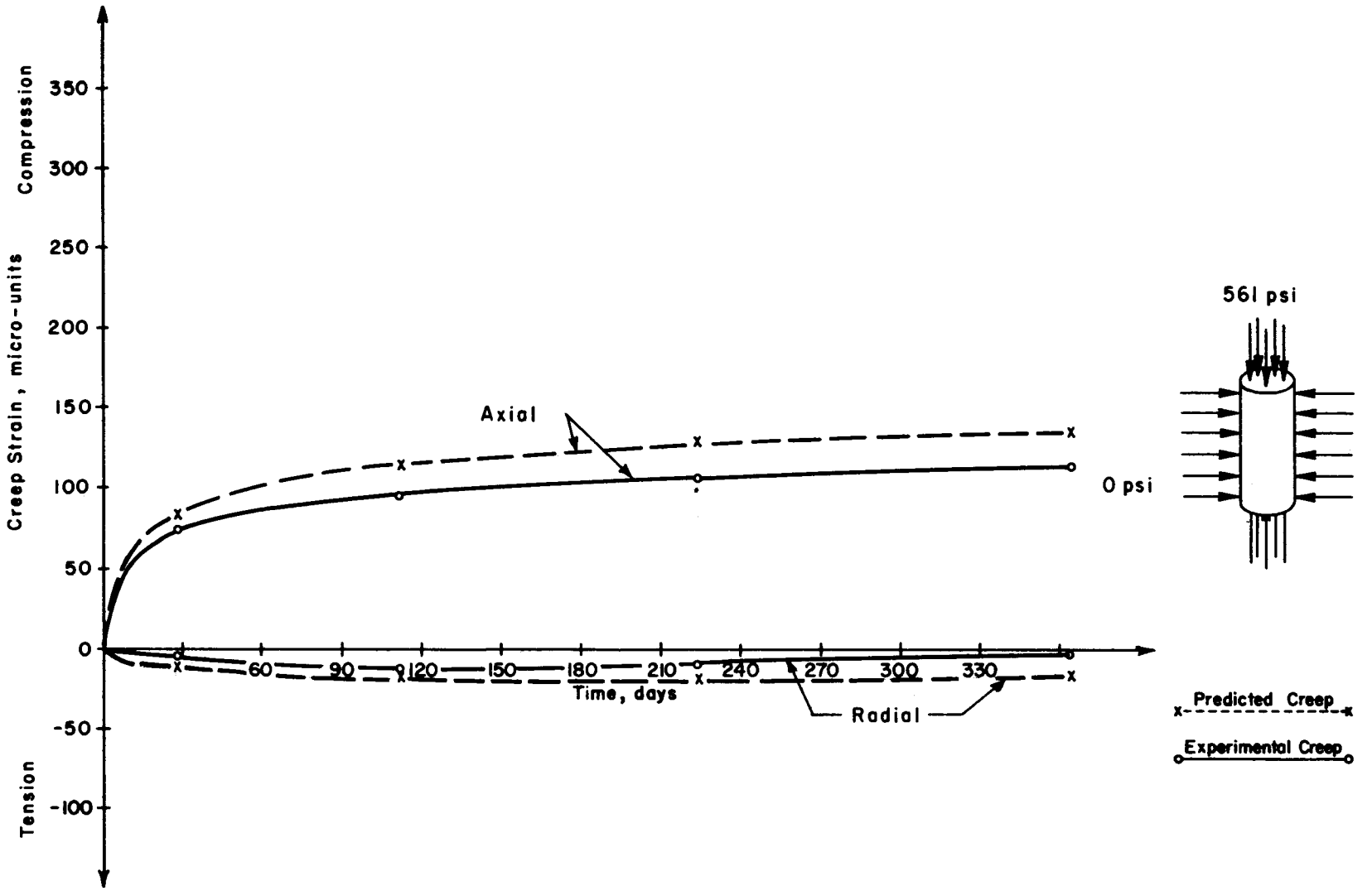

Fig 58. Predicted and experimental creep strain-time relationships for uniaxially loaded air-dried specimen (B-1) at 150° F.

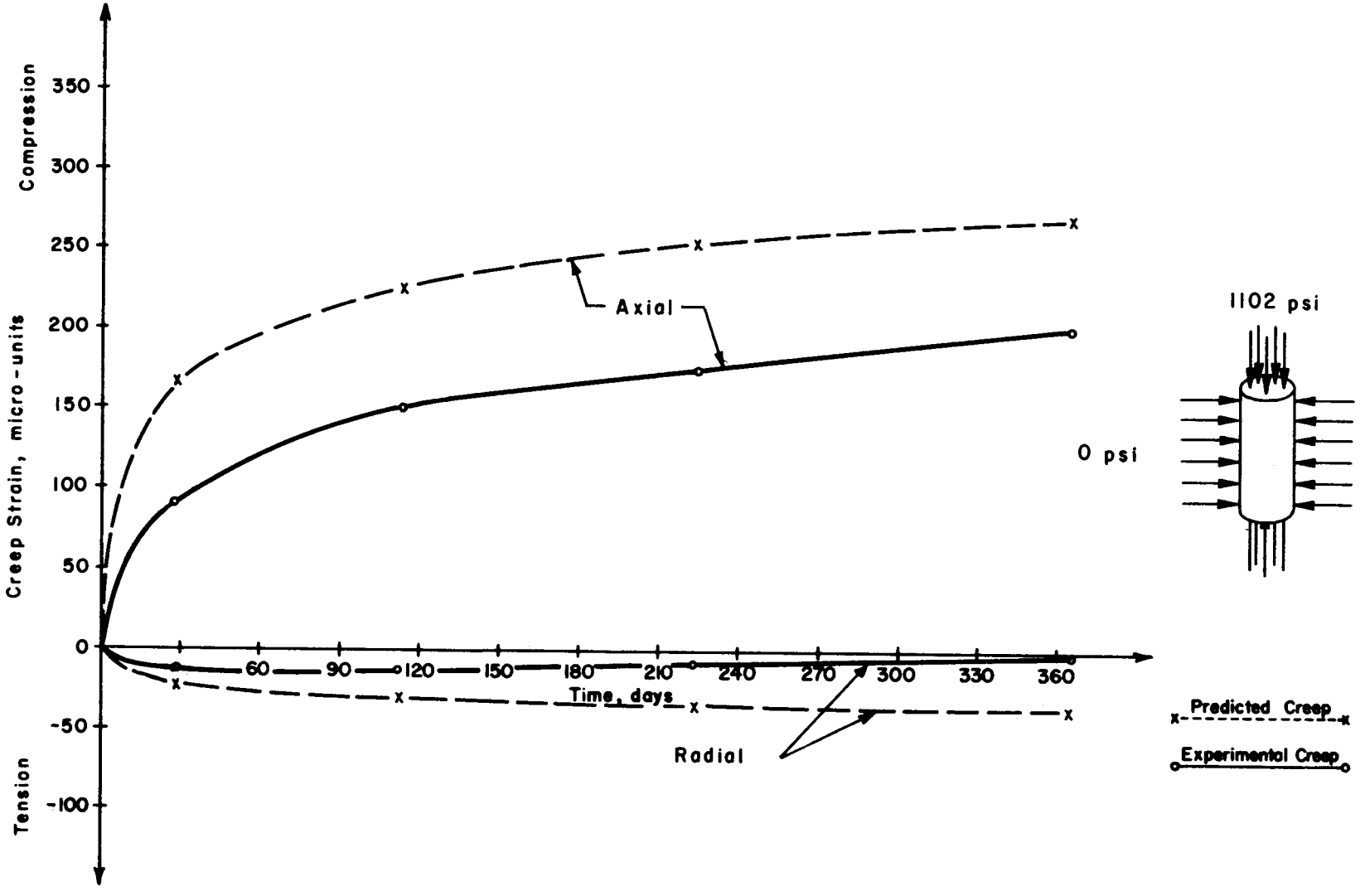

Fig 59. Predicted and experimental creep strain-time relationships for uniaxially loaded air-dried specimen (D-22) at 150° F.

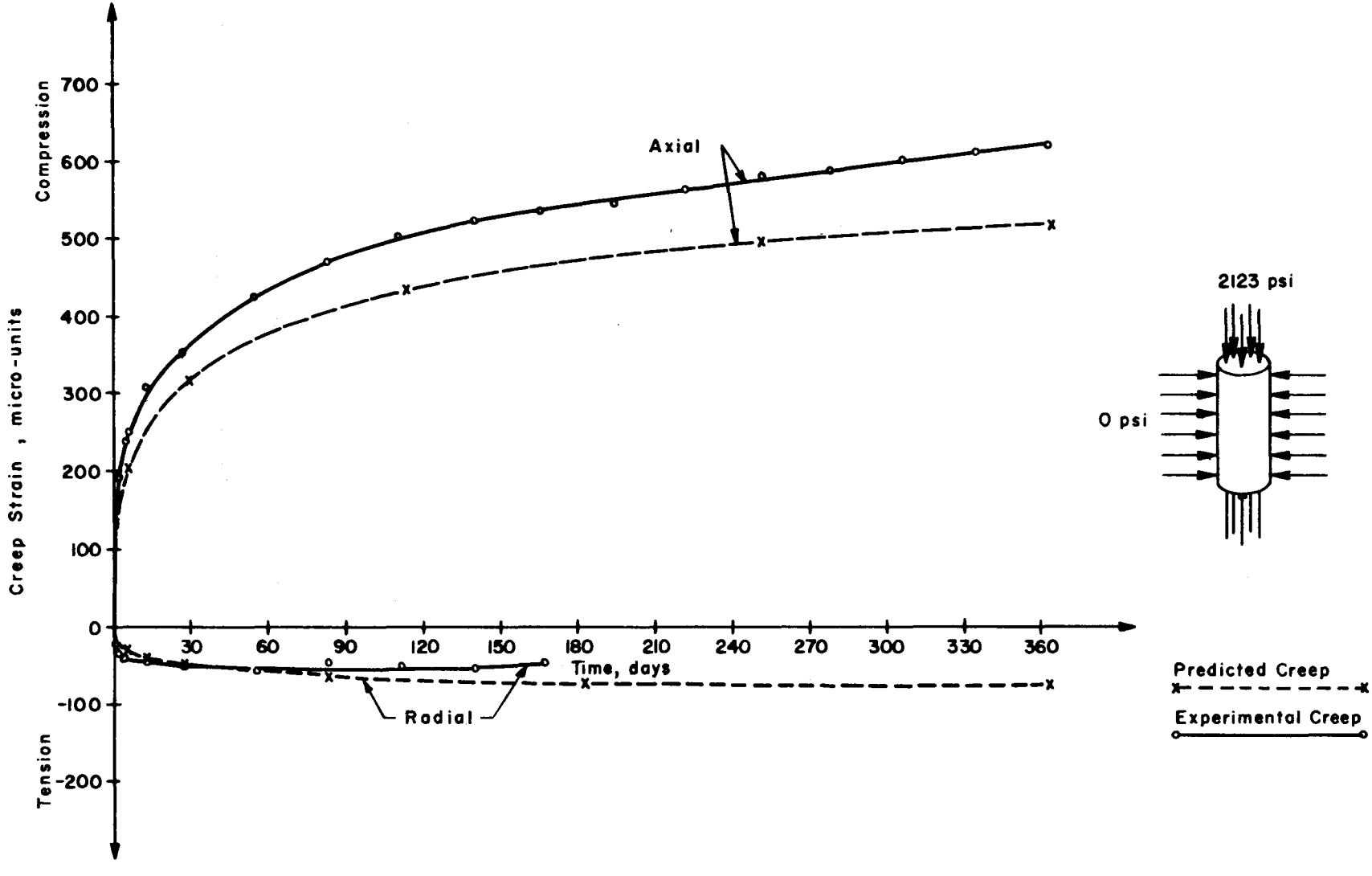

Fig 60. Predicted and experimental creep strain-time relationships for uniaxially loaded air-dried specimen (F-34) at 150° F.

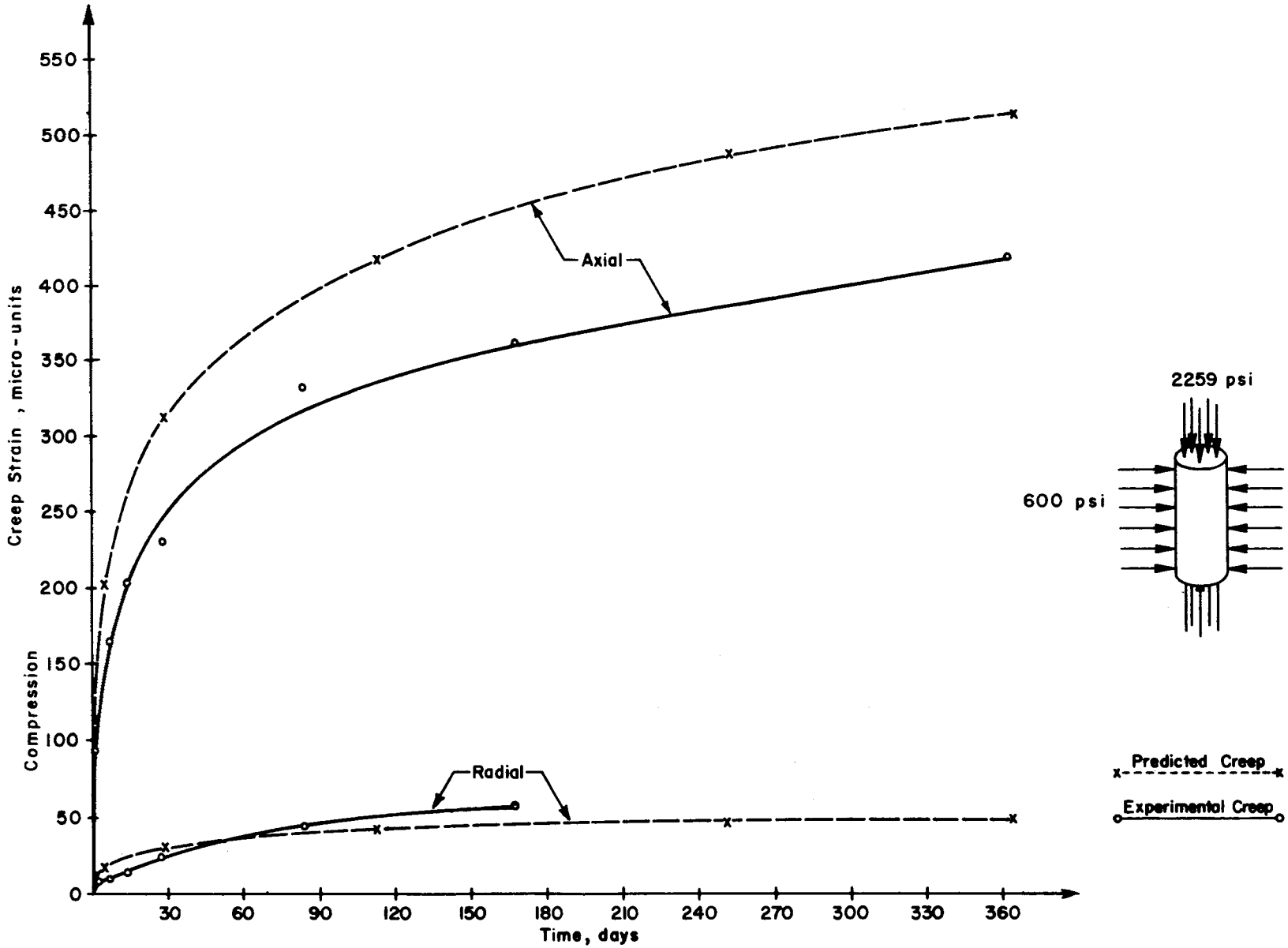

Fig 61. Predicted and experimental creep strain-time relationships for triaxially loaded air-dried specimen (E-4) at 150° F.

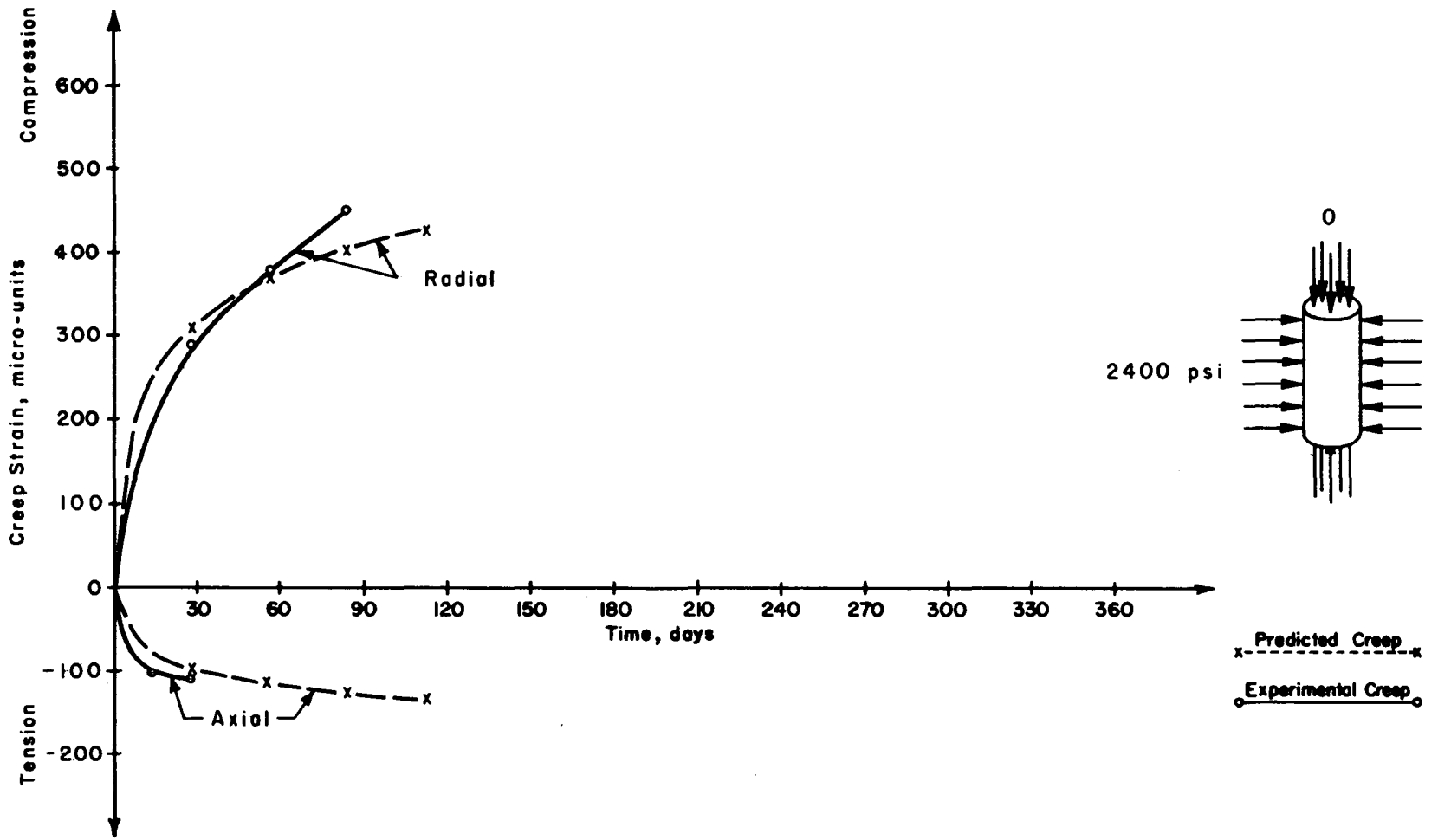

Fig 62. Predicted and experimental creep strain-time relationships for biaxially loaded air-dried specimen (E-1) at 150° F.

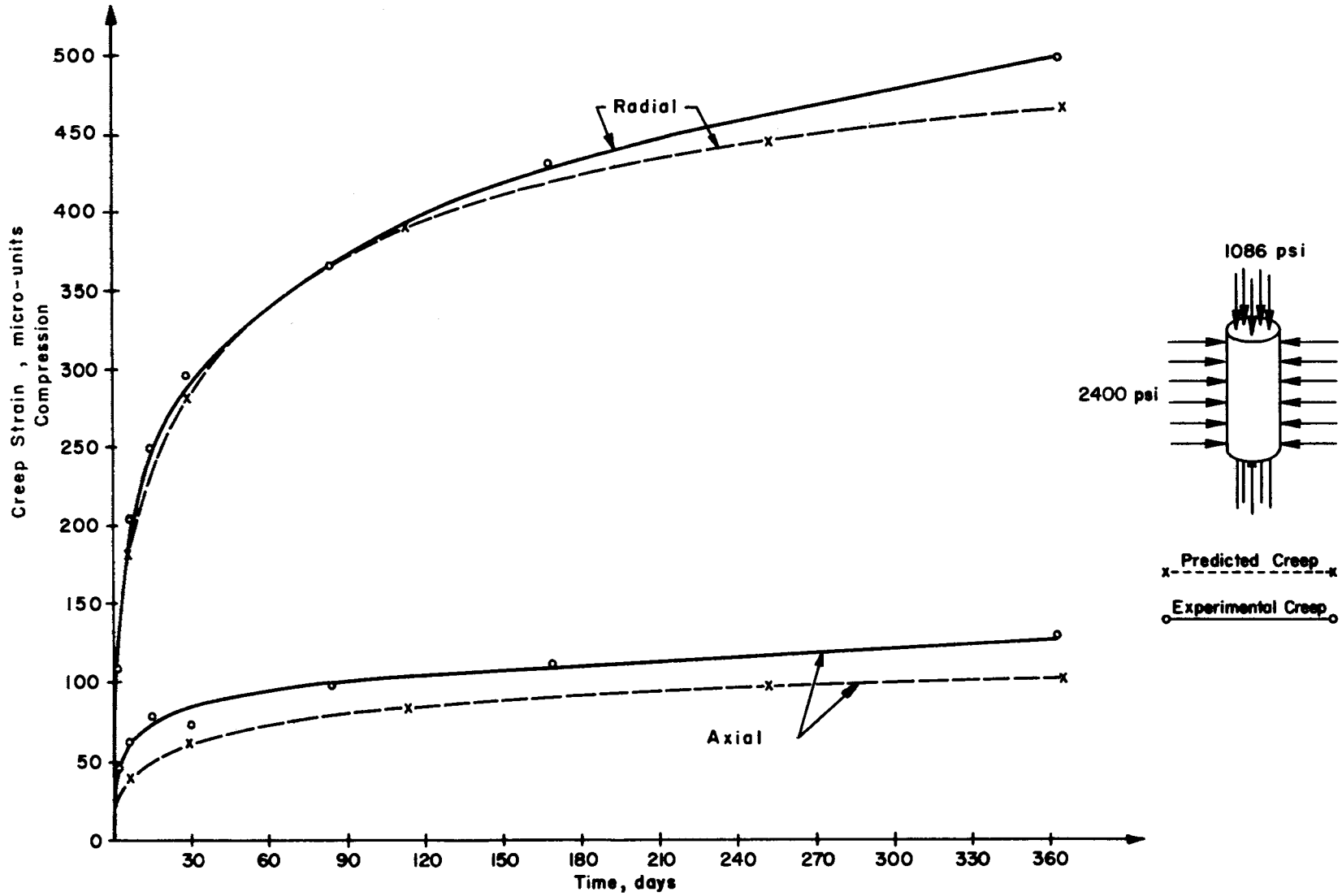

Fig 63. Predicted and experimental creep strain-time relationships for triaxially loaded air-dried specimen (D-41) at 150° F.

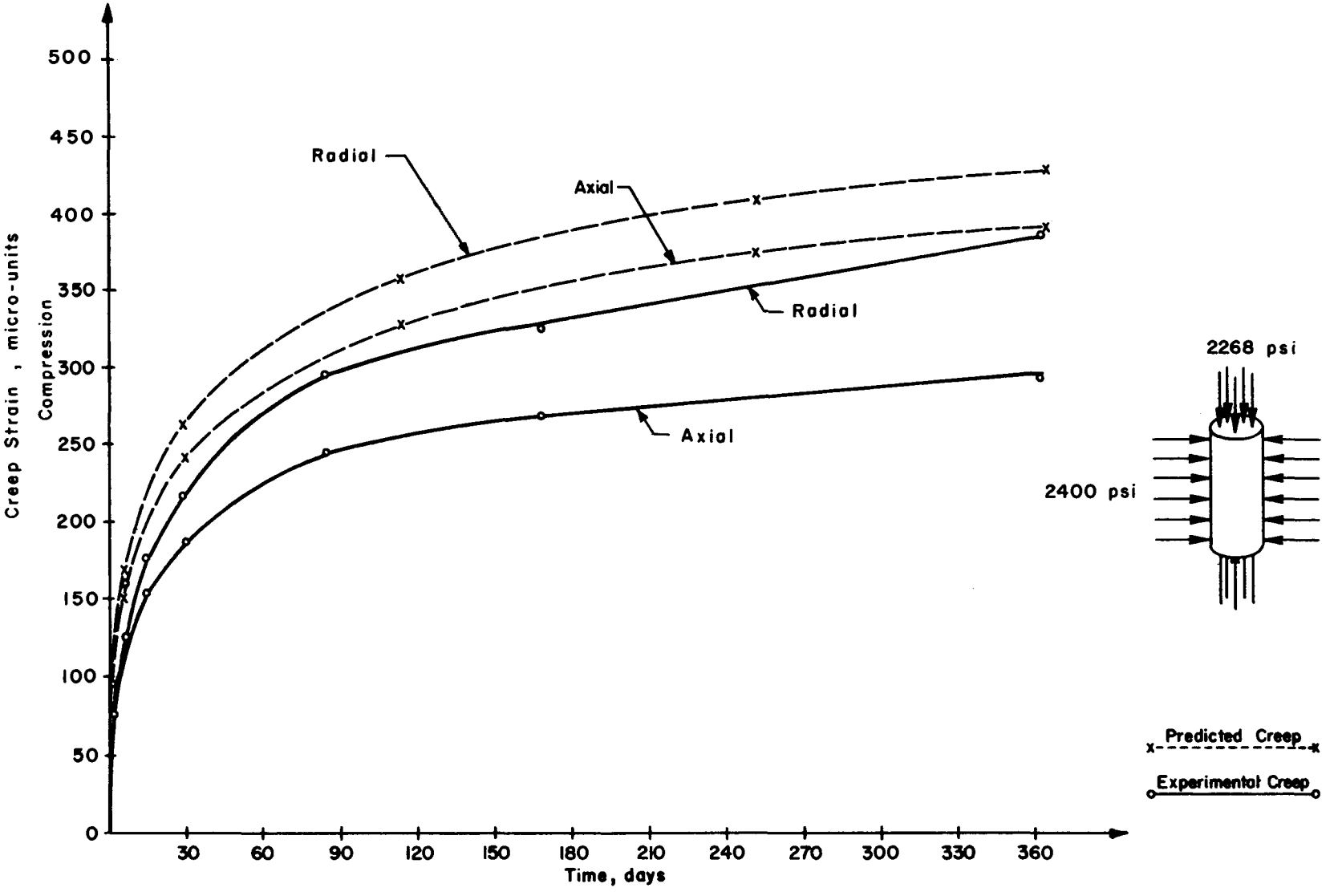

Fig 64. Predicted and experimental creep strain-time relationships for triaxially loaded air-dried specimen (G-19) at 150° F.

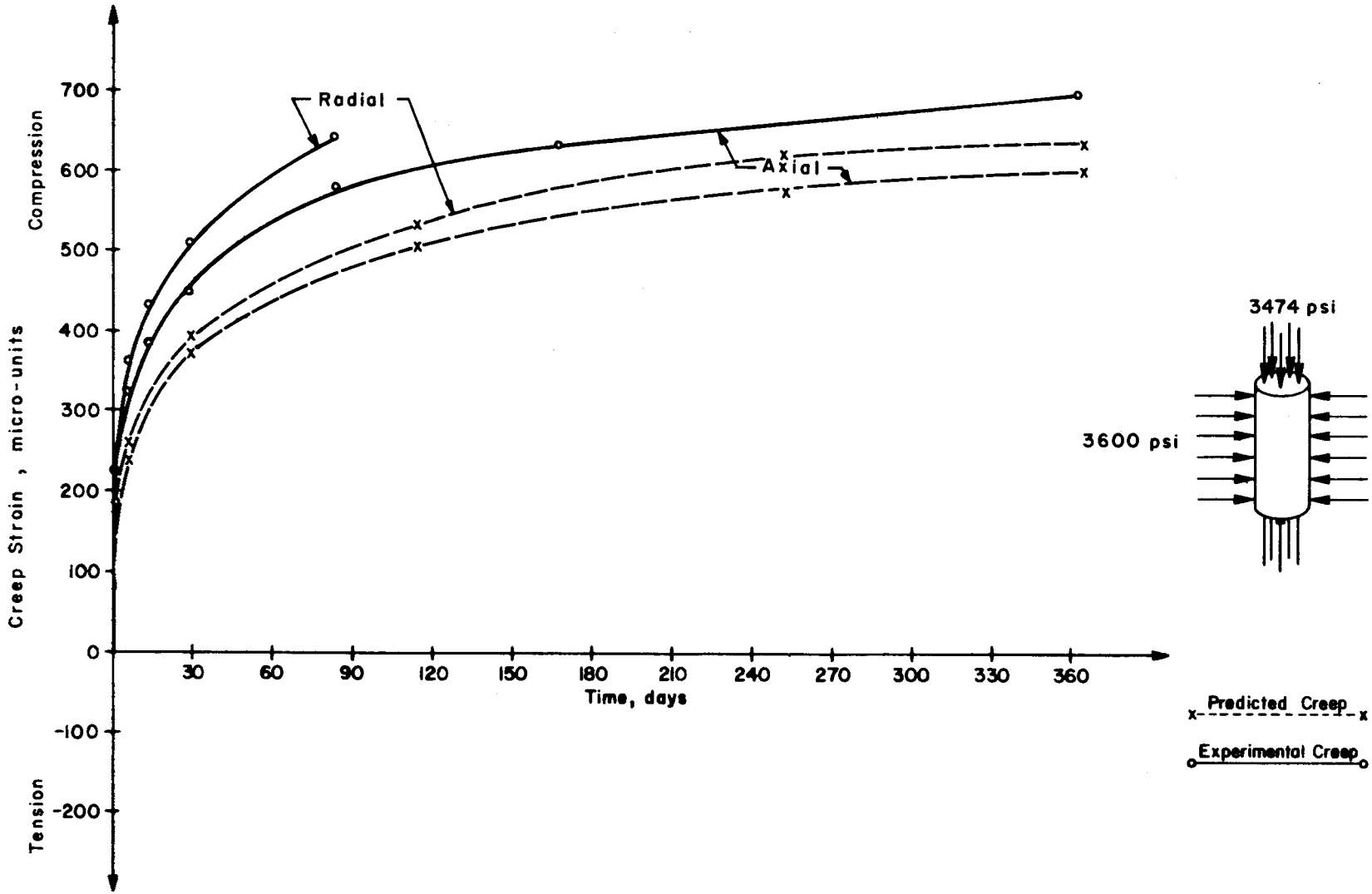

Fig 65. Predicted and experimental creep strain-time relationships for triaxially loaded air-dried specimen (F-6) at 150° F.

(text continued from page 73)

DISCUSSION AND MODIFICATION OF EQUATIONS

Discussion

The results shown and discussed above indicate that at stress levels less than the creep proportional limit, the creep prediction equations are relatively accurate. Nevertheless, with the exception of the air-dried specimens at 75° F, the predicted creep strains generally were larger than the measured creep strains. The difference was essentially a constant percentage of the measured strain for each test condition (Figs 29 through 32).

A number of reasons for the differences are evident. The first, of course, is concerned with experimental error associated with the tests. In addition to the normal variation between specimens there could also have been batch-to-batch variations in the concrete and variations between loading units. Normally such variation would not be expected to bias the results since the various specimens were assigned to the batches and loading units by randomization. Nevertheless, since there were relatively few specimens loaded uniaxially it is possible that an error could have been introduced.

More important is the fact that the unit creep function was developed from data obtained from very few specimens. Only two stress levels were used to develop the unit creep function and to estimate creep Poisson's ratio for the as-cast and air-dried condition at 150° F and for the as-cast condition at 75° F. For the air-dried condition at 75° F only one stress level was used. In addition, some of these stress levels were very near the creep proportional limit. Thus, in addition to being unable to define the function well, the high stress levels would tend to produce predictive equations which would overestimate creep strains.

A third area of possible error is concerned with the method of loading the triaxially loaded specimens since the axial and radial stresses were applied at two different rates. The maximum stress was applied at a rate of 35 psi per second with the ratio of the two stresses maintained equal to the ratio of their final magnitudes. Thus, the smaller of the two stresses was applied at a much slower rate. It would be expected that the portion of the total strain attributable to an instantaneous elastic strain would be greater for a slower loading rate, and therefore, the creep strain would be less. Thus, the measured creep strains could be less than the predicted strains since the predictive

equations were developed utilizing results from uniaxial tests in which the loads were applied at the higher rate.

A fourth and very definite possibility is that the uniaxially loaded specimens were losing moisture. If this were the case the measured strains would have included both shrinkage strain and creep strain. Thus, these strains would have resulted in unit creep prediction equations which would overestimate creep strains.

Finally, it is possible that the principle of superposition cannot be applied. It is therefore felt that additional tests are needed and justified in order to adequately define the unit creep function, to estimate creep Poisson's ratio, and to determine the validity of the concept. In recognition of the fact that it was not possible to conduct additional tests under this investigation, the unit creep predictive equations were modified.

Modification of Equations

In view of the fact that the unit creep predictive equations systematically overestimated creep strains in three of the four test conditions, all four equations have been modified by multiplying the K constant (Eq 3.2) by the ratio of the slope of the 45 degree line and the line of best fit.

Thus, the predictive equations for as-cast and air-dried conditions at 75° F and 150° F have been multiplied by a factor of 0.961, 1.098, 0.880, and 0.922, respectively, yielding the modified predictive equations shown in Table 13. The relationships between the predicted and measured creep strains are graphically illustrated in Figs 66 through 69. In these figures it can be seen that the predicted strains are very close to the measured strains for the conditions and measurements made in the experimental portion of this investigation. The standard error of estimate for as-cast and air-dried specimens at 75° F and 150° F loaded at stresses lower than the creep proportional limit were 13, 21, 35, and 31 micro-units, respectively.

These modified equations adequately predict the creep strains measured for specimens loaded at stress levels below the creep proportional limit in this investigation. This does not mean that they are necessarily adequate for application to other conditions. However, in view of the systematic variation between the predicted and measured creep strains, it is felt that these modified equations can be used until additional experimental verification can be conducted.

TABLE 13. MODIFIED UNIT CREEP PREDICTIVE EQUATIONS F(t,90)

	At 75° F
Air-Dried	$(\epsilon_c)_a = 0.324 \left[1 - e^{-0.102t^{0.401}}\right] \left[\sigma_a - 0.216\sigma_r\right]$
	$(\epsilon_c)_r = 0.324 \left[1 - e^{-0.102t^{0.401}}\right] \left[\sigma_r - 0.108(\sigma_r + \sigma_a)\right]$
As-Cast	$(\epsilon_c)_a = 0.303 \left[1 - e^{-0.088t^{0.350}}\right] \left[\sigma_a - 0.30\sigma_r\right]$
	$(\epsilon_c)_r = 0.303 \left[1 - e^{-0.088t^{0.350}}\right] \left[\sigma_r - 0.150(\sigma_r + \sigma_a)\right]$
	At 150° F
Air-Dried	$(\epsilon_c)_a = 0.262 \left[1 - e^{-0.207t^{0.405}}\right] \left[\sigma_a - 0.280\sigma_r\right]$
	$(\epsilon_c)_r = 0.262 \left[1 - e^{-0.207t^{0.405}}\right] \left[\sigma_r - 0.140(\sigma_r + \sigma_a)\right]$
As-Cast	$(\epsilon_c)_a = 0.323 \left[1 - e^{-0.118t^{0.374}}\right] \left[\sigma_a - 0.298\sigma_r\right]$
	$(\epsilon_c)_r = 0.323 \left[1 - e^{-0.118t^{0.374}}\right] \left[\sigma_r - 0.149(\sigma_r + \sigma_a)\right]$

σ_a = axial stress, psi

σ_r = radial stress, psi

t = time after loading, days

$(\epsilon_c)_a$ = creep strain in axial direction, micro-units

$(\epsilon_c)_r$ = creep strain in radial direction, micro-units

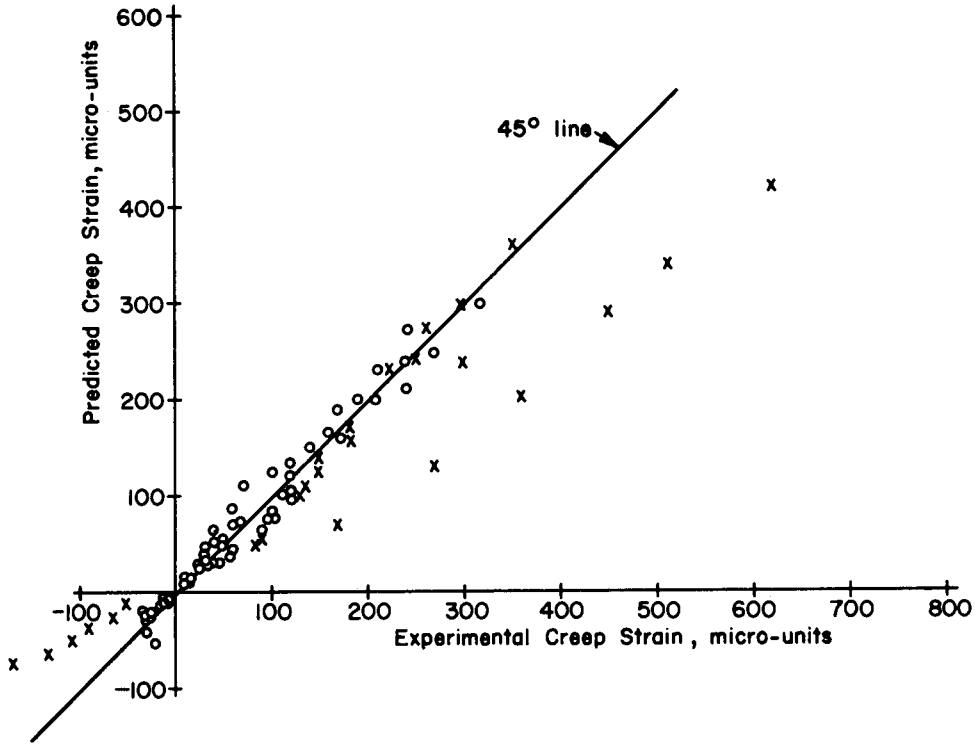

Fig 66. Experimental and predicted creep strains from modified unit creep prediction equations for triaxially loaded as-cast specimens at 75° F.

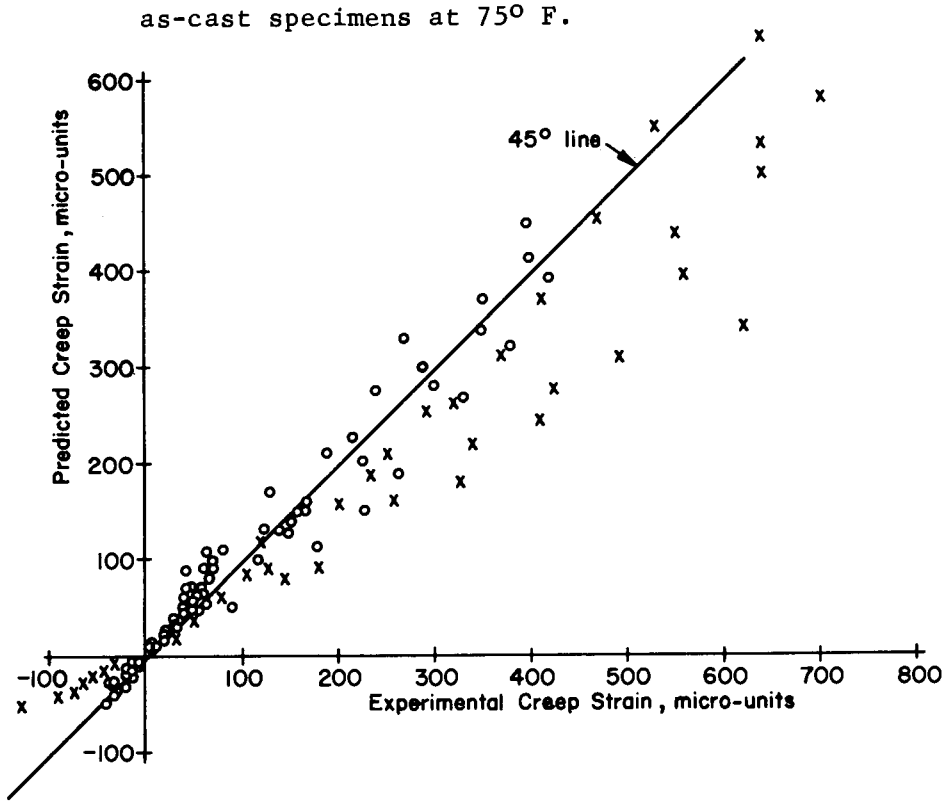

Fig 67. Experimental and predicted creep strains from modified unit creep prediction equations for triaxially loaded air-dried specimens at 75° F.

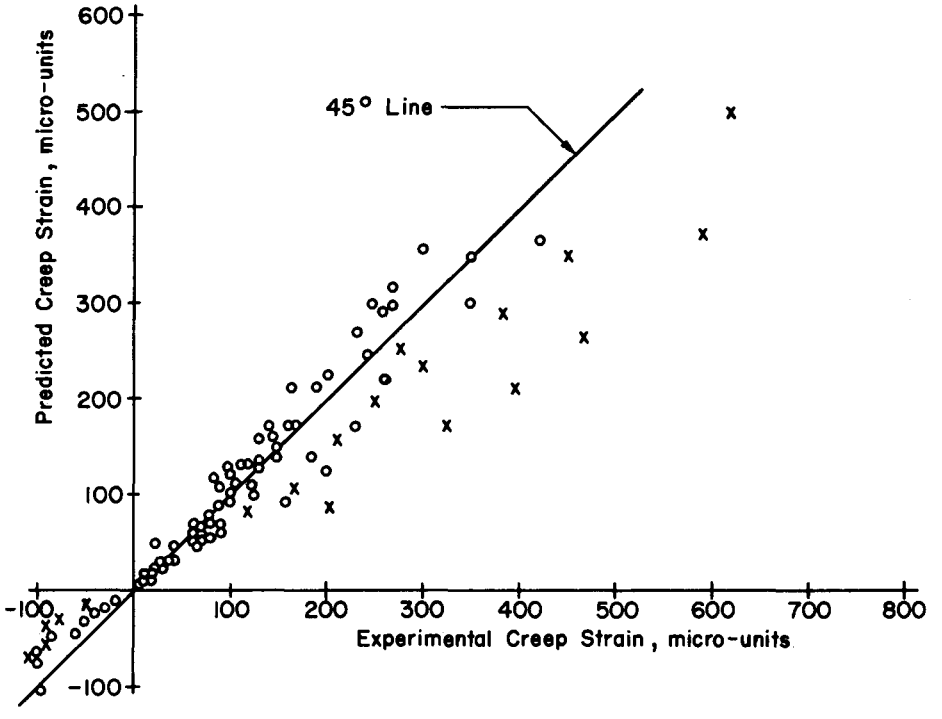

Fig 68. Experimental and predicted creep strains from modified unit creep prediction equations for triaxially loaded as-cast specimens at 150° F.

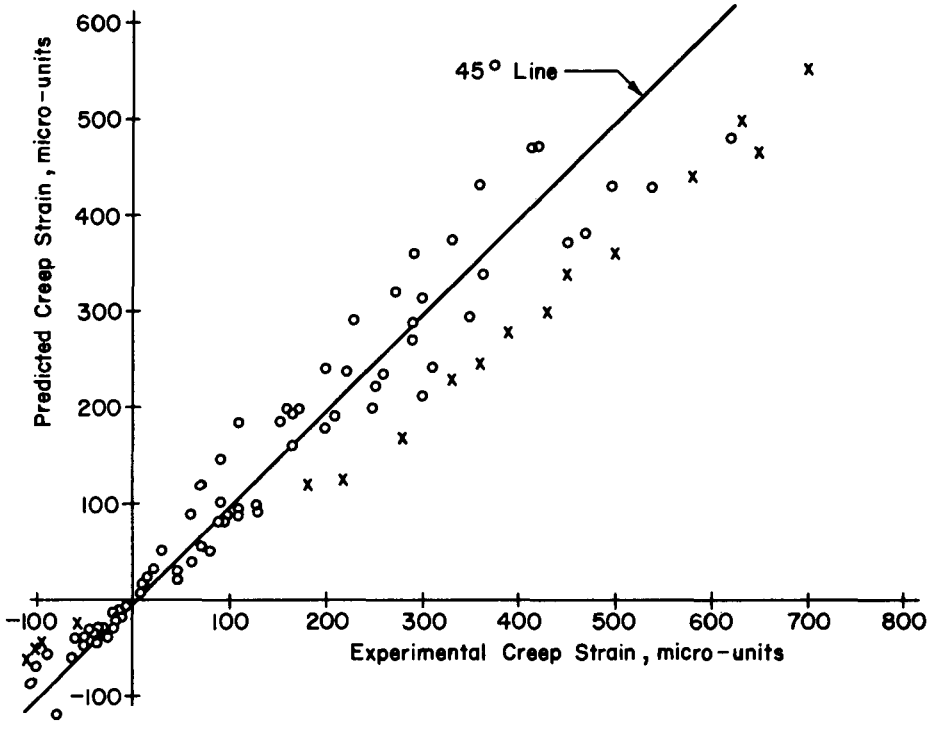

Fig 69. Experimental and predicted creep strains from modified unit creep prediction equations for triaxially loaded air-dried specimens at 150° F.

ESTIMATION OF TOTAL STRAINS

In addition to estimating creep strains the unit creep function concept probably can be used to predict total strains (Eqs 3.25, 3.26, and 3.27). For the loading conditions utilized in the experimental portion of this investigation, in which $\sigma_y = \sigma_z = \sigma_r$, these equations become

$$\epsilon_x = H(t,\tau)\sigma_a - 2\omega(t,\tau)\ (\sigma_a + \sigma_r) \tag{6.4}$$

$$\epsilon_r = H(t,\tau)\sigma_r - \omega(t,\tau)\ (\sigma_a + \sigma_r) \tag{6.5}$$

where

$H(t,\tau) = \frac{1}{E} + F(t,\tau)$, for time-dependent flexibility, and

$\omega(t,\tau) = \frac{\nu}{E} + \nu_c F(t,\tau)$, for the time-dependent coefficient of lateral strain.

Thus, by introducing appropriate values for the instantaneous modulus of elasticity E and Poisson's ratio ν , obtained from uniaxial tests, estimates of the total strains could be obtained. Additional study, however, is needed to evaluate this suggested approach to estimating total strains.

CHAPTER 7. CONCLUSIONS AND RECOMMENDATIONS

The object of this study was to investigate creep strains in concrete subjected to multiaxial compressive stresses under various moisture and temperature conditions and to develop predictive equations capable of predicting creep strains for multiaxial stresses by utilizing creep strains obtained from uniaxial tests.

Laboratory tests on seventy-eight 6 × 16-inch concrete cylinders with embedded vibrating wire gages were performed. Several conclusions and recommendations based on the results are summarized below.

CONCLUSIONS

(1) Unit creep of concrete under constant temperature and with a given curing history is a function of concrete age at loading, time after loading, and stress levels. When the applied stress is less than the creep proportional limit, unit creep of concrete is independent of stress levels.

(2) The creep proportional limit varied with moisture conditions and testing temperatures.

(3) The creep Poisson's ratio of as-cast specimens was higher than that of air-dried specimens. At 75° F, the average creep Poisson's ratios were 0.150 for as-cast specimens and 0.108 for air-dried specimens. At 150° F the average creep Poisson's ratios were 0.149 for as-cast specimens and 0.140 for air-dried specimens.

(4) The creep prediction technique developed by employing the unit creep function was satisfactory for predicting creep strains resulting from multiaxial stresses when stress levels were less than the creep proportional limit. For stress levels higher than the creep proportional limit, the measured creep strains were higher than the predicted values.

(5) The unit creep function based on one-year creep test results can be used for predicting creep at later ages. However, creep tests longer than one year are needed to valudate this technique.

RECOMMENDATIONS

(1) The possibility of introducing creep strain into stress-strain analysis for plain or reinforced concrete structures using the unit creep function should be investigated.

(2) Tests at higher stress levels should be performed to obtain the maximum failure creep strain and to complete the creep-failure portion of the unit creep function.

(3) The possibility of using the unit creep concept to evaluate stress relaxation of concrete should be investigated.

(4) An attempt should be made to determine whether reliable prediction equations can be obtained by using loading periods of less than 12 months.

(5) An attempt should be made to define the stress-creep strain-time relationships for stress levels higher than the creep proportional limit in order that the nonlinear creep behavior can be included as a part of the unit creep function.

(6) Additional uniaxial tests should be conducted at stress levels below the creep proportional limit in order to better define the unit creep function, to obtain better estimates of creep Poisson's ratio, and to determine the validity of applying the principle of superposition.

(7) Additional uniaxial creep tests at elevated temperatures should be conducted to determine the effect of temperature on the unit creep function. Until such tests are conducted, it is felt that linear interpolation or extrapolation can be used to estimate creep strains at other temperatures.

(8) Additional uniaxial creep tests should be conducted to obtain the unit creep function subjected to different curing histories.

REFERENCES

1. Ali, Iqbal, and Clyde E. Kesler, "Creep in Concrete With and Without Exchange of Moisture With the Environment," Dept. of Theoretical and Applied Mechanics Report, No. 641, University of Illinois.

2. Ali, Iqbal, and Clyde E. Kesler, "Mechanisms of Creep in Concrete," Symposium on Creep of Concrete, American Concrete Institute, Publication SP-9, pp 35-63

3. Arthanari, S., and C. W. Yu, "Creep of Concrete under Uniaxial and Biaxial Stresses at Elevated Temperatures," Magazine of Concrete Research, Vol 19, No. 60, September 1967, pp 149-156.

4. Arutyunyan, N. H., Some Problems in the Theory of Creep, Translated by H. E. Nowottny, Pergamon Press, 1966, p 290.

5. Bresler, B., and L. Selna, "Analysis of Time-Dependent Behavior of Reinforced Concrete Structures," Symposium on Creep of Concrete, American Concrete Institute, Publication SP-9, pp 115-128.

6. Cruz, C. R., "Apparatus for Measuring Creep of Concrete at High Temperatures," Journal of Portland Cement Association Research and Develop- Laboratories, Vol 10, No. 3, 1968.

7. Duke, C. Martin, and Harmer E. Davis, "Some Properties of Concrete Under Sustained Combined Stresses," Proceedings, American Society for Testing and Materials, Vol 44, 1944, pp 888-896.

8. England, G. L., and A. D. Ross, "Reinforced Concrete Under Thermal Gradients," Magazine of Concrete Research, Vol 14, No. 40, 1962.

9. Fluck, P. G., and G. W. Washa, "Creep of Plain and Reinforced Concrete," Journal of the American Concrete Institute, Title No. 54-49, April 1958, pp 879-895.

10. Glucklick, J. and O. Ishai, "Creep Mechanism in Cement Mortar," Journal of the American Concrete Institute, Proceedings, Vol 63, No. 2, February 1966, pp 267-290.

11. Gopalakrishnan, K. S., Adam M. Neville, and Amin Ghali, "Creep Poisson's Ratio of Concrete Under Multiaxial Compression," Journal of the American Concrete Institute, Title No. 66-90, December 1969, pp 1008-1019.

12. Hannant, D. J., "The Strain Behavior of Concrete Under Compressive Stress at Elevated Temperatures," Research and Development Report, Central Electricity Research Laboratories, London, June 1966.

13. Hansen, T. C., "Creep and Stress Relaxation of Concrete - A Theoretical and Experimental Investigation," Swedish Cement and Concrete Research Institute, Proceedings NR 31, September 1960.

14. Hanson, J. A., "A 10-Year Study of Creep Properties of Concrete," Report SP-38, Concrete Laboratory, U. S. Bureau of Reclamation, Denver, Colorado, July 1953.

15. Ishai, Ori, "Elastic and Inelastic Behavior of Hardened Mortar in Torsion," Symposium on Creep of Concrete, American Concrete Institute, Publication SP-9, pp 65-94.

16. Kennedy, Thomas W., and Ervin S. Perry, "An Experimental Approach to the Study of the Creep Behavior of Plain Concrete Subjected to Triaxial Stresses and Elevated Temperatures," Union Carbide Report No. 2864-1, The University of Texas at Austin, June 1970.

17. Leong, Tuch Wah, and Robert F. Warner, "Creep and Shrinkage in Reinforced Concrete Beams," Journal of the Structural Division, Proceedings of the American Society of Civil Engineers, March 1970, pp 509-533.

18. Lorman, W. R., "The Theory of Concrete Creep," Proceedings, American Society for Testing and Materials, Vol 40, 1940, pp 1082-1102.

19. McCormick, John M., and Mario G. Salvadori, Numerical Methods in Fortran, Prentice Hall, Inc., Englewood Cliffs, New Jersey, 1964, pp 52-54.

20. McHenry, D., "A New Aspect of Creep in Concrete and Its Application to Design," Proceedings, American Society for Testing and Materials, Vol 43, 1943, pp 1069-1084.

21. Nasser, K. W., and A. M. Neville, "Creep of Concrete at Elevated Temperatures, "Journal of American Concrete Institute, Proceedings, Vol 62, No. 12, December 1965, pp 1567-1578.

22. Neville, Adam M., Properties of Concrete, John Wiley, 1964, pp 274-328.

23. Neville, Adam M., and B. L. Meyers, "Creep of Concrete: Influencing Factors and Prediction," Symposium on Creep of Concrete, American Concrete Institute, Publication SP-9, p 31.

24. Neville, A. M., M. M. Staunton, and G. M. Bonn, "A Study of the Relation Between Creep and the Gain of Strength of Concrete," Symposium on Structure of Portland Cement Paste and Concrete, Highway Research Board Special Report 90.

25. Pauw, A., and B. L. Meyers, "Effect of Creep and Shrinkage on the Behavior of Reinforced Concrete Members," Symposium on Creep of Concrete, American Concrete Institute, Publication SP-9, pp 129-156.

26. Roll, F., "Long-Time Creep-Recovery of Highly Stressed Concrete Cylinders," Symposium on Creep of Concrete, American Concrete Institute, Publica- SP-9, pp 95-114.

27. Ross, A. D., "Concrete Creep Data," Structural Engineer, Vol 15, No. 8, August 1937, pp 314-326.

28. Ross, A. D., "Experiments on the Creep of Concrete Under Two-Dimensional Stressing," Magazine of Concrete Research, Vol 16, No. 46, March 1964, pp 12-30.

29. Rusch, Hubert, "Research Toward A General Flexural Theory for Structural Concrete," Journal of the American Concrete Institute, Title No. 57-1, July 1960, pp 1-28.

30. Shank, J. R., "Plastic Flow of Concrete at High Overload," Proceedings, American Society for Testing and Materials, Vol 45, February 1949, pp 493-498.

31. Subcommittee, ACI Committee 209, "The Effect of Concrete Constituents, Environments and Stress on the Creep and Shrinkage of Concrete," A Paper presented at the Annual Convention, American Concrete Institute, New York, April 11-17, 1970.

32. Troxell, G. E., J. M. Raphael, and R. E. Davis, "Long-Time Creep and Shrinkage Tests of Plain and Reinforced Concrete," Proceedings, American Society for Testing and Materials, Vol 58, 1958, pp 1101-1120.

33. York, Guy P., Thomas W. Kennedy, and Ervin S. Perry, "Experimental Investigation of Creep in Concrete Subjected to Multiaxial Compressive Stresses at Elevated Temperatures," Union Carbide Report No. 2864-2, The University of Texas at Austin, June 1970.

APPENDIX

CREEP STRAIN-TIME RELATIONSHIPS

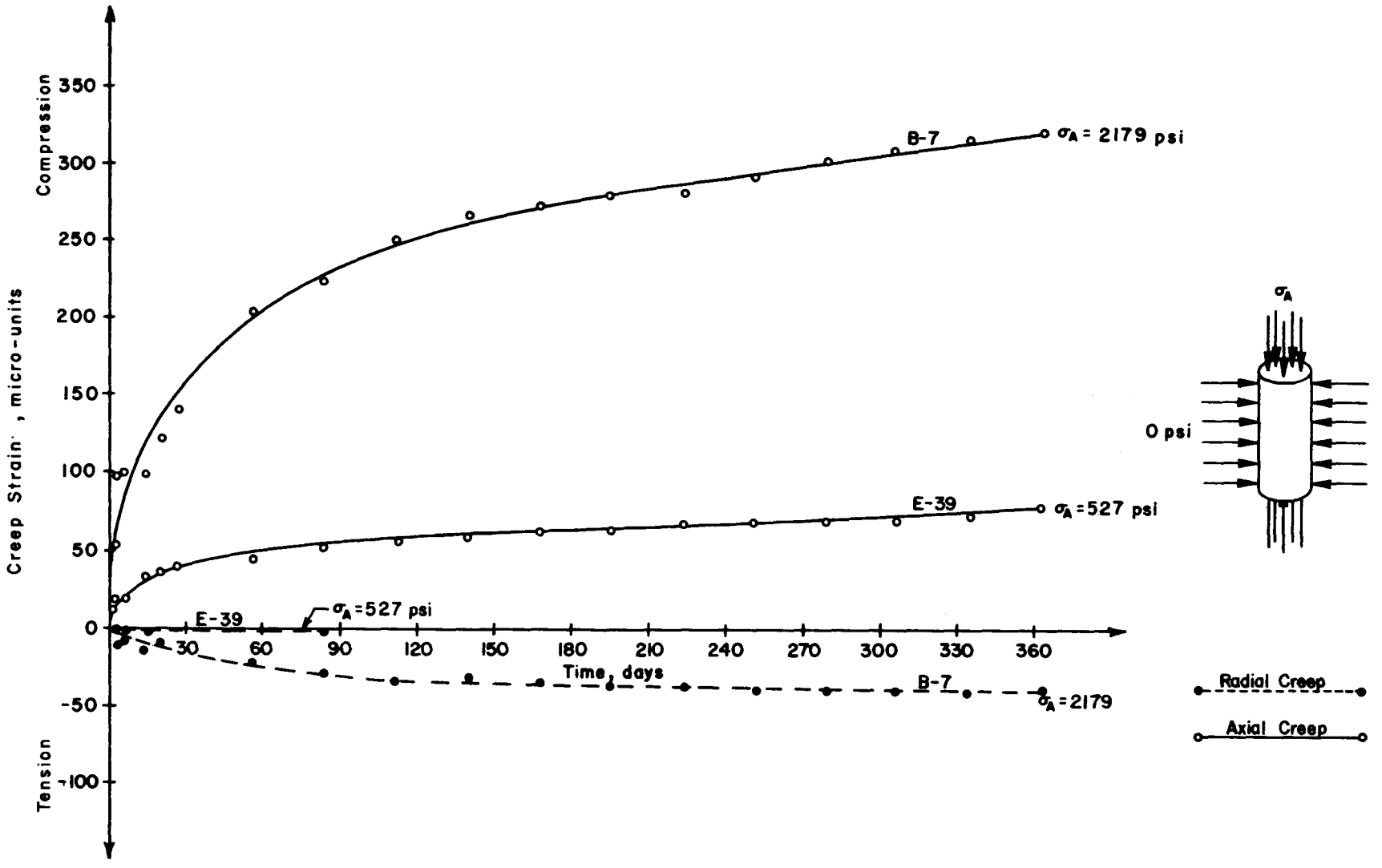

Fig A1. Creep strain-time relationships for uniaxially loaded as-cast specimens at 75° F.

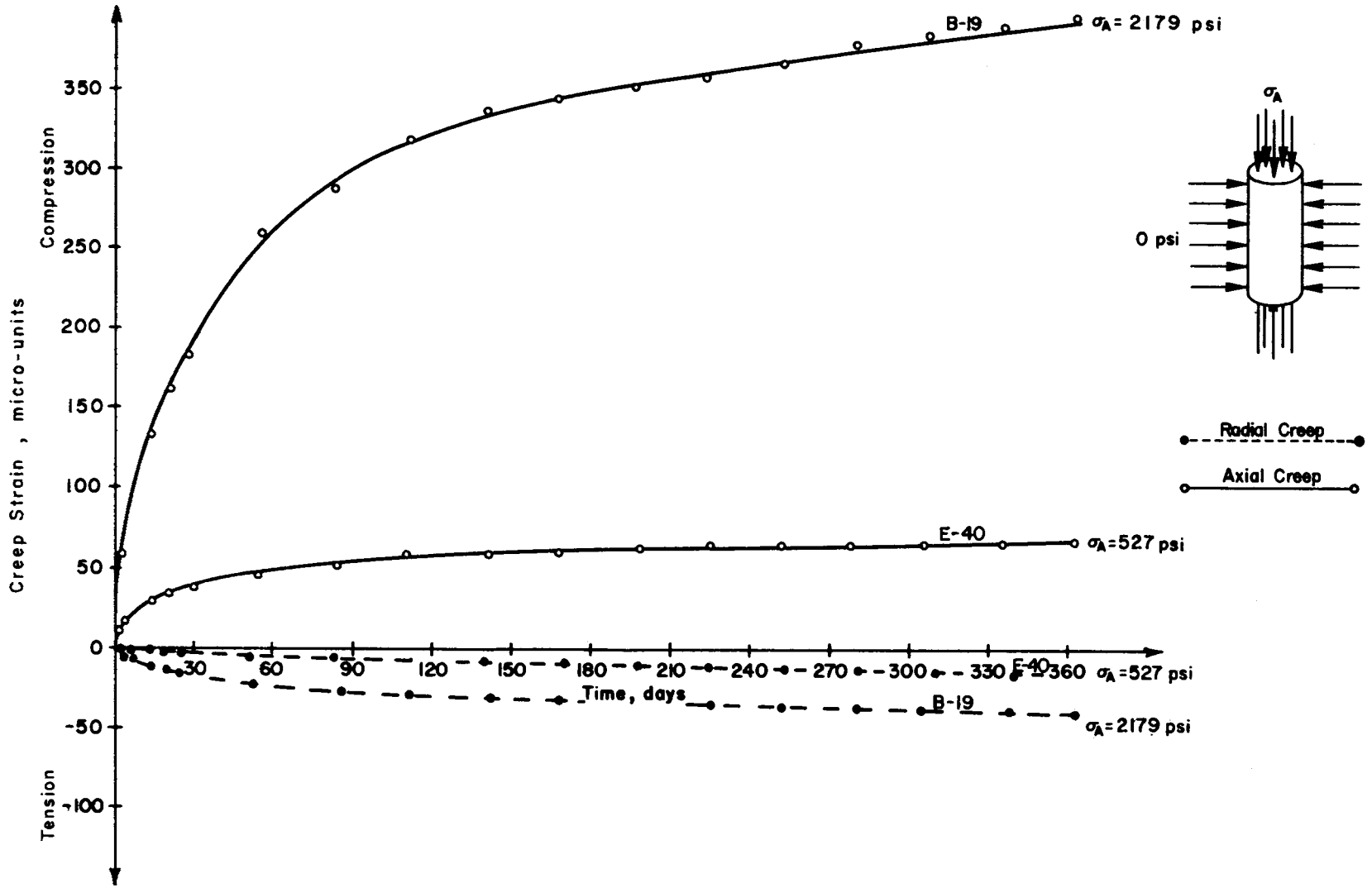

Fig A2. Creep strain-time relationships for uniaxially loaded air-dried specimens at 75° F.

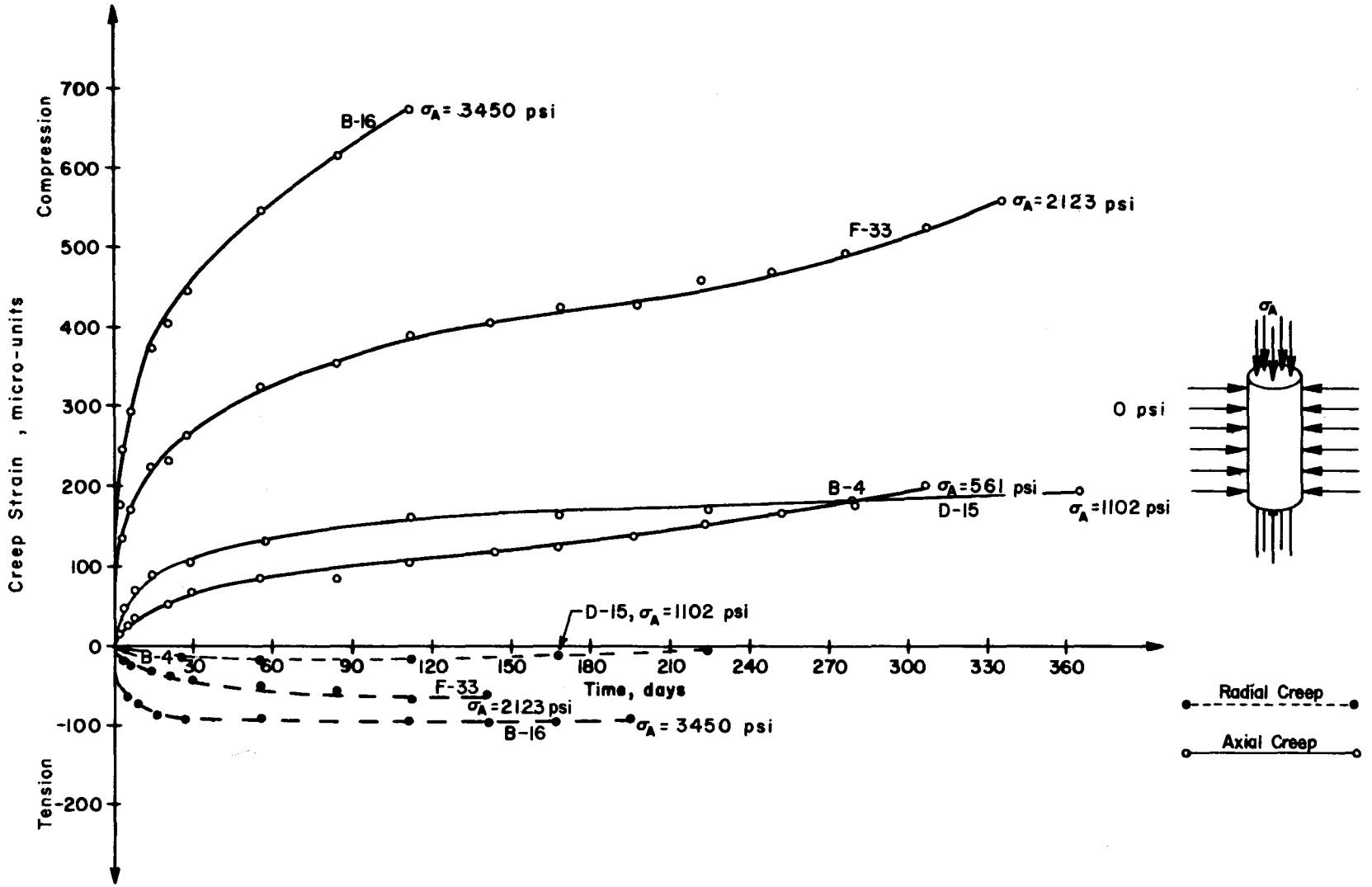

Fig A3. Creep strain-time relationships for uniaxially loaded as-cast specimens at 150° F.

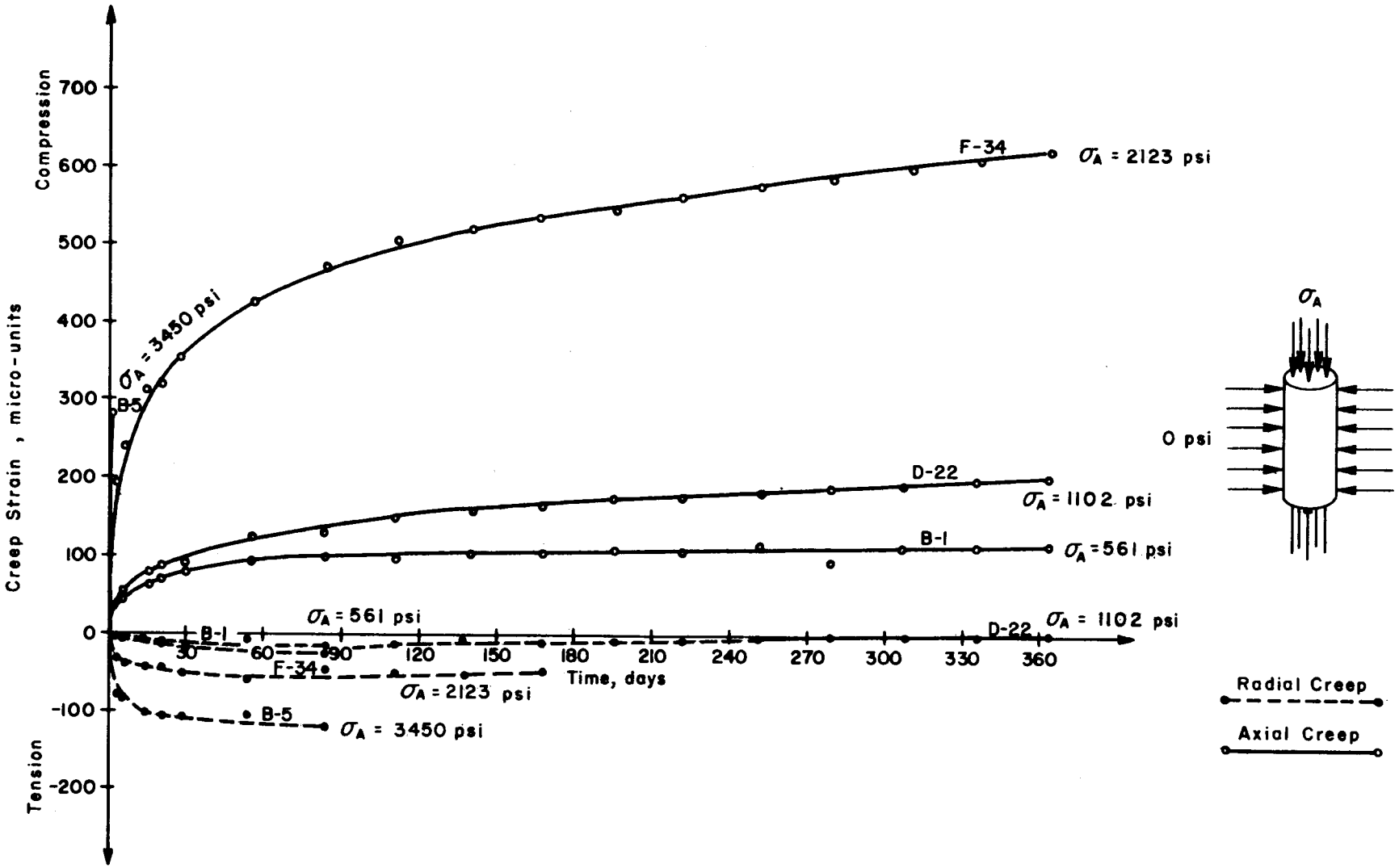

Fig A4. Creep strain-time relationships for uniaxially loaded air-dried specimens at 150° F.

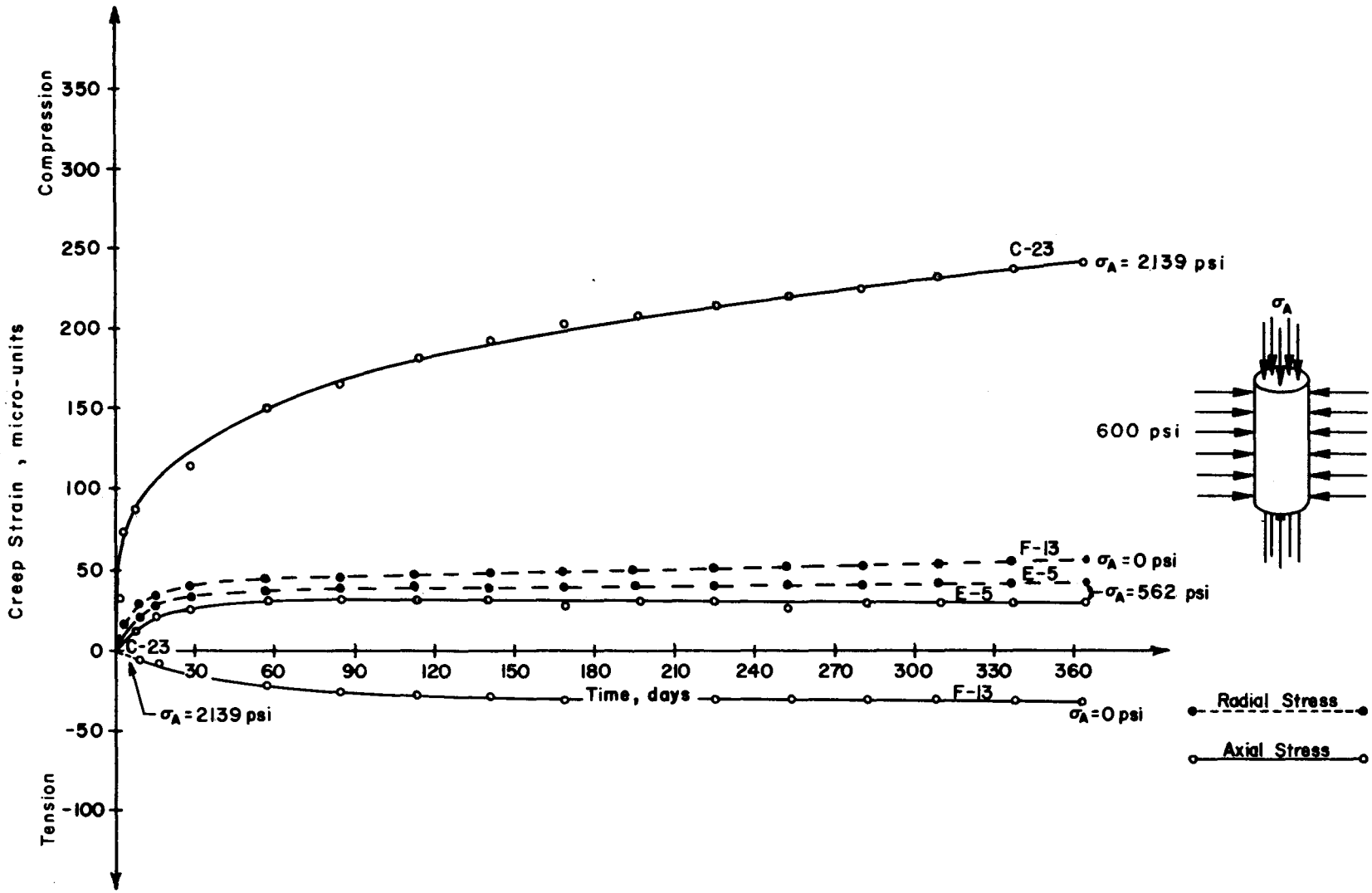

Fig A5. Creep strain-time relationships for triaxially loaded as-cast specimens with 600 psi confining pressure at 75° F.

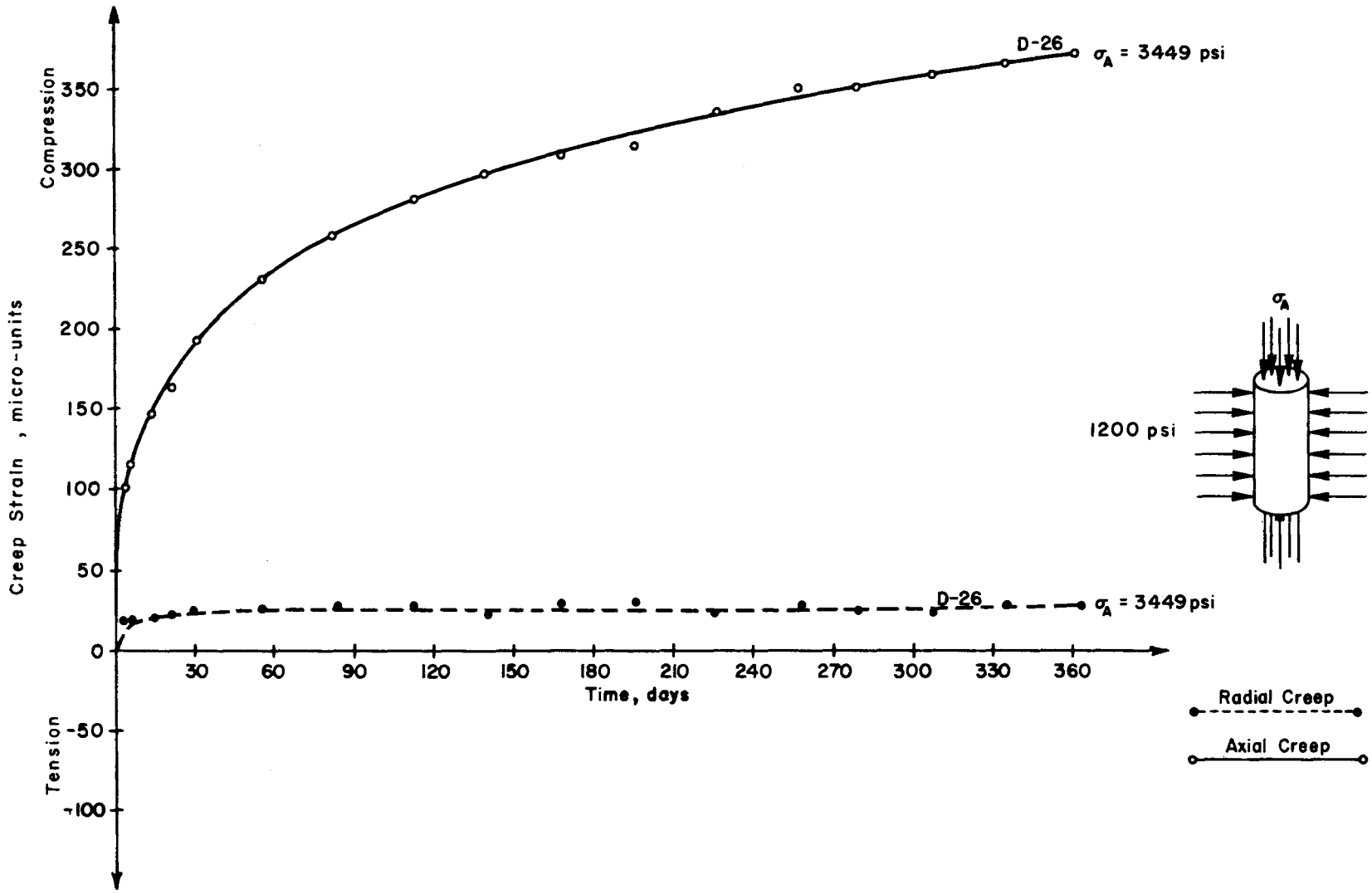

Fig A6. Creep strain-time relationships for triaxially loaded as-cast specimens with 1200 psi confining pressure at 75° F.

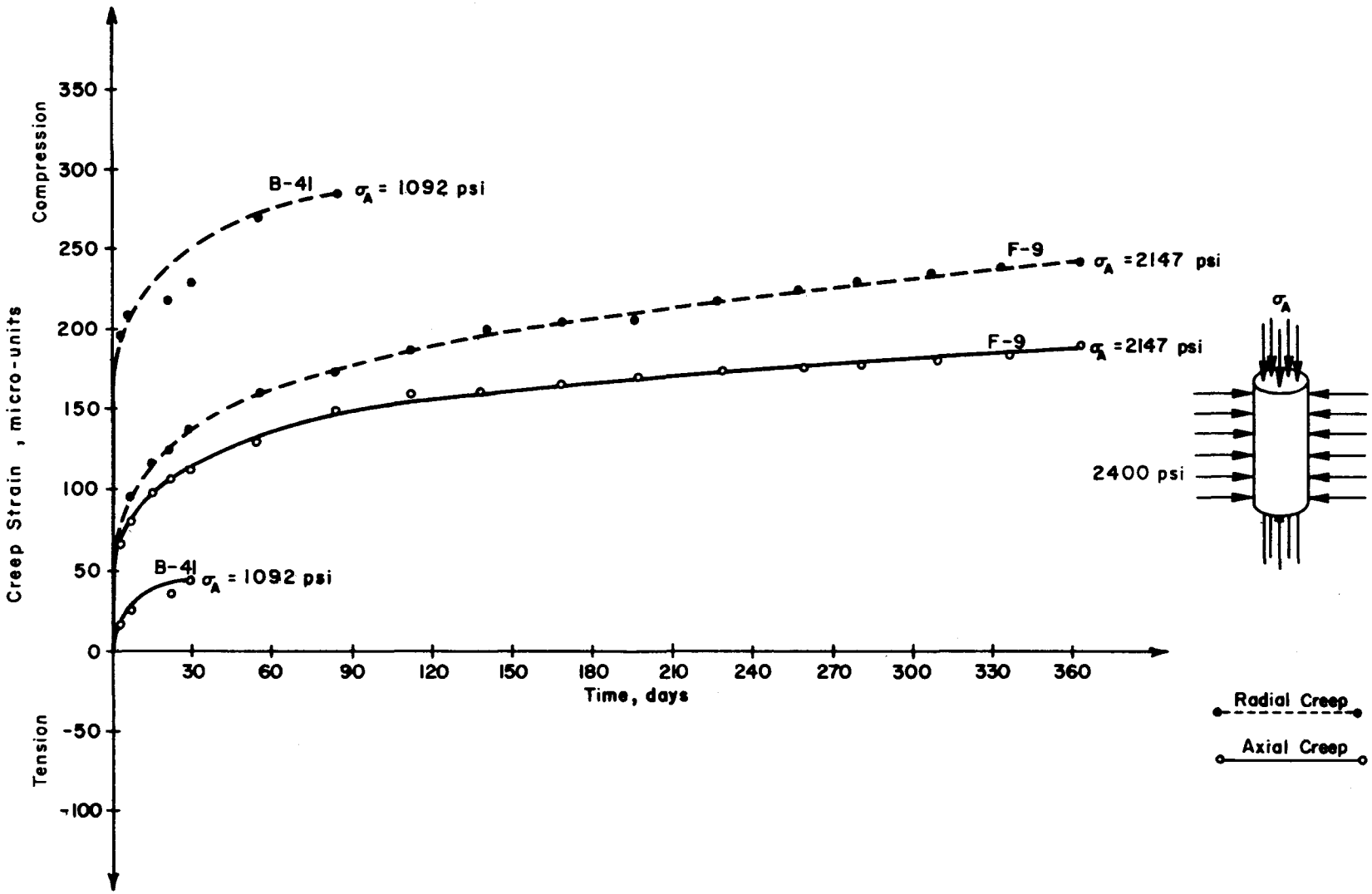

Fig A7. Creep strain-time relationships for triaxially loaded as-cast specimens with 2400 psi confining pressure at 75° F.

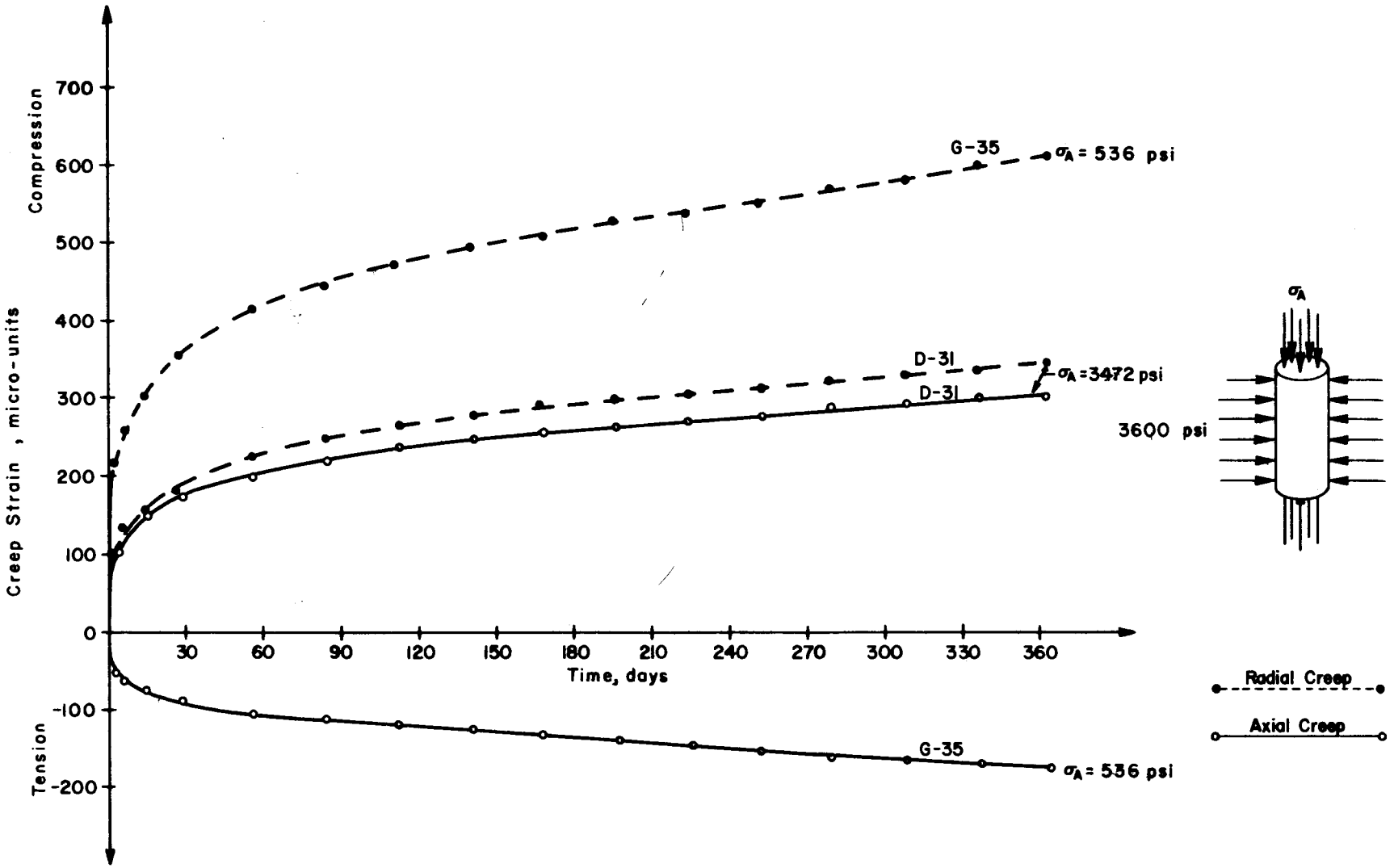

Fig A8. Creep strain-time relationships for triaxially loaded as-cast specimens with 3600 psi confining pressure at 75° F.

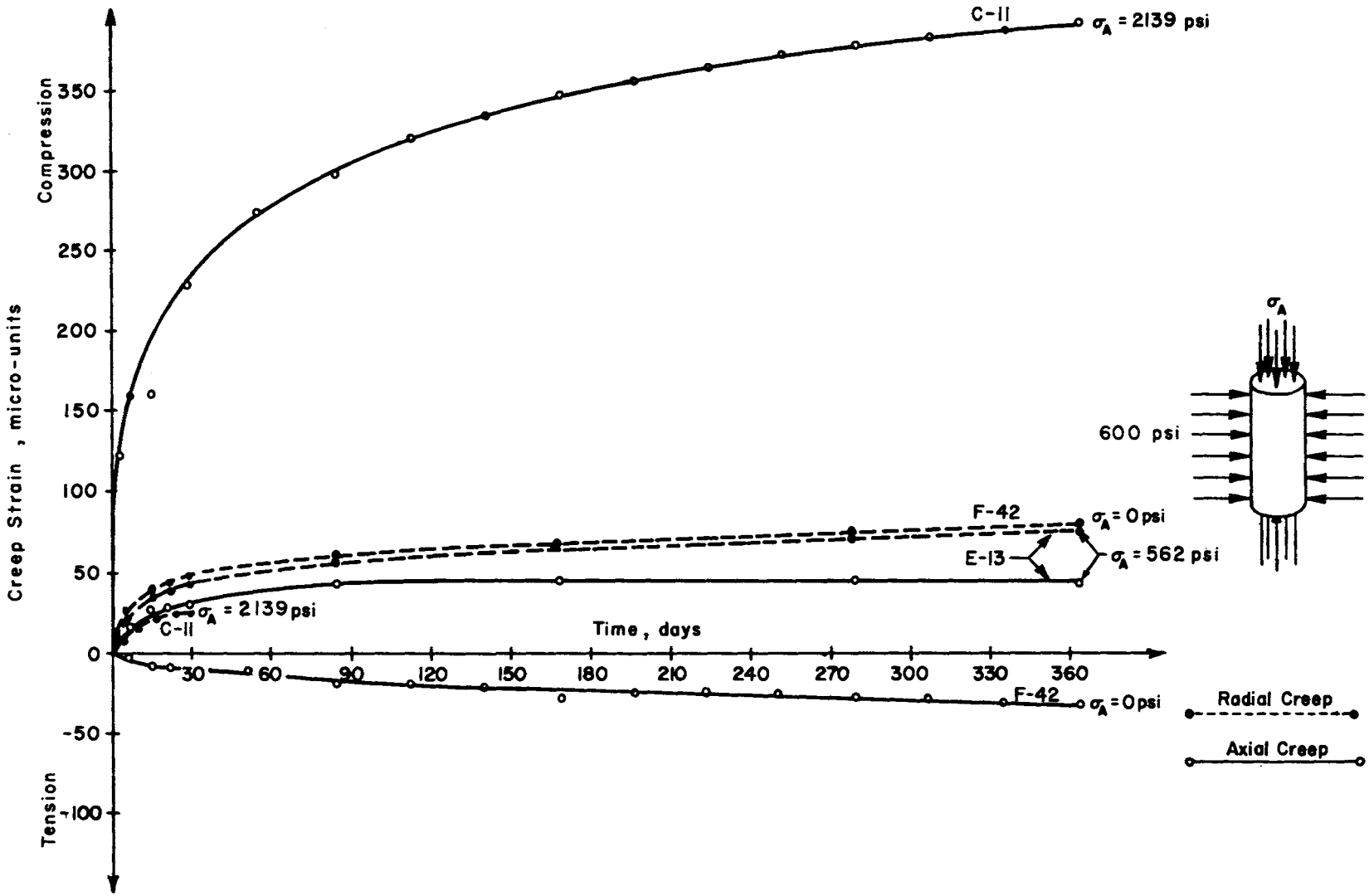

Fig A9. Creep strain-time relationships for triaxially loaded air-dried specimens with 600 psi confining pressure at 75° F.

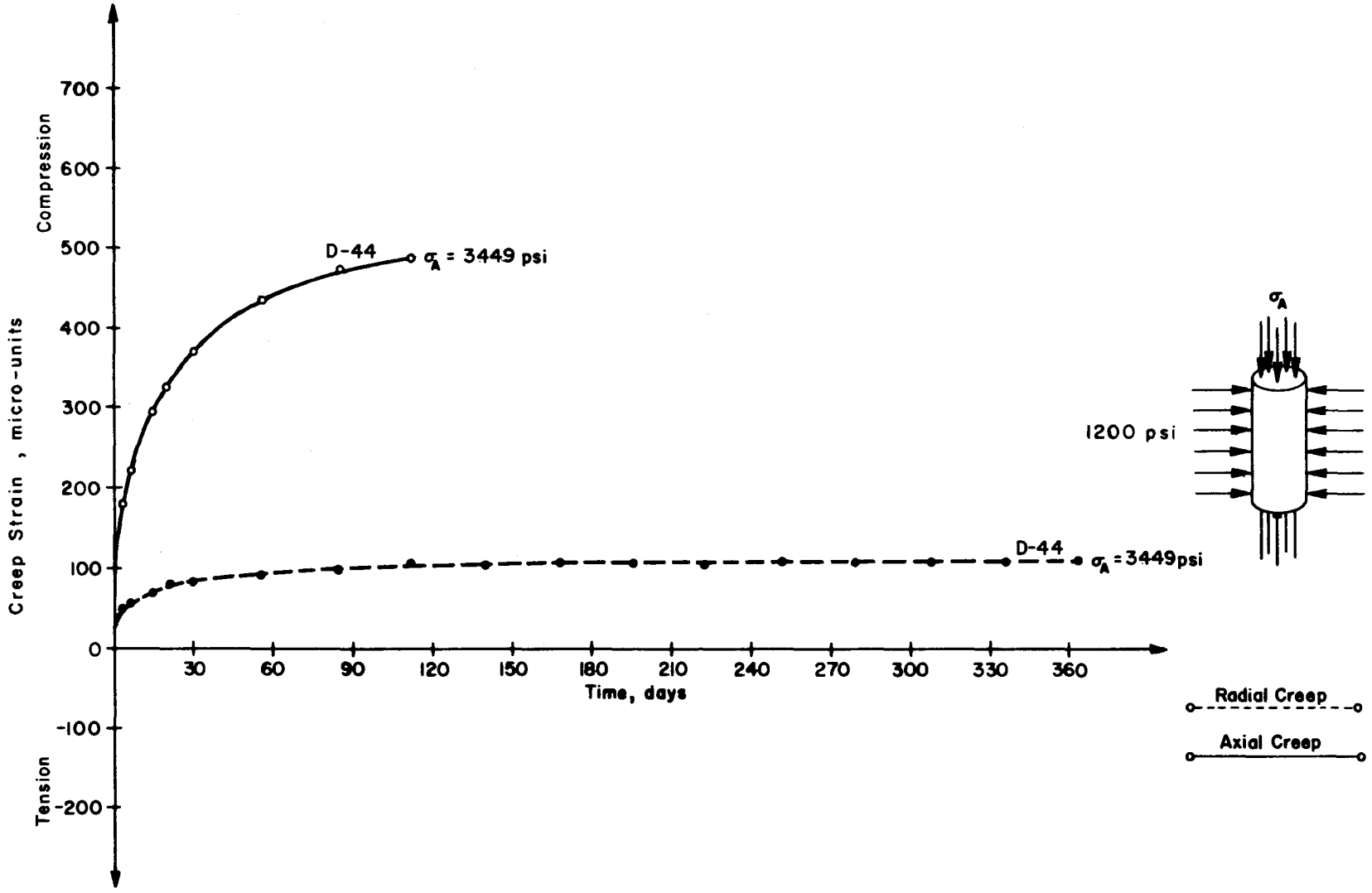

Fig A10. Creep strain-time relationships for triaxially loaded air-dried specimens with 1200 psi confining pressure at 75° F.

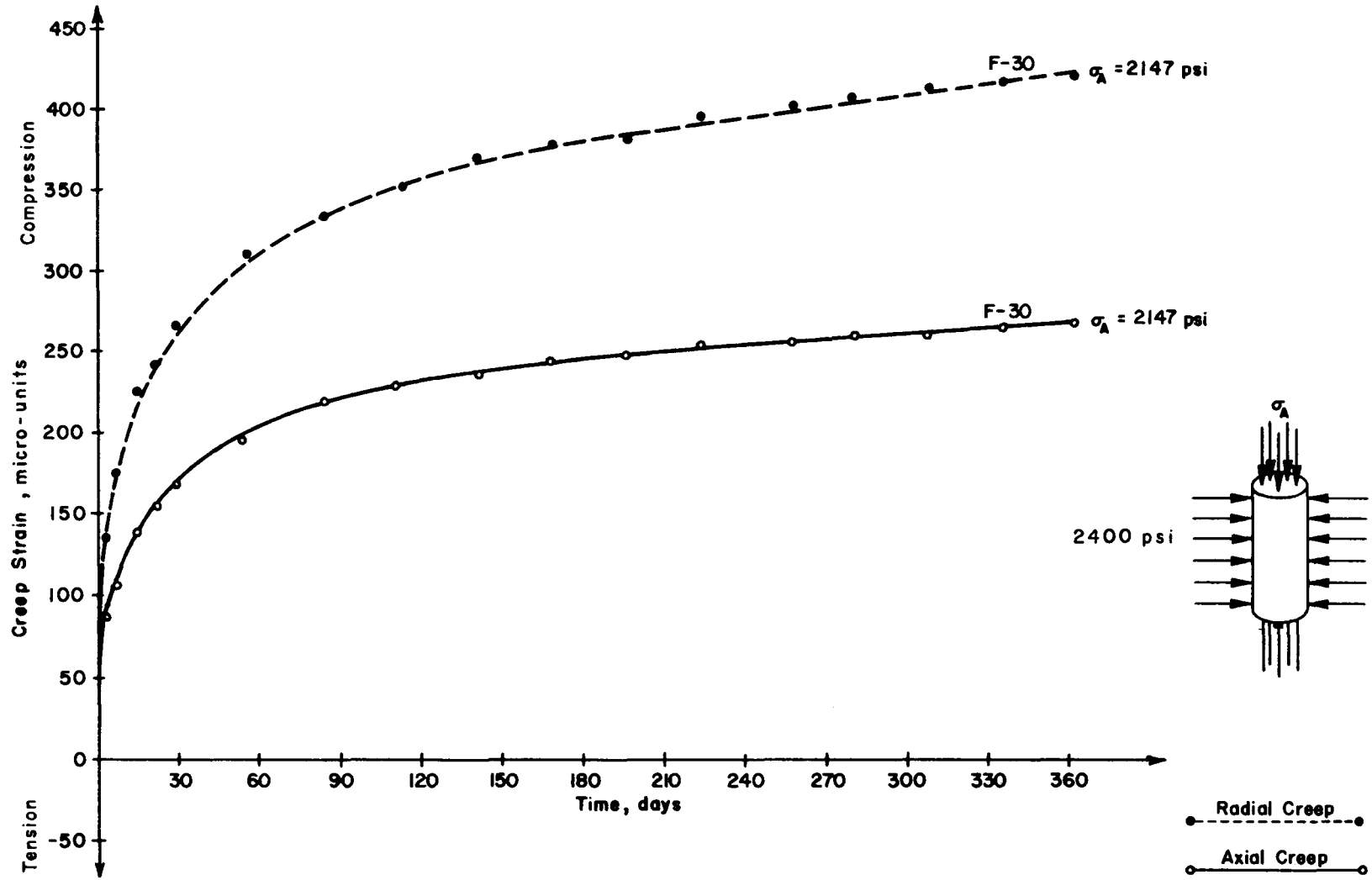

Fig A11. Creep strain-time relationships for triaxially loaded air-dried specimens with 2400 psi confining pressure at 75° F.

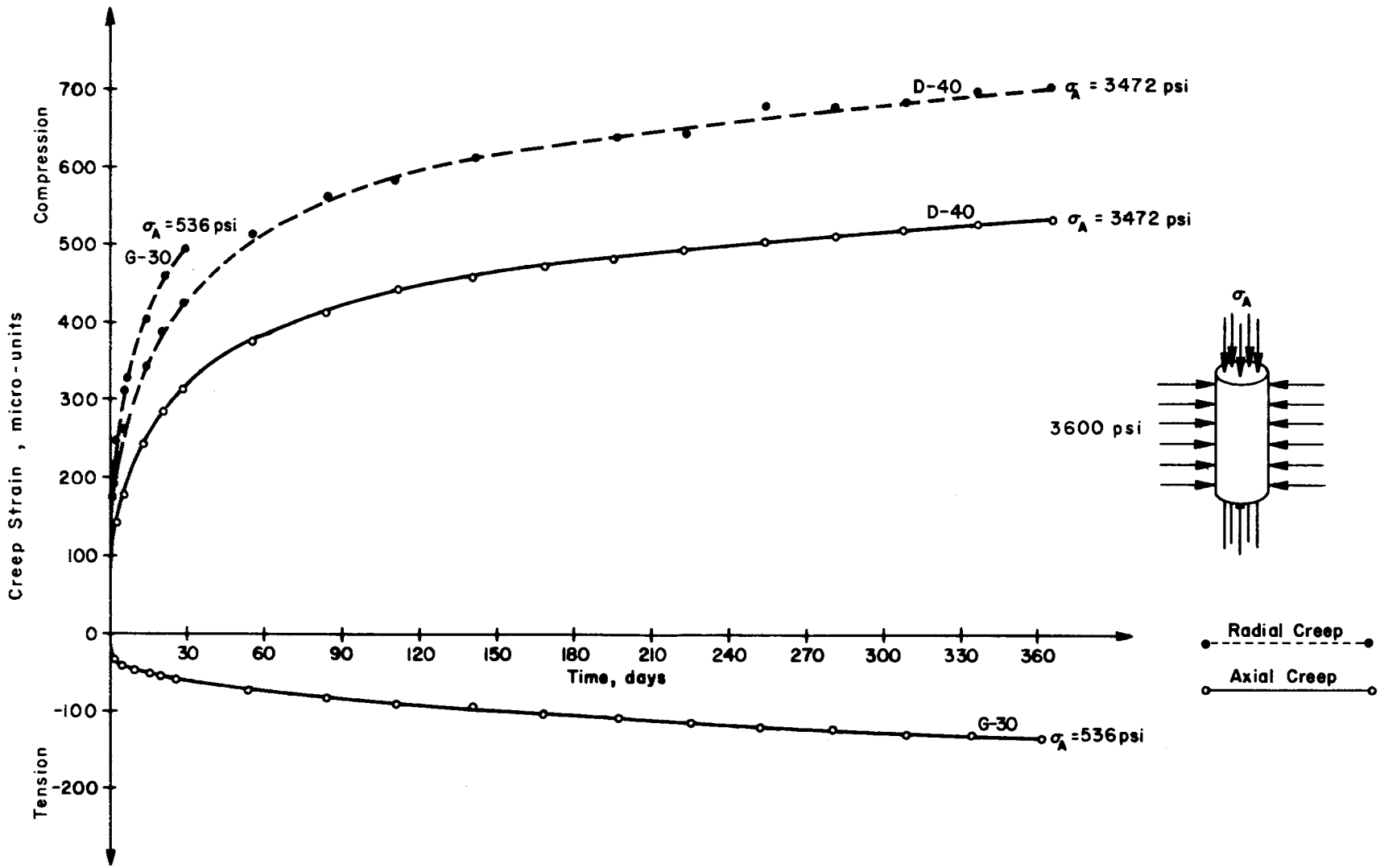

Fig A12. Creep strain-time relationships for triaxially loaded air-dried specimens with 3600 psi confining pressure at 75° F.

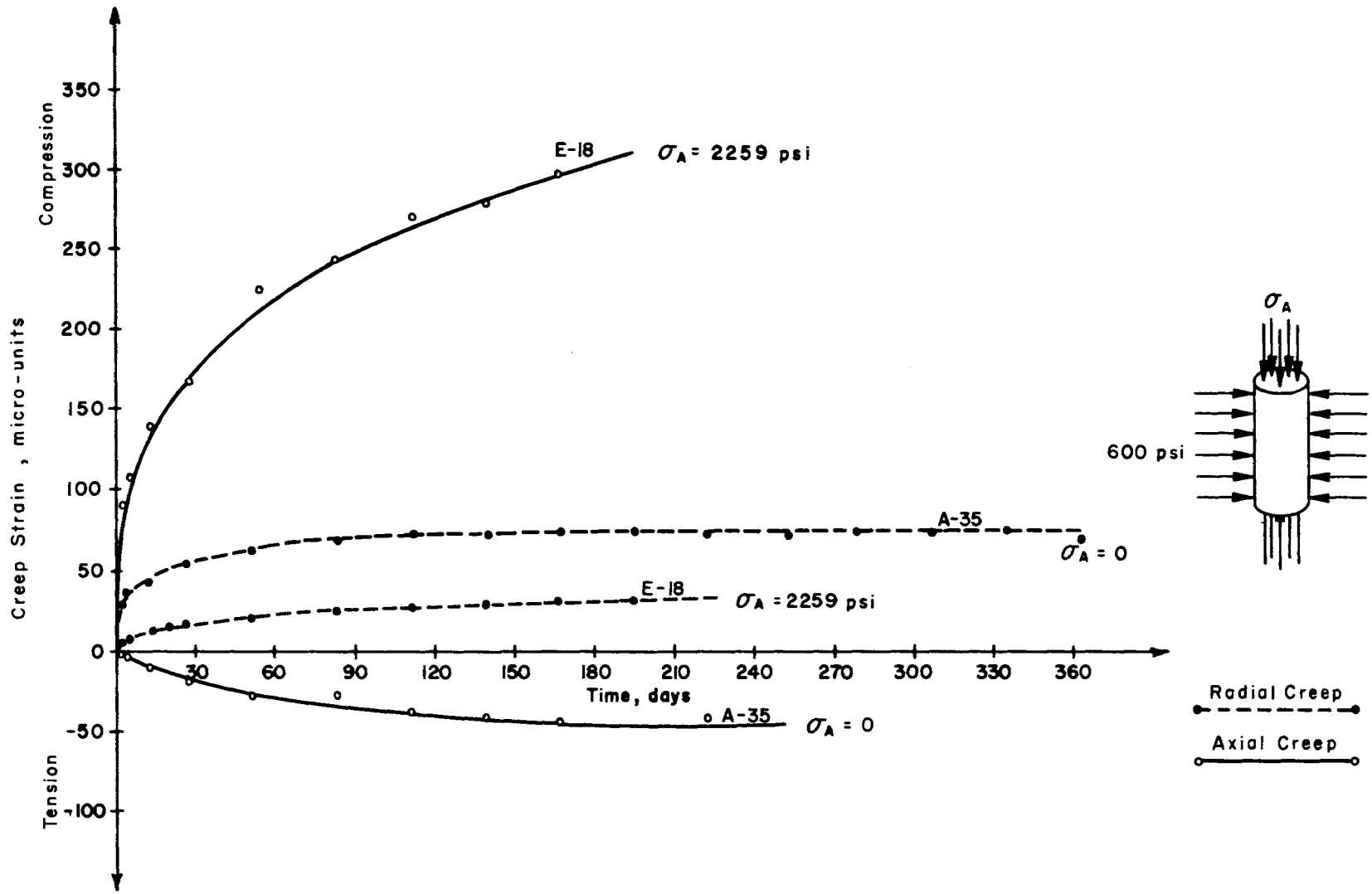

Fig A13. Creep strain-time relationships for triaxially loaded as-cast specimens with 600 psi confining pressure at 150° F.

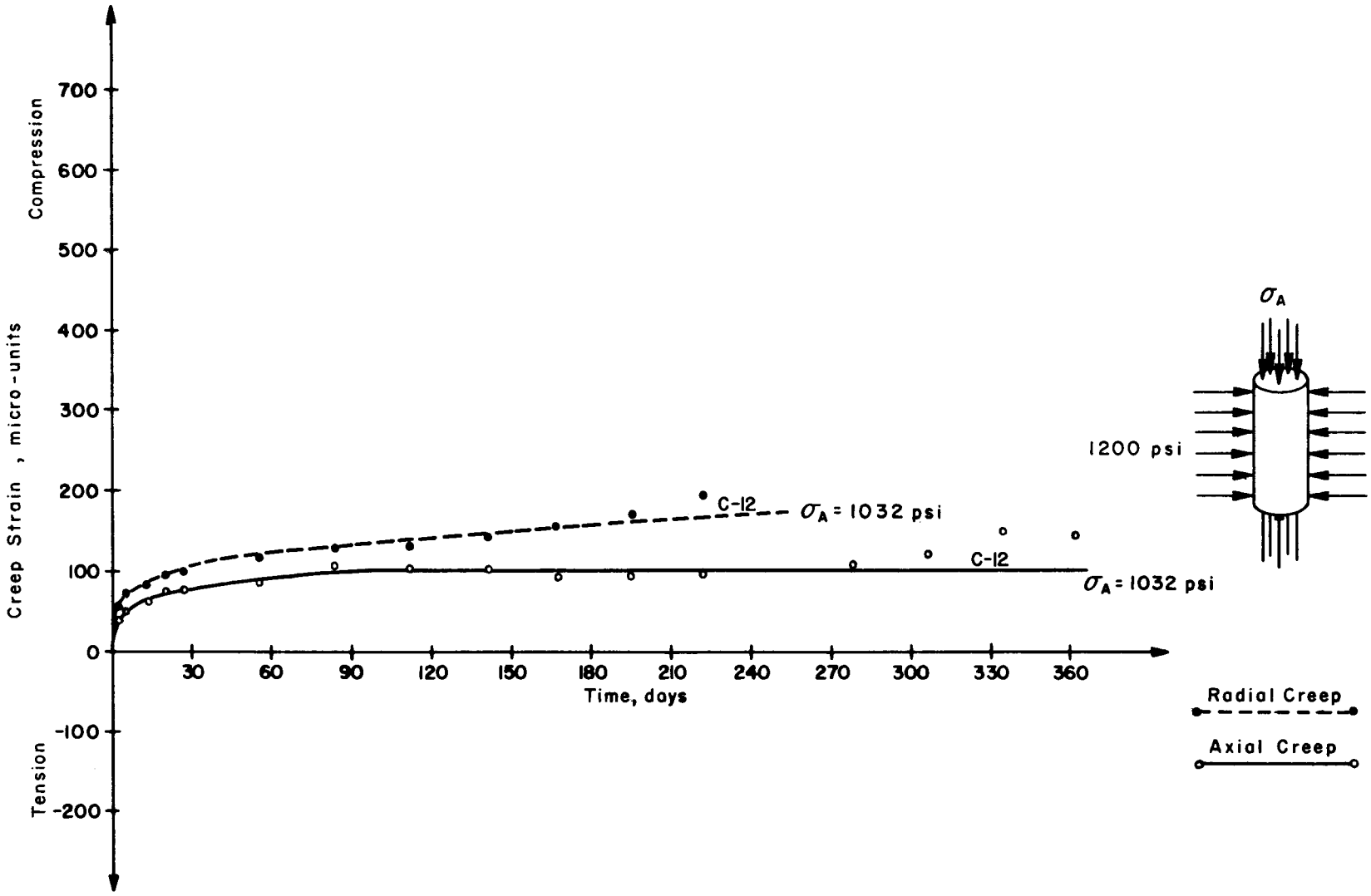

Fig A14. Creep strain-time relationships for triaxially loaded as-cast specimen with 1200 psi confining pressure at 150° F.

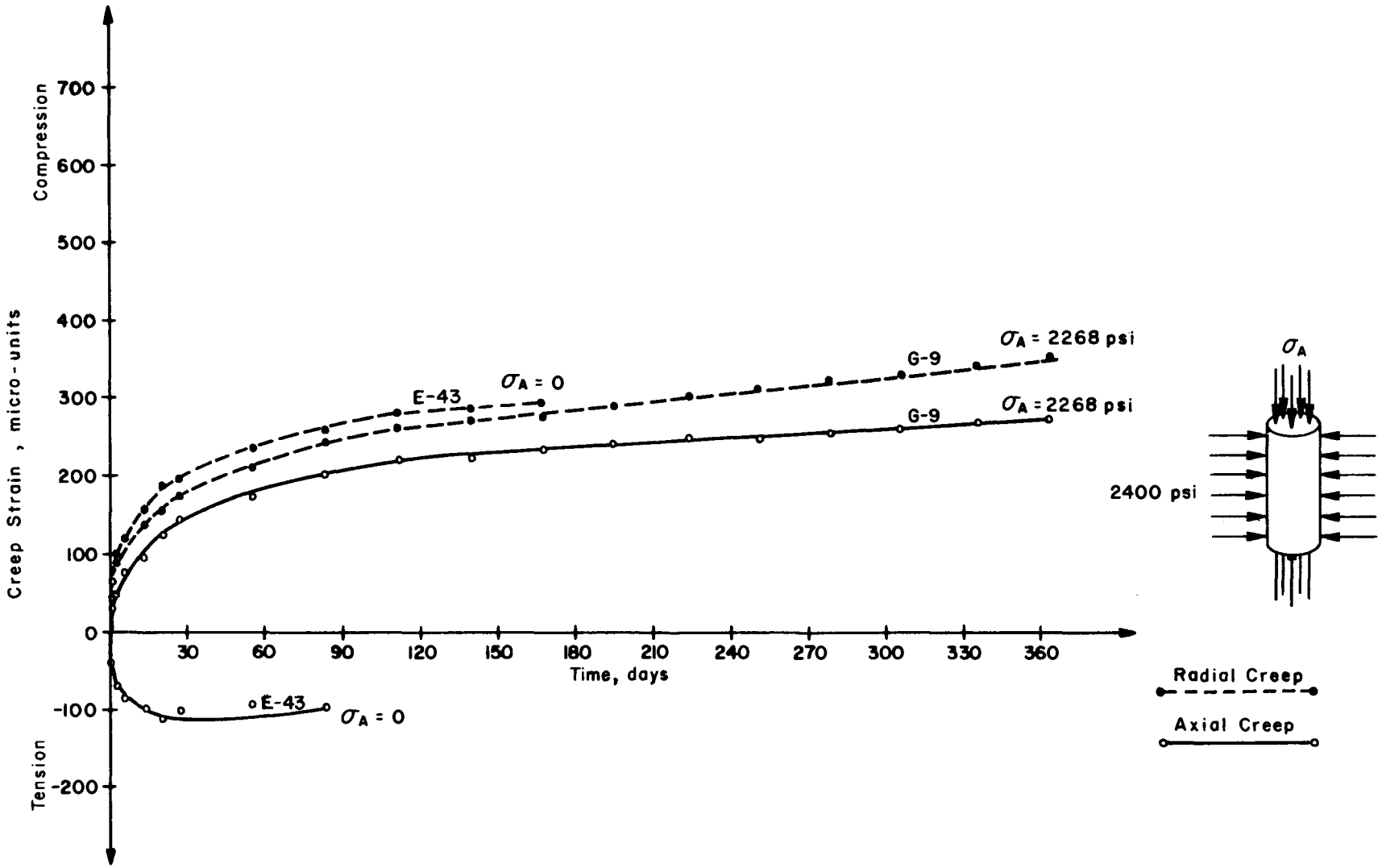

Fig A15. Creep strain-time relationships for triaxially loaded as-cast specimens with 2400 psi confining pressure at 150° F.

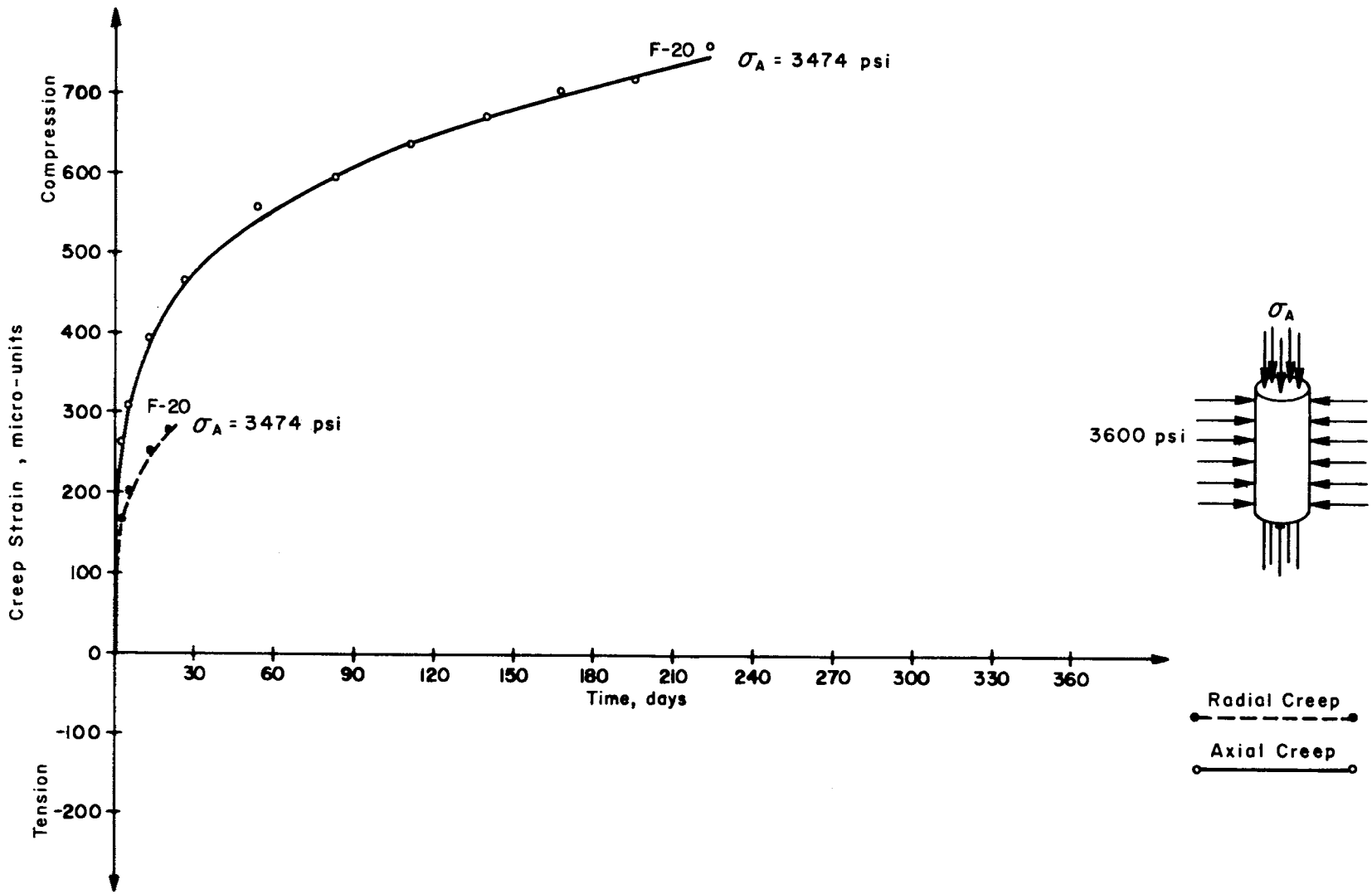

Fig A16. Creep strain-time relationships for triaxially loaded as-cast specimens with 3600 psi confining pressure at 150° F.

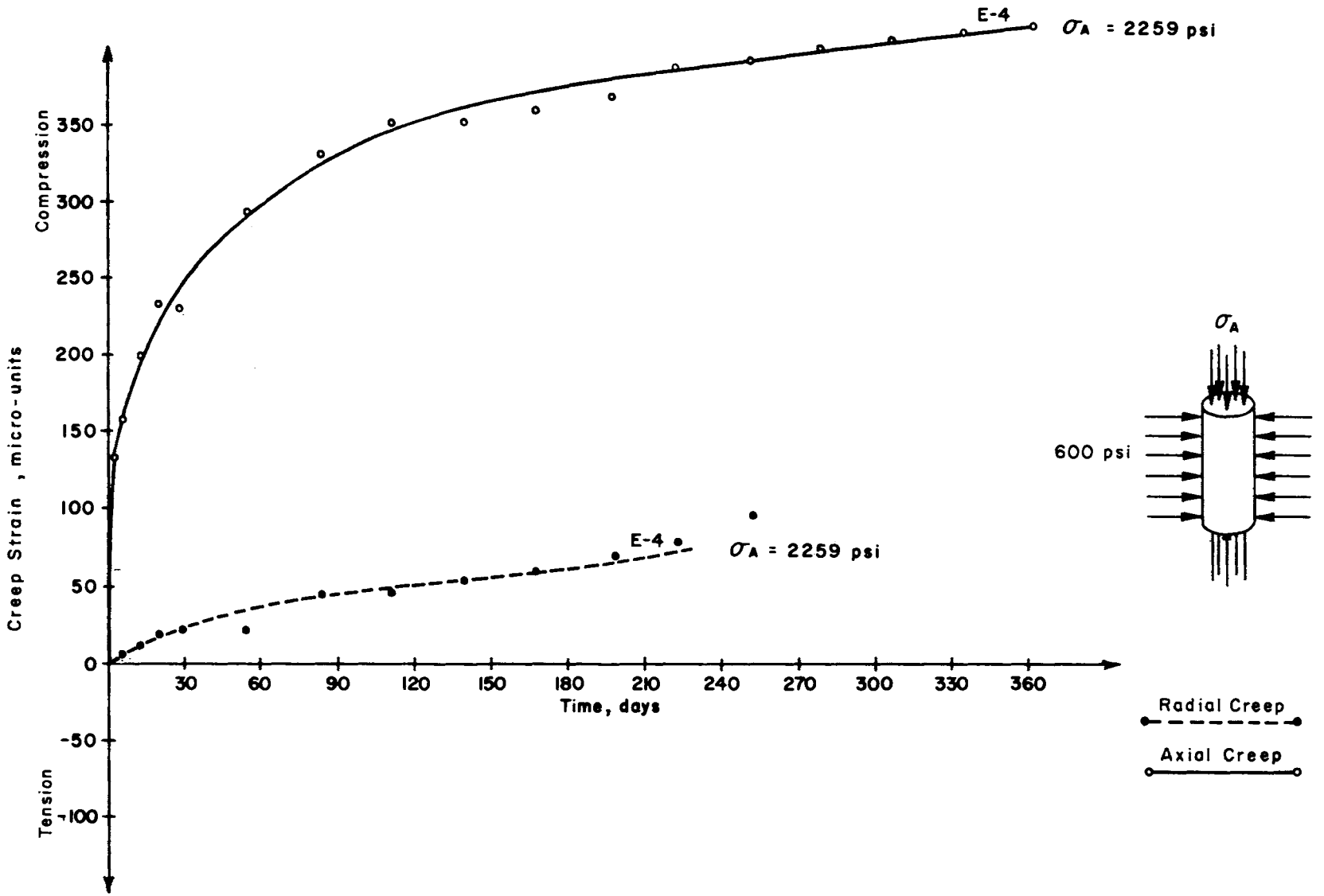

Fig A17. Creep strain-time relationships for triaxially loaded air-dried specimens with 600 psi confining pressure at 150° F.

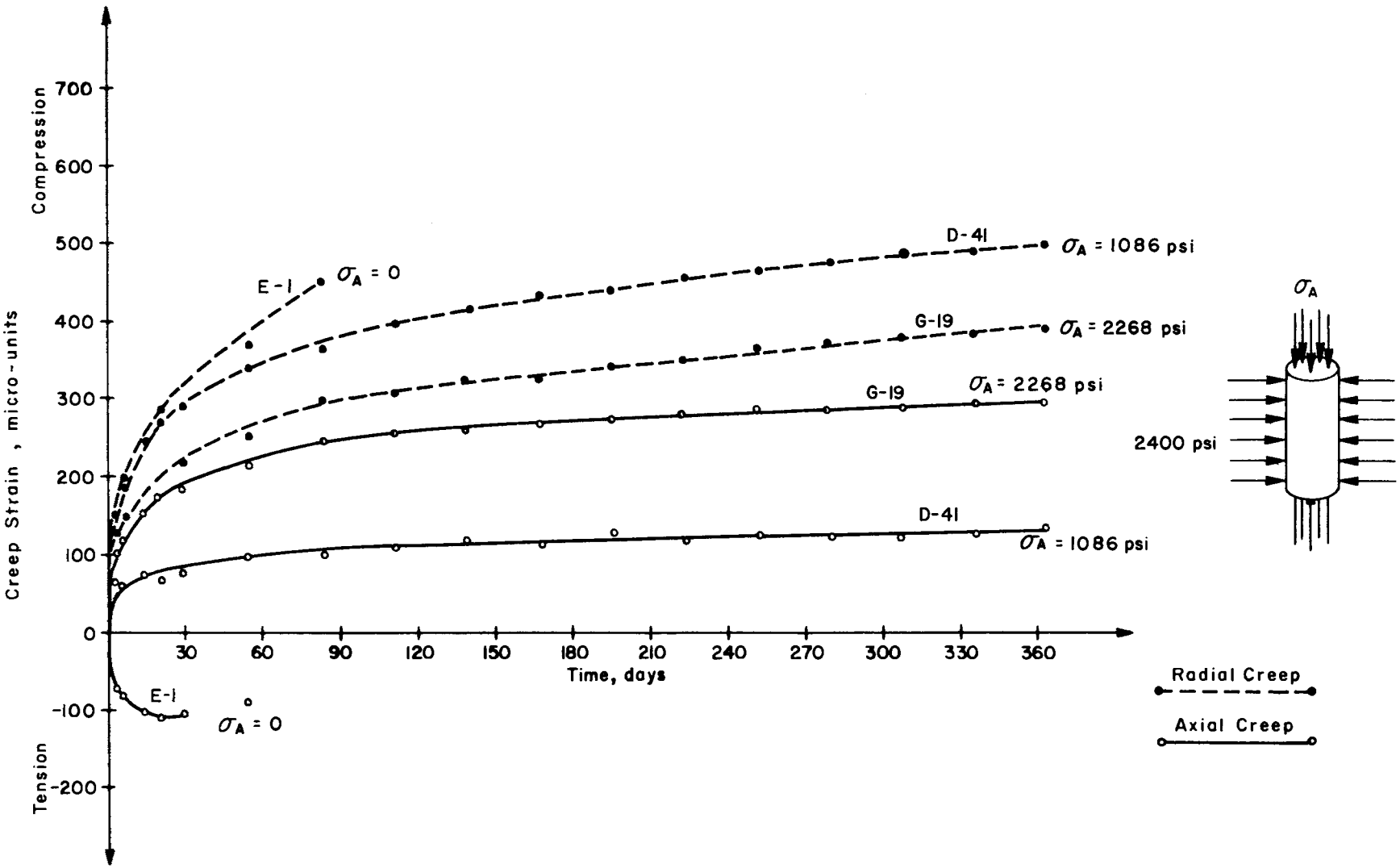

Fig A18. Creep strain-time relationships for triaxially loaded air-dried specimens with 2400 psi confining pressure at 150° F.

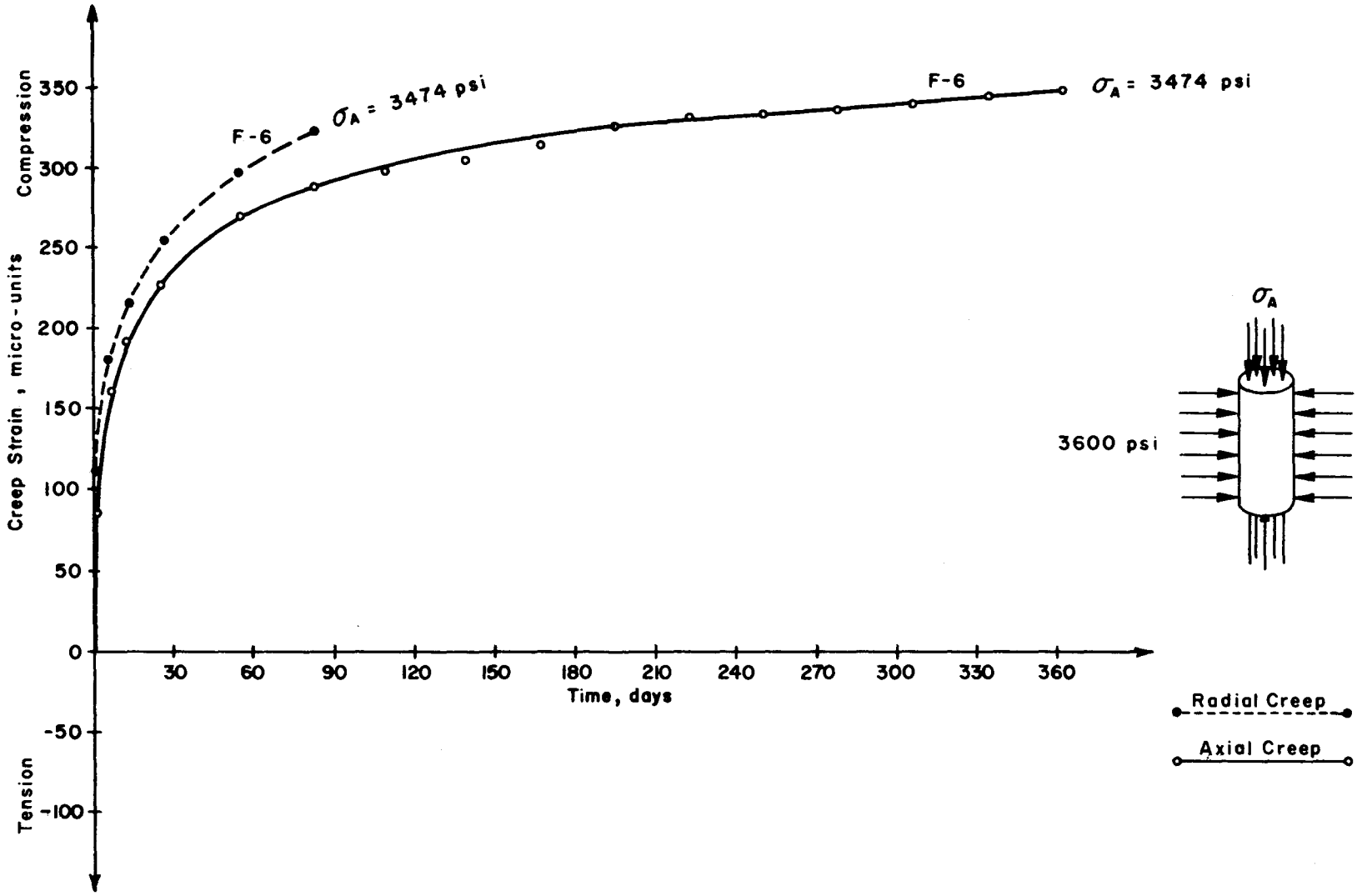

Fig A19. Creep strain-time relationships for triaxially loaded air-dried specimens with 3600 psi confining pressure at 150° F.